NITROGEN-DOPED GRAPHENE-BASED METAL COMPOSITES FOR THE NON-ENZYMATIC DETECTION OF HYDROGEN PEROXIDE

MOHAMMAD TAGHI TAJABADI POOR

FACULTY OF SCIENCE
UNIVERSITI MALAYA
KUALA LUMPUR

2020

NITROGEN-DOPED GRAPHENE-BASED METAL COMPOSITES FOR THE NON-ENZYMATIC DETECTION OF HYDROGEN PEROXIDE

MOHAMMAD TAGHI TAJABADI POOR

THESIS SUBMITTED IN FULFILMENT OF THE REQUIREMENTS FOR THE DEGREE OF DOCTOR OF PHILOSOPHY IN CHEMICAL SCIENCE

DEPARTMENT OF CHEMISTRY
FACULTY OF SCIENCE
UNIVERSITI MALAYA
KUALA LUMPUR

2020

UNIVERSITI MALAYA

ORIGINAL LITERARY WORK DECLARATION

Name of Candidate: **MOHAMMAD TAGHI TAJABADI POOR**

Matric No: **SHC120103**

Name of Degree: **DOCTOR OF PHILOSOPHY**

Title of Thesis ("this Work"):

NITROGEN-DOPED GRAPHENE BASED METAL COMPOSITES FOR THE NON-ENZYMATIC DETECTION OF HYDROGEN PEROXIDE

Field of Study:

PHYSICAL CHEMISTRY

I do solemnly and sincerely declare that:

(1) I am the sole author/writer of this Work;
(2) This Work is original;
(3) Any use of any work in which copyright exists was done by way of fair dealing and for permitted purposes and any excerpt or extract from, or reference to or reproduction of any copyright work has been disclosed expressly and sufficiently and the title of the Work and its authorship have been acknowledged in this Work;
(4) I do not have any actual knowledge nor do I ought reasonably to know that the making of this work constitutes an infringement of any copyright work;
(5) I hereby assign all and every rights in the copyright to this Work to the University of Malaya ("UM"), who henceforth shall be owner of the copyright in this Work and that any reproduction or use in any form or by any means whatsoever is prohibited without the written consent of UM having been first had and obtained;
(6) I am fully aware that if in the course of making this Work I have infringed any copyright whether intentionally or otherwise, I may be subject to legal action or any other action as may be determined by UM.

Candidate's Signature Date:

Subscribed and solemnly declared before,

Witness's Signature Date:

Name:

Designation:

NITROGEN-DOPED GRAPHENE BASED METAL COMPOSITES FOR THE NON-ENZYMATIC DETECTION OF HYDROGEN PEROXIDE

ABSTRACT

Recently, much attention has been devoted to detecting hydrogen peroxide (H_2O_2) because of its extensive range of applications in chemical synthesis, the textile industry, food production, fuel cell devices, and even in many oxidative biological reactions. Among the various methods of detection of H_2O_2, electrochemical sensors has many advantages, such as simplicity, high efficiency and sensitivity, as well as good selectivity., To improve the sensitivity of non-enzymatic sensors, noble metal nanoparticles with particular electrocatalytic activities can be utilized. The present research is aimed to design a hybrid approach for the development of novel nanostructures for non-enzymatic detection of H_2O_2. Herein, the electrochemical measurements were performed using a potentiostat/galvanostat. A X-ray powder diffractometer (XRD), transmission electron microscopy (TEM) and field emission scanning electron microscopy (FESEM) were utilized to investigate the phase structure and composition, as well as morphology and particle size of the electrodes. In addition, Raman spectroscopy and X-ray photoelectron spectroscopy (XPS) were also utilized to further investigate the structural and electronic properties and to identify the nitrogen-bonded groups in the as-synthesized nitrogen doped graphene (NG), respectively. For this purpose, NG was initially prepared using a microwave-assisted method that comprises of a three-step process of graphite oxidation, exfoliation, and chemical reduction using a reducing agent at low temperature. In the first step, NG was electrophoretically deposited (EPD) on an indium tin oxide (ITO) electrode, following by silver nanodendrites (AgNDs) and platinum nanoflowers (PtNFs) as the subsequent layers via electrochemical deposition. The as-prepared AgNDs/NG-modified ITO electrode was used as a non-enzymatic H_2O_2 sensor and exhibited high stability,

outstanding reproducibility and good electrocatalytic activity for the quick detection of H_2O_2 over a wide linear range from 100 μM to 80 mM. In the second case, PtNFs/NG-modified ITO electrode with different NG loadings were utilized as non-enzymatic H_2O_2 sensors, where ITO modified with 0.05 mg ml^{-1} NG loading exhibited improved properties for H_2O_2 detection over a linear range from 1 μM to 1 mM.

Keywords: Nitrogen doped graphene, Silver nanodendrite, Platinum nanoflower, Hydrogen peroxide, Sensor.

KOMPOSIT LOGAM BERASAS GRAFIN TERDOP-NITROGEN BAGI MENGESAN HIDROGEN PEROKSIDA SECARA BUKAN ENZIM

ABSTRAK

Baru-baru ini, banyak perhatian telah ditumpukan untuk mengesan hidrogen peroksida (H_2O_2) kerana pelbagai aplikasinya dalam sintesis kimia, industri tekstil, pengeluaran makanan, sel bahanapi, dan juga dalam banyak tindak balas biologi oksidatif. Di antara pelbagai kaedah untuk mengesan H_2O_2, penderia elektrokimia mempunyai banyak kelebihan, seperti kesederhanaan, kecekapan tinggi dan kepekaan, serta kepemilihan yang baik, di mana untuk meningkatkan kepekaan penderia bukan enzim, nanopartikel logam mulia dengan elektro-mangkin tertentu yang meningkatkan aktiviti boleh digunakan. Penyelidikan sekarang bertujuan untuk merancang pendekatan hibrid untuk pembangunan struktur nano baru untuk pengesanan penderia bukan enzim H_2O_2. Di sini, pengukuran elektrokimia dilakukan menggunakan potentiostat/galvanostat. Difraktometer serbuk sinar X (XRD), mikroskop elektron penghantaran (TEM) dan mikroskop elektron pengimbasan pelepasan medan (FESEM) telah digunakan untuk memeriksa struktur fasa dan komposisi, serta morfologi dan saiz zarah elektrod. Di samping itu, spektroskopi Raman dan spektroskopi X-ray fotoelektron (XPS) juga digunakan untuk menyiasat sifat-sifat struktur dan elektronik untuk mengenal pasti kumpulan-kumpulan terikat nitrogen dalam asid sintetik graphene didopkan nitrogen (NG). Untuk tujuan ini, NG pada mulanya disediakan dengan kaedah micro-gelombang yang terdiri daripada proses tiga langkah pengoksidaan grafit, pengelupasan dan pengurangan kimia dengan menggunakan agen penurunan pada suhu rendah. Dalam langkah pertama, NG adalah disadurkan secara electrophoretik (EPD) pada elektrod indium tin oksida (ITO), diikuti dengan nano-dendrit perak (AgNDs) dan platinum nano-bunga (PtNFs) yang disadurkan sebagai lapisan kedua melalui saduran elektrokimia. Elektrod ITO yang diubahsuai AgNDs/NG telah digunakan sebagai penderia bukan

enzimatik H_2O_2 dan menunjukkan kestabilan yang tinggi, kebolehulangan dan aktiviti elektrokatalik yang baik untuk pengesanan cepat H_2O_2 dengan julat linear yang luas dari 100 μM hingga 80 mM. Dalam kes kedua, elektrod ITO (PtNF/NG) diubahsuai PtNF/N-Grafine dengan sebatian N-doped G yang berbeza digunakan sebagai penderia bukan enzimatik H_2O_2, di mana ITO diubahsuai dengan 0.05 mg ml^{-1} NG yang mempamerkan sifat-sifat yang lebih baik untuk pengesanan H_2O_2 melalui julat linear antara 1 μM hingga 1 mM.

Kata kunci: Grafin terdop-nitrogen, diikuti dengan nano-dendrit perak, dan platinum nano-bunga, hidrogen peroksida, Sensor.

ACKNOWLEDGEMENTS

I would like to acknowledge Professor. Dr. Wan Jeffrey Basirun for their very useful advice and support throughout my graduate career. I am also in deep appreciate towards Dr. Mehran Sookhakian for helpful assistance on my thesis. Without their recommendation during my studies, I will not be capable of complete my PhD degree. I would like to thank Universiti Malaya for the financial support. In the end, I would like to acknowledge my dear family for their endless encouragement throughout my PhD.

TABLE OF CONTENTS

LIST OF FIGURES

LIST OF TABLES

LIST OF SYMBOLS AND ABBREVIATIONS

Ag	:	Silver
AgBP	:	Antigen binding proteins
AgNDs	:	Silver nanodendrites
AgNDs/NG	:	AgNDs-Nitrogen doped graphene-modified ITO
$AgNO_3$	:	Silver nitrate
AgNPs	:	Silver nanoparticles
ATP	:	Adenosine-5'-triphosphate
Au-CPE		Gold-modified carbon paste electrode
BWAs	:	Biowarfare agents
CAT	:	Catalase
CE	:	Counter electrode
CMOS	:	Complementary metal-oxide-semiconductor
CNT	:	Carbon nanotube
CVs	:	Cyclic voltammograms
EIS	:	Electrochemical impedance spectroscopy
ELISA	:	Enzyme-linked immunosorbent assay
EPD	:	Electrophoretically deposited
Fab	:	Fragment antigen-binding
FACS	:	Fluorescence-activated cell sorting
FDA	:	US food and drug administration
FESEM	:	Field emission scanning electron microscopy
FRET	:	Förster resonance energy transfer
GC	:	Glassy carbon
GCEs	:	Glassy carbon electrodes

GO	:	Graphene oxide
GOD	:	Glucose oxidase
H_2O_2	:	Hydrogen peroxides
H_2PtCl_6	:	Chloroplatinic acid
HDAC	:	Histone deacylase
HEX	:	Hexokinase
HfO_2	:	Hafnium oxide
HRP	:	Horseradish peroxidase
ICSBs	:	Ion channel switch biosensors
ITO	:	Indium tin oxide
JCPDS	:	Joint Committee on Powder Diffraction and Standards
LOD	:	Limit of detection
MSF	:	Mesoporous silica film
MWCNTs-COOH	:	Functionalized multi-walled carbon nanotubes
NG	:	Nitrogen doped graphene
NF	:	Nafion
PANI	:	Polyaniline
PBS	:	Phosphate buffered saline
PLL/f-MWCNT	:	Ploy-L-Lysine/multiwalled carbon nanotube
POCT	:	Point-of-care testing
Pt	:	Platinum
PtNF	:	Platinum nanoflower
PtNF/NG	:	PtNF-Nitrogen-doped graphene
PVA	:	Polyvinyl alcohol
RFBs	:	Reagentless fluorescent biosensors

rGO	:	Reduced graphene oxide
RSD	:	Relative standard deviation
SAMs	:	Self-assembled monolayers
SAW	:	Surface acoustic waves
SBET	:	Specific surface area
SCFV	:	Single-chain variable fragment
SS	:	Single-stranded
t-BLM	:	Tethered bilayer membranes
TEM	:	Transmission electron microscopy
TFS	:	Transcription factors
UTI	:	Urinary tract infection
WE	:	Working electrode
XPS	:	X-ray photoelectron spectroscopy
XRD	:	X-ray powder diffractometer

LIST OF APPENDICES

CHAPTER 1: INTRODUCTION

1.1 Background of Study

Recently, there has been a growing interest in hydrogen peroxide (H_2O_2) detection owing to its broad range of applications, such as in food production (as a disinfecting agent), the textile industry (as a bleaching agent), fuel cell devices (as an energy storage system), chemical synthesis (as an active reagent) and even in many oxidative biological reactions (as an essential mediator) (Yang *et al.*, 2013). Various methods have been proposed for the detection of H_2O_2 such as chemiluminescence, fluorescence, titration, chromatography and electrochemistry (Yang *et al.*, 2013). Among these methods, the utilization of electrochemical sensors has proven to be a simple and efficient approach, and these sensors have been broadly used because of their high sensitivity, good selectivity and easy operation (Mahmoudian *et al.*, 2014). In addition, electrochemical sensors based on the non-enzymatic technique possess the advantages of low cost, high stability and good reproducibility compared to enzymatic detection. Thus, to improve the sensitivity of non-enzymatic sensors, noble metal nanoparticles, such as Pt (You *et al.*, 2003), Au (Qiu *et al.*, 2007) and Pd (Huang *et al.*, 2008), with particular electrocatalytic activities have been employed as modified electrodes for the detection of H_2O_2.

It is well known that Ag nanostructures exhibit good catalytic activity toward H_2O_2 reduction, and they have been commonly expanded for enzymeless-based H_2O_2 sensors. Recently, several efforts have been focused on the design of Ag nanostructures with a variety of morphological features, such as nanowires (Sun and Xia, 2002), nanobars (Wiley *et al.*, 2007), nanobelts (Sun *et al.*, 2003) and multiple twinned structures (Wiley *et al.*, 2005). Among these nanostructures, nanodendritic configurations comprised of trunks and multiple hierarchical symmetrical branches have attracted considerable

research interest due to their unique optical, electronic and catalytic properties (Abbasi *et al.*, 2013). Silver nanodendrites (AgNDs) are able to form porous structures on the surfaces of electrodes owing to the high surface area (AgNPs), which create a dense film on the surface of electrode (Bonačić-Koutecký *et al.*, 2012). Accordingly, AgNDs show better catalytic performance compared to AgNPs. Several methods have been proposed in order to prepare Ag nanostructures, which include electrochemical deposition (Kumar *et al.*, 2004), thermal evaporation (Zhu *et al.*, 2003), chemical vapor deposition (Cardini *et al.*, 2002) and template approach (Xiao *et al.*, 2001). Among the various techniques, electrochemical deposition is a comparatively simple and versatile technique for this purpose.

On the other hand, Pt shows high catalytic activity for many reactions and has found application in a wide range of fields, such as catalytic hydrogenation, oxygen reduction and fuel-cell catalysis (Kulp *et al.*, 2013). However, Pt is expensive and rare, and new approaches are required to minimize the amount of Pt used for various technological applications. Hence, the support materials on which the Pt catalysts are attached, have also received much attention due to the increased analytical performance. The support materials of the catalysts are influenced by many factors including the hydrophobicity, biocompatibility, surface roughness and morphology. An ideal catalyst support material as the sensing interface should possess strong affinity towards the catalyst particles for their immobilization, high electrical conductivity and good chemical stability. Besides, this material should be non-toxic and have a high surface area and long-term stability (Vinayan *et al.*, 2012). Thus materials such as redox proteins (Liu *et al.*, 2004), conductive polymers (Mahmoudian *et al.*, 2014) and carbon (Lawal, 2015), have been utilized as support materials for non-enzymatic biosensors.

Conversely, graphene is a single sheet of two-dimensional sp^2-hybridized carbon nanosheets arranged in a honeycomb lattice, has attracted much attention in recent decades due to its outstanding physical and chemical properties, such as high thermal conductivity, high surface area, high chemical stability and rapid charge carrier mobility (Sookhakian *et al.*, 2013; Sookhakian *et al.*, 2014a). In addition to its intrinsic structure, many theoretical and experimental efforts have been made to modify graphene using various doping agents, such as nitrogen, boron, chlorine, phosphorus, fluorine, hydrogen and sulfur. This modification is a promising approach to further modulate and tailor the electronic properties of graphene, to manipulate its surface chemistry and to introduce a considerable number of defects into its lattice (Sookhakian *et al.*, 2014b; Azarang *et al.*, 2014). Among these elements, nitrogen is considered an excellent dopant for graphene owing to its comparable atomic size and valence electrons. Moreover, strong valence bonds can be formed between the nitrogen lone pair electrons and the graphene π-electron system. Thus, nitrogen doping can form a band gap in the graphene energy levels, which is accompanied by the transformation of graphene to an n-type semiconductor. This process results in a dramatic increase in the electron conductivity, spin density and charge distribution of the carbon atoms, which lead to the development of an activation region on the graphene surface (Wu *et al.*, 2012) that enhances its ability to bind with guest molecules. Compared to other active inorganic compounds such as Prussian blue (Wang *et al.*, 2013) and conductive polymers-metal nanocomposites, such as polyaniline-palladium nanocomposites (Ivanov *et al.*, 2013), N-doped G not only shows superb electrocatalytic activity and biocompability, but exhibit large surface area, which is helpful for adsorption of more nanodendrites on the surface by π-π stacking. This feature is vital for improving the sensitivity of H_2O_2 detection. So far, several methods of synthesis of NG were reported, such as chemical vapor deposition, laser ablation and

ammonia plasma treatment (Mayavan *et al.*, 2012); however, these methods involve high energy consumption and high cost.

1.2 Problem statement

Despite the inherent benefits of AgNDs/NG and PtNF/NG and their potential towards H_2O_2 detection, little attention has been paid to producing these nanostructured electrodes for biosensor applications. In fact, there are also no reports on the layer-by-layer electrochemical deposition route for the rapid synthesis of AgNDs and PtNFs as second layers on NG-modified indium tin oxide (ITO) electrodes.

On the other hand, the synthesis of graphene and NG is another challenging issue, which may have a significant impact on the electrode performance. This process should be simple and cost-effective. Among the proposed methods, most of them involve high energy consumption. One unique approach to improve production efficiency is to use the microwave-assisted method. Another solution is to take advantage of the thermal treatment of graphene oxide (GO). Thus, a detail investigation of NG loading and its influence on the analytical performance of non-enzymatic biosensors is essential. This makes it necessary to determine the optimal amount of graphene in the system.

It should be noted that although the assessment of the hybrid electrodes towards H_2O_2 reduction using chronoamperometry, cyclic voltammetry and electrochemical impedance spectroscopy (EIS) are very important, it is also no less important to specify the synergistic effect between the electrocatalytic activity of the nanoparticles and the high conductivity and large surface area of NG.

1.3 Objectives

This study aims to develop hybrid approaches for the development of novel nanostructures for the non-enzymatic detection of H_2O_2. The phase structure and composition, morphological features, as well as the structural and electronic properties of the as-modified ITO electrodes are examined. The objectives of this study are the following:

1. To fabricate AgNDs/NG- and PtNF/NG-modified ITO electrodes using electrophoretic and electrochemical deposition in order to improve the sensitivity of non-enzymatic biosensors.
2. To assess the support of NG and effect of NG loadings on the electrocatalytic activity toward H_2O_2 reduction.
3. To examine the effect of the presence of Ag and Pt on the performance of the nanostructured sensor.

1.4 Research Contribution

The first phase of the present research deals with the preparation of AgNDs/NG-modified ITO electrode for the non-enzymatic detection of hydrogen peroxide, where the support of NG and the presence of silver NDs on the performance of the nanostructured sensor are examined. The outcome and contribution of this work to the world of knowledge consists of one research article published in specialized scientific journal.

The second phase of the present study concentrates on the electrodeposition of flower-like platinum on electrophoretically grown NG as a highly sensitive electrochemical non-enzymatic biosensor for hydrogen peroxide detection. In this part, the presence of Pt and NG loading on the analytical performance of the non-enzymatic

biosensor are investigated. The outcome of this phase of research has also been published in a specialized scientific journal.

1.5 Scope of Research

The current study aims to merge the chemical science and materials engineering to fabricate biosensors with advantageous electrochemical performances toward H_2O_2 detection. The development of such biosensor makes it necessary to study the effect of processing parameters. Accordingly, the as-prepared sensors must be evaluated in terms of their phase and chemical purity, morphological features, as well as structural and electronic properties using various characterization methods such as X-ray powder diffraction (XRD), transmission electron microscopy (TEM) and field emission scanning electron microscopy (FESEM), Raman spectroscopy and X-ray photoelectron spectroscopy (XPS). The electrochemical measurements were performed using a potentiostat/galvanostat.

1.6 Outline

A brief description of each of the chapters follows: Chapter 1 identifies the existing challenges in the present study. In this chapter, a brief introduction of the project concept is mentioned. Given the existing restrictions, the research goals are elucidated and the research scope is outlined.

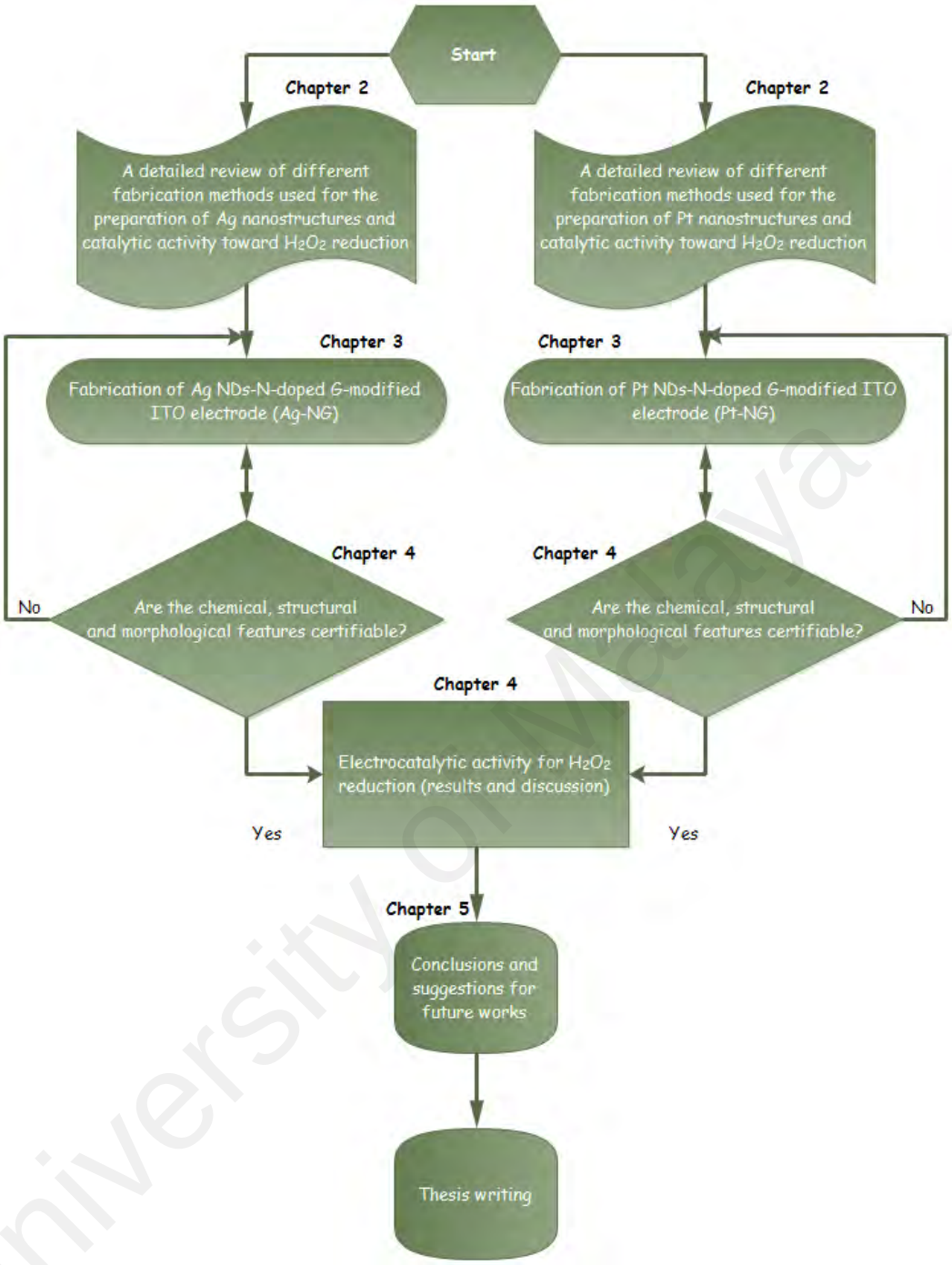

Figure 1.1: A summary of the activities carried out in the present project.

In chapter 2, a comprehensive background into the analytical performances of the nanostructured biosensors is presented. This chapter also covers a detailed review of a range of fabrication techniques for the preparation of the electrochemical biosensors, especially non-enzymatic approach, as well as the productivity parameters, which require

to be controlled in order to attain products with the highest performance. Chapter 3 presents the methodology utilized for the preparation of NG, deposition of AgNDs and PtNFs as the secondary layers, as well as the characterization techniques employed for the assessment of the chemical, structural, morphological and electrochemical properties of the as-prepared nanostructured biosensors. Chapter 4 focuses on the analysis of various characteristics of the as-prepared biosensors and descriptions of the results of experimental investigation. Chapter 5 ultimately concludes the obtained data and offers suggestions for future research or investigations. A summary of the activities carried out in the present study is shown in Figure 1.1.

CHAPTER 2: LITERATURE REVIEW

2.1 Introduction

In general, biosensors are analytical devices that converts a biological response into an electrical signal. Quintessentially biosensors must be highly specific, independent of physical parameters such as pH and temperature, and should be reusable. This term was coined by Cammann (Cammann, 1977). Design and preparation of biosensors, their chemical compositions, transducing devices and immobilization methods involve multidisciplinary studies in materials, chemistry, biology and engineering. The materials utilized in biosensors are classified into three groups on the basis of their mechanisms: biocatalytic group comprising enzymes, bioaffinity group including antibodies and nucleic acids, as well as microbe based containing microorganisms (Mehrotra, 2016).

The sensitive biological element, for example tissue, organelles, cell receptors, microorganisms, enzymes, antibodies, nucleic acids, etc. is a biologically material or biomimetic component, which acts reciprocally with the analyte under study. These elements can also be formed by biological engineering. The transducer or the detector element works in a physicochemical mode (optical, piezoelectric, electrochemical, etc.) converts the signal caused by the interaction of the analyte with the biological element into another signal that can be more effortlessly evaluated and quantified. The biosensor reader device with the associated electronics or signal processors is principally responsible for the demonstration of the outcomes, which sometimes gives a reason for the most expensive part of the sensor device. Nevertheless, it is possible to generate a user friendly display that comprises transducer and sensitive element. It should be noted that the readers are typically custom-designed and produced to suit the diverse working principles of biosensors (Turner *et al.*, 1987; Bănică, 2012).

2.2 Biosensor Component

A biosensor characteristically comprises a biodiagnosis element, biotransducer component and electronic system, which involve a signal amplifier, processor and display (Figure 2.1).

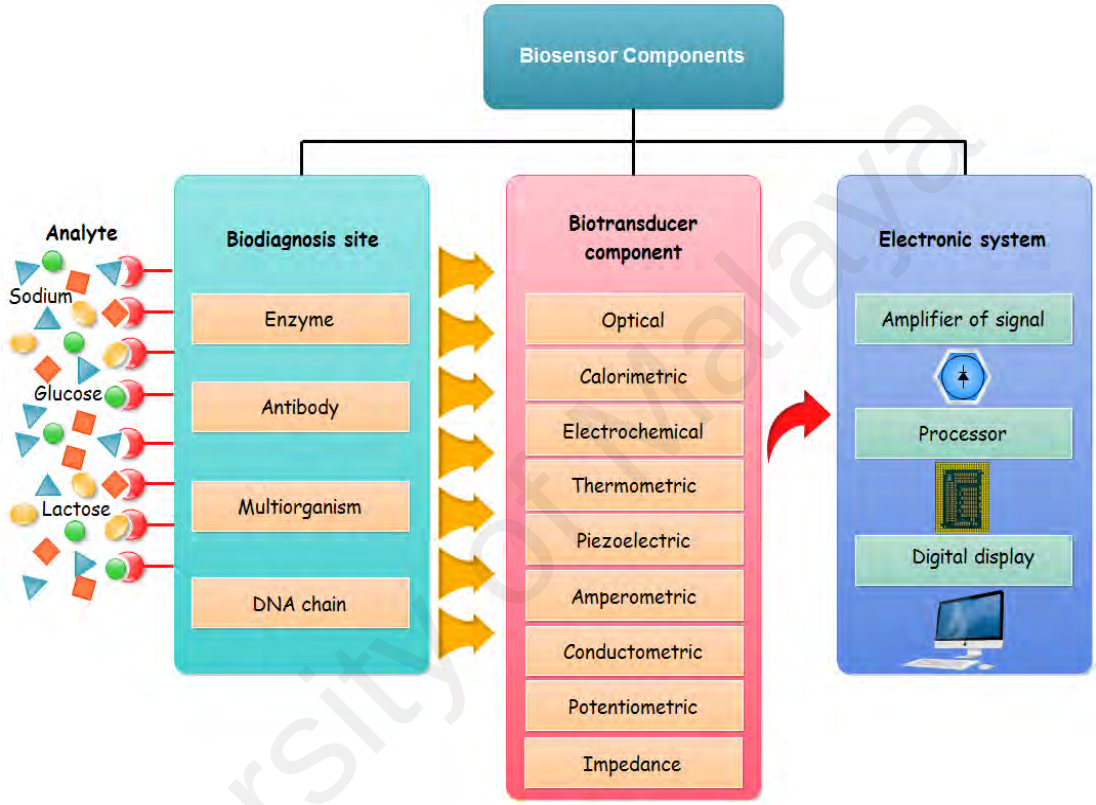

Figure 2.1: Scheme view of biosensor components consisting of different transducers depending on signal response type.

The transducers and electronics can be integrated in a complementary metal-oxide-semiconductor (CMOS)-based microsensors. The diagnosis part, also known as a bioreceptor, employs biomolecules from organisms or receptors modeled after biological systems to interact with the analyte of interest. This interaction is measured by the biotransducer which outputs a measurable signal proportional to the presence of the target analyte in the sample. The overall goal of the design of a biosensor is the facile and convenient testing at the point of concern or care, where the specimen was acquired (Hierlemann *et al.*, 2003; Hierlemann and Baltes *et al.*, 2003).

2.2.1 Recognition Component (Bioreceptors)

In a biosensor, the bioreceptor is designed to interact with the particular analyte of interest to produce an outcome measurable by the transducer. An important requirement of the bioreceptor is the high selectivity towards the analyte, among a matrix of other chemical or biological interfering compounds. While the kind of biomolecule used can differ broadly, biosensors can be categorized pursuant to usual types of bioreceptor interactions such as: anitbody/antigen, enzymes/ligands, nucleic acids/DNA, cellular structures/cells, or biomimetic materials (Vo-Dinh and B. Cullum, 2000).

2.2.1.1 Antibody/Antigen Interactions

An immunosensor uses a very particular binding affinity of antibodies for a certain compound or antigen. The special nature of the antibody-antigen interaction is similar to a lock and key fit, where the antigen will only bind to the antibody with the correct adaptation. The binding events cause a physicochemical alteration that in combination with a tracer, such as a fluorescent molecules, enzymes, or radioisotopes, can create a signal. There are limitations with using antibodies in sensors:

The antibody binding capacity is heavily dependent upon the testing conditions, e.g. pH and temperature.

The antibody-antigen interaction is normally irreversible. Nevertheless, it has been reported that binding can be interrupted by chaotropic reagents, organic solvents, or even ultrasonic radiation (Marazuela and Moreno-Bondi, 2002).

2.2.1.2 Artificial Binding Proteins

It has been found that the utilization of antibodies as the bioreceptor component of biosensors has several disadvantages, such as high production costs, high molecular weights and limited constancy, and possession of essential disulfide bonds. In order to

prevail over these restrictions, recombinant binding fragments, i.e. fragment antigen-binding (Fab), antibody variable domain (Fv), single-chain variable fragment (scFv) or domains heavy chain (V_H, V_HH), of antibodies have been engineered (Crivianu-Gaita and Thompson, 2016). In another approach, smaller protein scaffolds with favorable biophysical features have been designed to create artificial families of Antigen Binding Proteins (AgBP), able to specifically bind to different target proteins while retaining the favorable features of the parent molecule. The elements of the family that specifically bind to the given target antigen, are often selected in vitro by display techniques: phage display, ribosome display, yeast display or mRNA display. The artificial binding proteins are much smaller than antibodies (generally less than 100 amino-acid residues), show a strong constancy, lacking of disulfide bonds and can be expressed in high yield in decreasing cellular environments such as the bacterial cytoplasm, contrary to antibodies and their derivatives (Škrlec *et al.*, 2015; Jost and Plückthun, 2014). Accordingly, they are particularly appropriate in the manufacture of biosensors (Miranda *et al.*, 2011).

2.2.1.3 Enzymatic Interactions

The specific binding abilities and catalytic activity of enzymes make them popular bioreceptors. The analyte recognition could be enabled through several possible mechanisms:

a. The change of the analyte into the product by the enzyme is sensor-detectable,
b. Detection of the enzyme inhibition or activation by the analyte.
c. Monitoring the changes in the enzyme features caused by interaction with the analyte.

The ability to catalyze a large number of reactions, potential to detect a group of analytes (substrates, products, inhibitors, and modulators of the catalytic activity), as well

as the suitability with several different transduction methods for detecting the analyte are the main reasons for the common use of enzymes in biosensors. It should be noted that biosensors can be utilized incessantly in view of the fact that enzymes are not consumed in reactions. Besides, the catalytic activity of enzymes also allows lower limits of detection compared to common binding techniques. Nonetheless, the lifetime of the sensor is limited by the constancy of the enzyme (Marazuela and Moreno-Bondi, 2002).

2.2.1.4 Affinity Binding Receptors

Antibodies exhibit a high binding constant more than 10^8 L mol^{-1}, which is a symbol of a nearly irreversible association once the antigen-antibody couple has developed. For particular analyte molecules such as glucose, the affinity binding proteins bind with the ligand with a high specificity like an antibody, but with a much smaller binding constant in the order of 10^2 to 10^4 L mol^{-1}. The relationship between the analyte and the receptor is reversible in nature. For example, in the case of glucose, *concanavalin A* may operate as an affinity receptor with a binding constant of 4×10^2 L mol^{-1} (Schultz *et al.*, 1982). The application of affinity binding receptors for biosensing goals has been proposed in 1979 (Schultz and Sims, 1979), and was then configured into a fluorescent assay for measuring glucose in the relevant physiological range between 4.4 and 6.1 mmol L^{-1} (Ballerstadt and Schultz, 2000). In this case, the sensor does not consume the analyte in a chemical reaction in enzymatic assays.

2.2.1.5 Nucleic Acid Interactions

Biosensors that utilize nucleic acid interactions can be noted as genosensors, where the detection process is on the basis of the principle of complementary base pairing, adenine: thymine, and cytosine: guanine in DNA. If the target nucleic acid sequence is known, complementary sequences can be prepared, tagged, and immobilized on the sensor. The hybridization probes can then base pair with the target sequences, creating an

optical signal. The preferential transduction principle engaged in this kind of sense has always been optical detection (Marazuela and Moreno-Bondi, 2002).

2.2.1.6 Epigenetics

It has been found that appropriately optimized integrated optical resonators can be exploited for identifying epigenetic modifications, e.g. DNA methylation, histone post-translational modifications, in body fluids from patients influenced by cancer or other diseases (Donzella and Crea, 2011). Nowadays, photonic biosensors with ultra-sensitivity are being expanded to detect cancerous cells within the patient's urine (Vollmer and Yang, 2012). Many efforts have been made to develop new portable devices that use cheap, environmentally friendly, disposable cartridges that need only simple handling with no need for further processing, washing, or manipulation by expert technicians (http://www.glam-project.eu/).

2.2.1.7 Organelles

Organelles create separate compartments in cells and perform biological function autonomously. Various types of organelles have different metabolic pathways and possess enzymes to fulfill its operation. Frequently used organelles are lysosome, chloroplast, and mitochondria. The spatial-temporal distribution pattern of calcium is closely related to the ubiquitous signaling pathway. Mitochondria actively participate in the metabolism of calcium ions to control the function and also modulate the calcium-related signaling pathways. The experimental outcomes have shown that mitochondria have the ability to respond to high calcium concentration generated in the proximity by opening the calcium channel (Rizzuto *et al.*, 1999). Therefore, mitochondria can be utilized to diagnose the calcium concentration in medium and the detection is very sensitive owing to the high spatial resolution. In addition, mitochondria can be used for

the detection of water pollution. The detergent compounds' toxicity damages the cell and subcellular configuration including the mitochondria. The detergents will cause a swelling effect which could be measured by an absorbance change. The experimental data illustrates that the alteration rate is proportional to the detergent concentration, supplying a high standard for detection accuracy (Bragadin *et al.*, 2001).

2.2.1.8 Cells

Cells are frequently utilized in bioreceptors as they are sensitive to the surrounding environment and can respond to all types of stimulants. Cells have a tendency to absorb onto the surface and immobilized. They remain active for a longer time and their reproduction capability has made them reusable compared to organelles. They are commonly utilized to diagnose global parameters, such as stress condition, toxicity, and organic derivatives. This type of bioreceptors can also be utilized to monitor the therapeutic effect of drugs. One application is to employ cells to determine herbicides, which are the main aquatic pollutants (Védrine *et al.*, 2003). Microalgae are entrapped on a quartz microfiber and the chlorophyll fluorescence modified by herbicides is collected at the tip of an optical fiber bundle and transmitted to a fluorimeter. The algae are incessantly cultured to acquire optimized measurement. Results indicate that the discernment limit of specific herbicide can reach sub-ppb concentration levels. In addition, some cells can be utilized to monitor microbial corrosion (Dubey and Upadhyay, 2001). *Pseudomonas sp*. as isolated from the corroded material surface can be immobilized onto acetylcellulose membrane. The respiration activity is specified by measuring oxygen consumption. There is a linear relationship between the current generated and the concentration of sulfuric acid. The response time depends on the loading of cells and surrounding environments and can be regulated to no more than 5 min.

2.2.1.9 Tissues

Tissues are utilized as biosensors due to the abundance of enzymes. The advantages of using tissues as sensors are as follows (Campàs *et al.*, 2008):

a. Easier immobilization compared to cells and organelles.
b. Higher activity and constancy from maintain enzymes in the natural environment.
c. Accessibility and lower price.
d. Avoid the tedious work of extraction, centrifuge, and purification of enzymes.
e. Necessary cofactors for enzyme function
f. The broad range of choices concerning various objectives.

However, there are also some drawbacks of tissues, such as the lack of specificity due to the interference of other enzymes, as well as longer response time attributed to the transport barrier.

2.2.2 Biotransducer

As shown in Figure 2.1, biosensors can be categorized by their type of biotransducer. The most common types of transducer in biosensors are electrochemical, optical, electronic, piezoelectric, gravimetric, and pyroelectric biosensors.

2.2.2.1 Electrochemical Biosensors

Electrochemical biosensors are usually based on enzymatic catalysis of a reaction that releases or consumes electrons (Figure 2.2). In fact, this kind of sensor targets the biological reactions that derived from redox reactions. This will initiate the charge transfer across the double layer of the physiochemical transducer that produces a

measurable signal (Sethi and Lowe, 1990; Thévenot et al., 2001). Such enzymes are truly named redox enzymes. The sensor substrate commonly includes three electrodes; a reference electrode, a working electrode, and a counter electrode. The target analyte is involved in the reaction that occurs on the active electrode surface, and the reaction may lead to either electron transfer across the double layer (producing a current) or induces the double layer potential (producing a voltage). It can either measure the current at a fixed potential, where the rate of electron flow is proportional to the analyte concentration, or the potential can be measured at zero current, which causes a logarithmic response. It should be noted that the potential of the working or active electrode is space charge sensitive and this is frequently used. Moreover, the label-free and direct electrical diagnosis of small peptides and proteins are possible by their inherent charges using biofunctionalized ion-sensitive field-effect transistors (Lud et al., 2006).

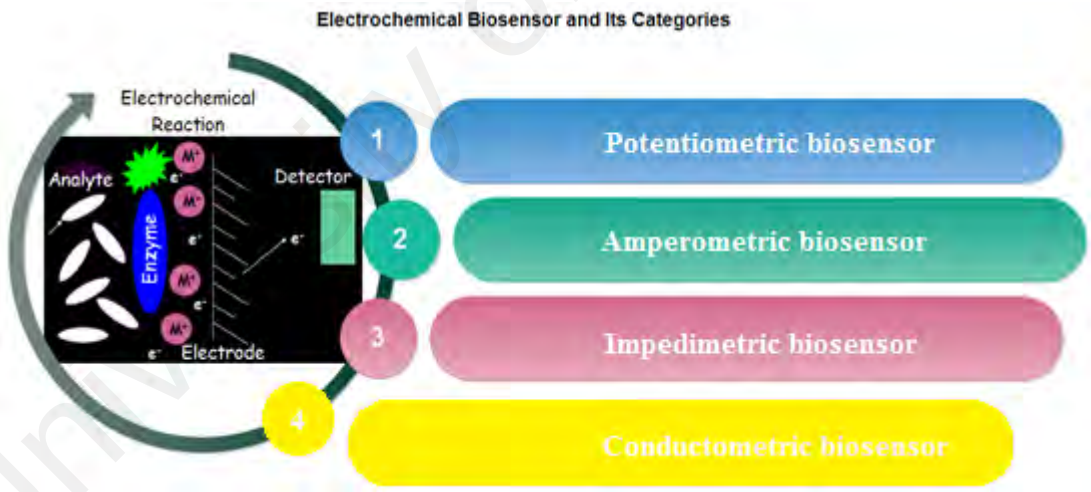

Figure 2.2: Schematic structure of an electrochemical biosensor and its categories.

Another example is the potentiometric biosensor, (potential produced at zero current) which causes a logarithmic response with a high dynamic range. Such biosensors are frequently fabricated by screen printing the electrode patterns on a plastic substrate, covered with a conducting polymer followed by protein (enzyme or antibody) immobilization. In these cases, there are only two electrodes which are sorely sensitive

and robust. They are able to detect analytes at levels previously attainable by only HPLC and LC/MS techniques, without rigorous specimen preparation. It is important to note that all biosensors commonly include minimal sample preparation, as the biological sensing component is highly selective for the analyte concerned. The signal is produced by electrochemical and physical changes in the conducting polymer layer as a result of changes taking place at the surface of the sensor. Such alterations can be ascribed to ionic strength, pH, hydration, and redox reactions, where the latter is due to the enzyme label turning over a substrate. Field effect transistors, wherein the gate region has been modified with an enzyme or antibody, can also detect very low concentrations of a variety of analytes. The binding of the analyte to the gate region of the FET which produces an alteration in the drain-source current. Based on the measured signal characterizations, the electrochemical biosensor has three main classifications of silicon-based chips as shown in Figure 2.2.

Potentiometric biosensor: The principle of this biosensor is based on the ion-selective field-effect transistor (ISFET). The output signal is created by the potential differences of the oxidation and reduction reactions. The electrochemical reaction generates ions that are accumulated at the ion-sensitive membrane of the ISFET interface. As this potential is applied to the electrode, it modulates the current flow through the FET which produces a measurable potential of the detector (Zhou *et al.*, 2012).

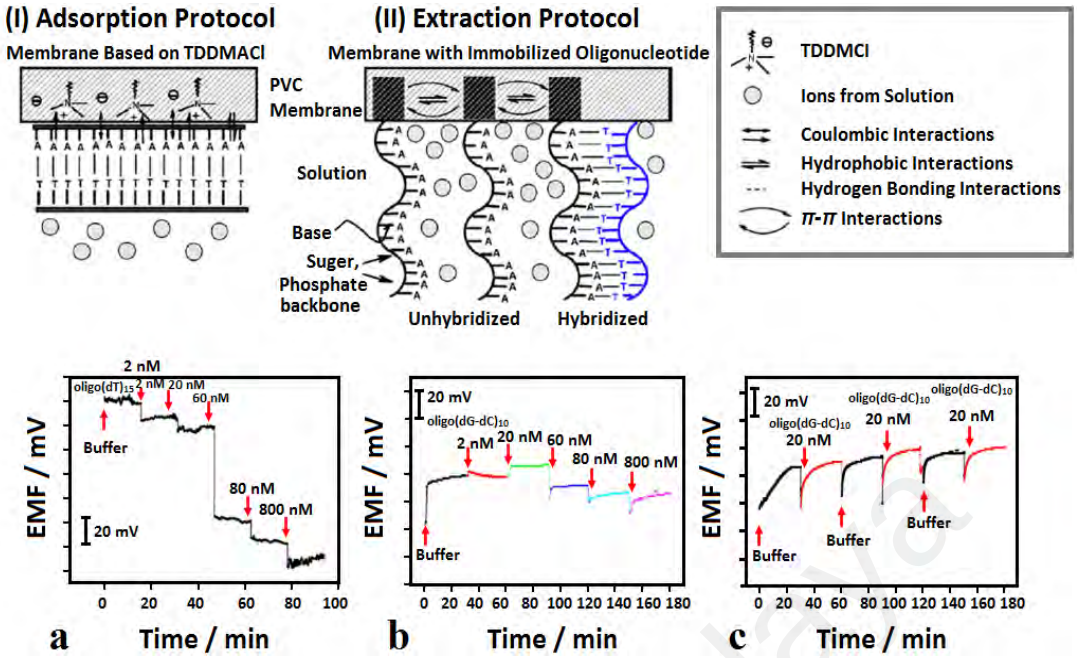

Figure 2.3: Schematic view and performance outputs of a potentiometric sensor for the diagnosis of hybridization between complementary single-stranded (ss) oligonucleotides on the phase boundary PVC membrane/solution. Hereon, two arrangements of the probe have been demonstrated, where the ss oligonucleotides are attached along (I) or parallel (II) to the PVC membrane surface. The potentiometric diagnosis of the hybridization with complementary strands is illustrated: (a) with complementary and unspecific interactions with non-complementary oligonucleotides; (b) with complementary oligonucleotides; (c) presentation of the reproducibility after restoration in a buffer of 0.01 M NaOH for 15 min (upward arrow) and succeeding injections of the corresponding oligonucleotides (downward arrow) (Shishkanova *et al.*, 2007).

An outstanding example of a potentiometric biosensor is shown in Figure 2.3. The diagnosis principle counted on the hybridization process of single-stranded oligonucleotides adjacent to a PVC membrane, which initiates an assessable redistribution of the ion concentration within intermolecular regions (Shishkanova *et al.*, 2007).

Amperometric Biosensor: The high sensitivity of this sensor supplies the sensing ability to diagnose electroactive substances in biological specimens. By applying a steady potential between the sensing and auxiliary electrode, the exchange of electroactive species occurs at the electrode, which produces electron transfer, and the current is directly correlated to the bulk concentration of tested electroactive species (Sethi and Lowe, 1990; Thévenot *et al.*, 2001).

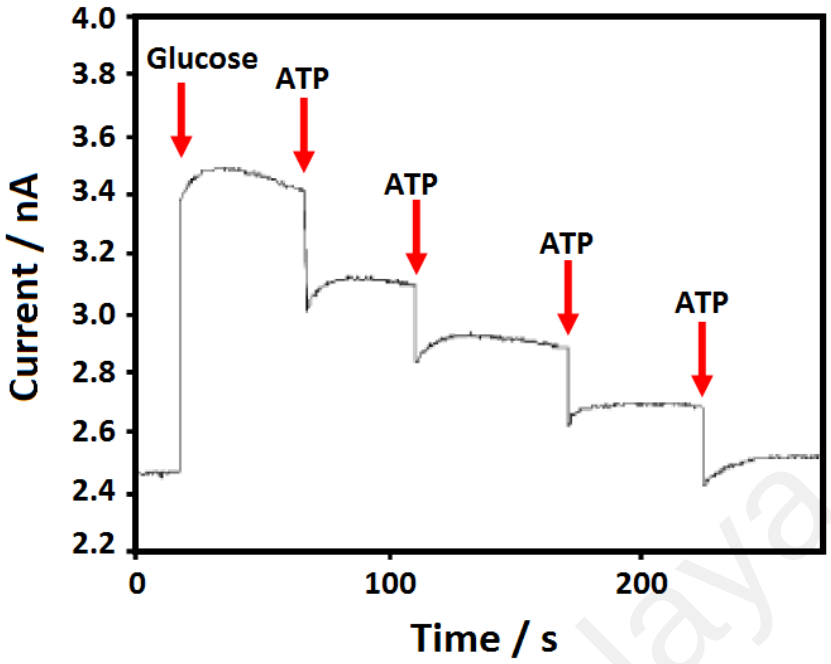

Figure 2.4: An illustration curve for amperometric measurement: this is a generic hydrodynamic response of the electroactive biosensor to glucose followed by several injections of ATP measured in phosphate buffer at 650 mV in reference to Ag/AgCl. As glucose is consumed at the glucose oxidase (GOD) and hexokinase (HEX) modified electrode surface, the alteration in the current response is proportional to the ATP concentration (Kueng *et al.*, 2004).

Kueng *et al.* (Kueng *et al.*, 2004) prepared a biosensing technique using an amperometric approach for the diagnosis of adenosine-5'-triphosphate (ATP) at physiological pH values with a recognition limit of 10 nmol/l. Firstly, they co-immobilized glucose oxidase and hexokinase (HEX) at the electrode surfaces. Glucose was consumed by the enzymatic reaction catalyzed by HEX upon introducing the electrode into a system comprising ATP, which caused a reduction in signal in proportion to the ATP concentration. Figure 2.4 shows an illustration curve for their amperometric measurements.

Impedimetric Biosensor: The chemical reactions causing either ion production or consumption will alter the conductivity of the solution. The solution impedance (Z) alteration is the basis of detection for this kind of sensor. The sensitivity of an impedimetric sensor is relatively low in view of the fact that the measure of conductance

is essentially non-specific. This problem can be overcome by targeting the specifically defined geometry of enzymatic reactions in a microelectronic cell (Sethi and Lowe, 1990).

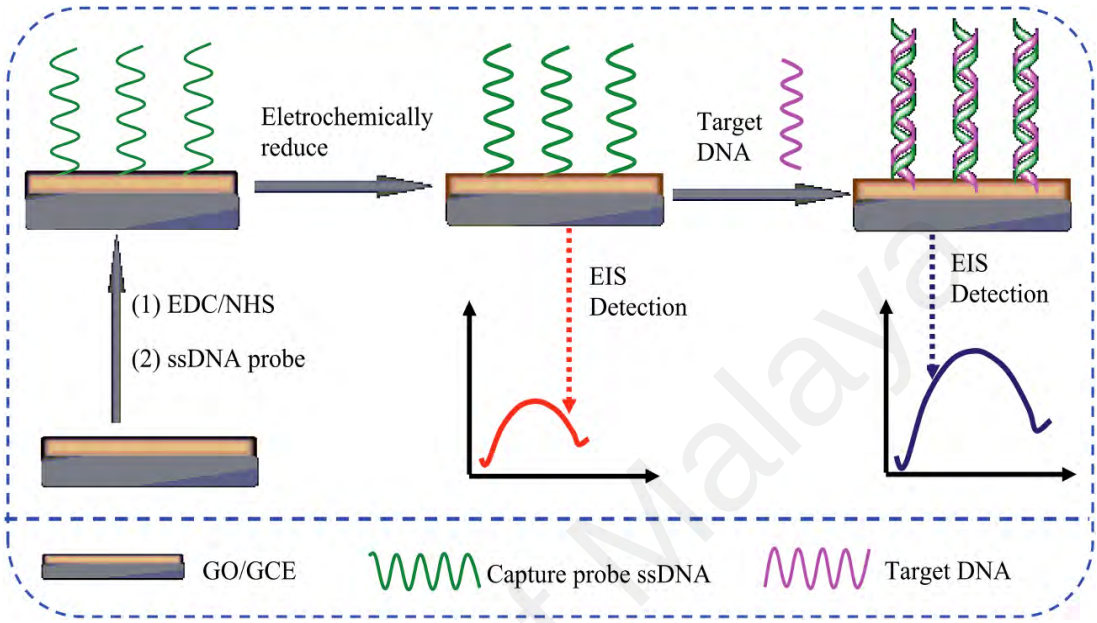

Figure 2.5: Schematic illustration of the preparation of the impedimetric DNA biosensor and the diagnosis of target DNA (Gong *et al.*, 2015).

Figure 2.5 shows a schematic illustration of the DNA biosensor with the preparation stages and its performance. As can be seen, this biosensor is designed by covalently immobilizing an amino-modified ssDNA probe onto the GO-modified glassy carbon (GC) electrode surface and investigating the electrochemical reduction on the GO/GC electrode. In this case, the electrochemical reduction of GO as the electronic transducer on the DNA biosensor effectively hastened the transfer of electron and increased the EIS response of the DNA biosensor (Gong *et al.*, 2015).

2.2.2.2 Ion Channel Switch Biosensors (ICSBs)

It was shown that the utilization of ion channels offers a highly sensitive diagnosis of target biological molecules (Vockenroth *et al.*, 2005). By embedding the ion channels in supported or tethered bilayer membranes (t-BLM) attached to a gold electrode, an

electrical circuit can be generated. The capture molecules, for instance, antibodies, can be bound to the ion channel, with the intention that the binding of the target molecule governs the ion flow through the channel. This gives rise to an assessable alteration in the electrical conduction, which is proportional to the concentration of the target molecule.

The ICSBs can be generated using gramicidin, a dimeric peptide channel, in a tethered bilayer membrane (Cornell *et al.*, 1997). One peptide of gramicidin, with the attached antibody, is mobile while the other is fixed. The breaking of the dimer discontinues the ionic current through the membrane, where the level of the electrical signal change is significantly increased by separating the membrane from the metal surface using a hydrophilic spacer. In addition, a quantitative diagnosis of a wide group of target species, i.e. bacteria, drugs, proteins, and toxins has been verified using various membrane and capture configurations (Cornell *et al.*, 2008; Krishnamurthy *et al.*, 2010).

2.2.2.3 Reagent-less Fluorescent Biosensors (RFBs)

This type of biosensors can monitor a target analyte in a complex biological mixture without additional reagent. Thus, it can operate incessantly if immobilized on solid support. A fluorescent biosensor reacts to the interaction with the target analyte by an alteration of its fluorescence features. The RFB can be fabricated by integrating a biological receptor, which is directed against the target analyte, and a solvatochromic fluorophore, whose emission features are sensitive to the nature of the local environment, in a single macromolecule. The fluorophore transduces the detection event into a measurable optical signal. The use of extrinsic fluorophores, whose emission features differ broadly from the intrinsic fluorophores of proteins, tryptophan, and tyrosine, enables one to instantaneously diagnose and measure the analyte in complex biological mixtures. The integration of the fluorophore must be performed in a site where it is sensitive to the binding of the analyte without perturbing the affinity of the receptor.

Antibodies and artificial families of AgBP are well suited to supply the diagnosis module of RF biosensors given that they can be directed against any antigen. A general approach to integrate a solvatochromic fluorophore in an AgBP when the atomic structure of the complex with its antigen is known, and thus transform it into an RF biosensor, has been described (Brient-Litzler *et al.*, 2010). A residue of the AgBP is identified in the vicinity of the antigen in their complex. This residue is changed into cysteine by site-directed mutagenesis. The fluorophore is chemically attached to the mutant cysteine. As the design is successful, the coupled fluorophore does not avoid the binding of the antigen, this binding protects the fluorophore from the solvent, and it can be diagnosed by an alteration of fluorescence. This approach is also valid for antibody fragments (Renard *et al.*, 2002; Renard and Bedouelle, 2004). Nevertheless, in the absence of certain structural data, other approaches must be employed. Antibodies and artificial families of AgBPs are constituted by a set of hypervariable (or randomized) residue positions, positioned in a unique sub-region of the protein, and supported by a constant polypeptide scaffold. The remains that create the binding site for a given antigen, are chosen among the hypervariable residues. It is possible to change any AgBP of these families into an RF biosensor, specific to the target antigen, simply by coupling a solvatochromic fluorophore to one of the hypervariable residues that have little or no importance for the interaction with the antigen, after changing this residue into cysteine by mutagenesis. More specifically, the approach consists in individually changing the residues of the hypervariable positions into cysteine at the genetic level, by the chemical coupling a solvatochromic fluorophore with the mutant cysteine, and then in keeping the resulting conjugates that have the highest sensitivity (a parameter that involves both affinity and variation of the fluorescence signal) (Miranda *et al.*, 2011). This approach is also valid for families of antibody fragments (Renard *et al.*, 2003).

Previous studies have shown that the best RFBs are achieved as the fluorophore does not produce non-covalent interactions with the surface of the bioreceptor when it interacts with a binding pocket at the surface of the target antigen (de Picciotto *et al.*, 2016). These biosensors that are designed by the above approaches, can operate and diagnose target analytes inside living cells (Kummer *et al.*, 2013).

2.2.2.4 Others Biosensors

Piezoelectric sensors use crystals that undergo an elastic deformation as an electrical potential is applied to them. An alternating potential (A.C.) makes a standing wave in the crystal at a characteristic frequency, which is highly dependent on the elastic features of the crystal, such that if a crystal is coated with a biological detection element, the binding of a (large) target analyte to a receptor will create an alteration in the resonance frequency, which provides a binding signal. In a mode that uses surface acoustic waves (SAW), the sensitivity is greatly increased. This is a particular application of the Quartz crystal microbalance as a biosensor. It should be mentioned that thermometric and magnetic-based biosensors are less in the spotlight.

2.2.3 Electronic System

As mentioned above, the transducer signal is transformed to an electronic signal and amplified by a detector circuit using a suitable reference and sent for processing by computer software to be converted to a meaningful physical parameter describing the process being investigated; finally, the resulting quantity has to be presented through an interface to the human operator (Grieshaber *et al.*, 2008).

2.3 Deployment of Biosensors

The proper deployment of biosensors counts on their field of operation, which may generally be divided into biotechnology, agriculture, food technology, and biomedicine. In the field of biotechnology, the examination of the chemical composition of cultivation broth can be done in-line, on-line, at-line, and off-line. As outlined by the US Food and Drug Administration (FDA), the specimen is not removed from the process stream for in-line sensors, while it is diverted from the manufacturing process for on-line measurements. In the case of at-line sensors, the specimen may be removed and assessed in close proximity to the process stream (US Department of Health and Human Services). An example of the latter is the monitoring of lactose in a diary processing plant. Besides, off-line biosensors are mainly utilized in agriculture, food technology, and biomedicine.

In medical applications, biosensors are commonly classified as *in vitro* and *in vivo* systems. An *in vitro* biosensor assessment occurs in a test tube, a culture dish, a microtiter plate, or elsewhere outside a living organism. In this case, the sensor uses a bioreceptor and transducer as described above. An enzyme-conductimetric biosensor is an example of an *in vitro* biosensor, which can be used for the monitoring of blood glucose. However, there are some challenges to fabricate biosensors that function by the principle of point-of-care testing (POCT), i.e. at the location where the test is required (Kling, 2006). This point is very important because the deletion of lab testing can save time and money. An application of a POCT biosensor is required for the detection of the HIV virus in areas difficult to be tested. In this approach, the biosensor can be utilized in the desired position for a quick and effortless assessment. On the other hand, an *in vivo* biosensor is an implantable device that functions inside the body. Of course, biosensor implants are required to satisfy the strict regulations on sterilization to prevent an initial

inflammatory response after implantation. Other worries are connected with the long-period biocompatibility, i.e. the innocuous interaction with the body environment during the intended period of use and failure (Kotanen *et al.*, 2012). The device should be detached and substituted if there is a failure which could result in additional surgery. Insulin monitoring in the body is an example of an *in vivo* biosensor, which is not mass-produced. The most advanced biosensor implants have been expanded for the incessant monitoring of glucose (Gough *et al.*, 2010; Mortellaro and DeHennis; 2014). Currently, biosensors are being joined into mobile phone systems, making them user-friendly and available to a large number of users (Quesada-González and Merkoçi, 2017).

2.4 Application of Biosensors

Biosensors can have various industrial, biomedical, and military applications as illustrated in Figure 2.6. One of the main uses is the monitoring of blood glucose due to its abundant market potential. Nevertheless, biosensors have the marvelous potential for commercialization in other fields of application as well. Despite this potential, commercial implementation is slow due to some technological constraints. For instance, biosensor contamination is one of the main issues owing to the presence of biomolecules along with the semiconductor (Mishra *et al.*, 2012). The following presents a range of biosensor applications in various fields.

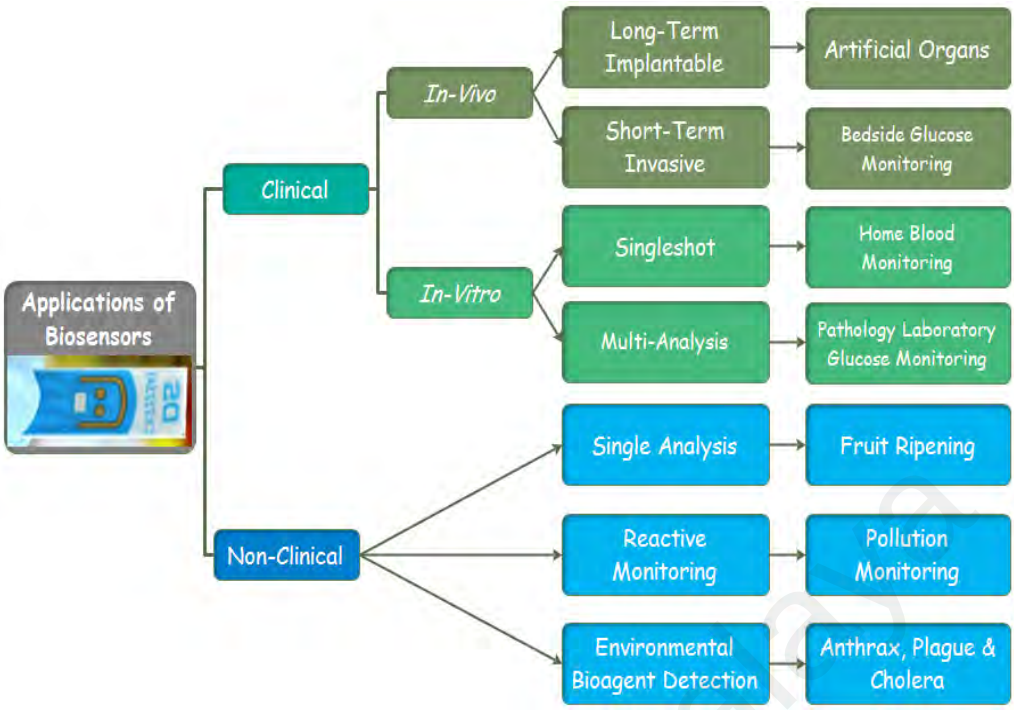

Figure 2.6: Classifications of biosensors based on potential applications.

2.4.1 In Food Processing and Safety

A difficult problem in food processing industry is the quality and safety, maintenance of food products and processing. Traditional techniques of chemical testing and spectroscopy have disadvantages of possible of human error, time consuming and expensive. The alternatives for food authentication and monitoring with the objective and consistent measurement of food products, in a cost effective approach, are favorable for the food industry. Therefore, the development of biosensors for effortless, real-time, adoptive and economical techniques are useful (Scognamiglio *et al.*, 2014). In this regard, the monitoring of ageing of beer using enzymatic biosensors on the basis of cobalt phthalocyanine was investigated, where these biosensors showed a good ability to monitor the ageing of beer during storage (Ghasemi-Varnamkhasti *et al.*, 2012). Biosensors are frequently used to diagnose pathogens in food. The presence of *Escherichia coli* in vegetables, is a bioindicator of faecal contamination in food (Arora *et*

al., 2011; Ercole *et al.*, 2003). *E. coli* has been measured by diagnosing alteration in pH, attributable to ammonia using potentiometric alternating biosensing systems. Enzymatic biosensors are also used in the dairy industry. A biosensor, on the foundation of a screen-printed carbon electrode, was integrated into a flow cell, where enzymes were immobilized on electrodes by engulfment in a photocrosslinkable polymer. The automated flow-based biosensor could measure three types of organophosphate pesticide contamination in milk (Mishra *et al.*, 2012).

One of the common food additives, which broadly utilized today, are sweeteners. These additives are the main cause of some common diseases, such as type-2 diabetes, dental caries, cardiovascular diseases and obesity. These artificial sweeteners are addictive to humans who consume more high-energy food instinctively, unintentionally causing weight gain. Hence, their diagnosis and quantification are of prime importance. Traditional approaches to differentiate the two kinds of sweeteners are ion chromatography, which are complex and arduous. A more effective approach, which combined lipid films with electrochemical techniques as biosensors for speedy and sensitive screening of sweeteners, has been investigated by multi-channel biosensor, which diagnose the electrophysiological activities of the taste epithelium. The signals are scrutinized using spatiotemporal techniques, on MATLAB, where glucose and sucrose depict natural sugars while saccharin and cyclamate include artificial sweeteners. Given that all sweeteners are mediated by heterodimeric G-protein coupled receptors in Type-II cells in the bud, they possess a plurality of binding sites to detect sweet stimuli of different structures respectively. Studies show two kinds of sweet stimuli: cyclic adenosine monophosphate pathway as well as inositol triphosphate and diacylglycerol pathway. The reaction to artificial sweeteners depends on the amino terminal domains of taste receptors as ligand binding sites. The signal responses of taste receptor cells towards natural and artificial sweeteners are discrete. The taste epithelium biosensor liberates sparse signals

with positive waveforms as glucose was consumed, while sucrose retained signals with negative spikes. The taste epithelium responds to artificial sweeteners with more intensive signals response to artificial sweeteners are wholly different from those of natural sugars, in terms of time and frequency domains (Mehrotra, 2016).

2.4.2 In Fermentation Industries

In the fermentation process, the quality of product and safety are necessary. Therefore, efficient monitoring of the fermentation process is very important to develop, optimize and sustain biological reactors at maximum efficiency. Biosensors accurately control the fermentation process and provide reproducible outcomes because of their simple instrumentation, impressive selectivity, low prices and effortless automation. Currently, numerous types of commercial biosensors are available, which are able to detect biochemical parameters such as glucose, lactate, lysine, ethanol etc.. They are broadly employed in China, around 90% of the market share. In general, saccharification can be monitored by traditional Fehling's method in the fermentation process. In view of the fact that this method includes titration of reducing sugar, its outcomes were imprecise. Nowadays, factories productively utilize glucose biosensors to control production of the saccharification and fermentation workshop and use the bioenzymatic method to produce glucose. In addition, biosensors can be used in ion exchange retrieval, where diagnosis of alteration of biochemical composition is executed. In the fermentation process, the on-line monitoring of critical metabolites is essential to facilitate quick optimization and to control biological processes (Mehrotra, 2016; Yan *et al.*, 2014).

2.4.3 In Medical Areas

During the last decade, the applications of biosensors have quickly grown in various medical fields. For instance, glucose biosensors are extensively utilized in clinical applications for detection of diabetes mellitus, which necessitates accurate control over

blood-glucose levels (Scognamiglio *et al.*, 2010). Domestic blood-glucose biosensors usage accounts for 85% of the world market (Rea *et al.*, 2009). Biosensors are widely used in the medical field for the detection of infectious diseases. An encouraging biosensor technology for urinary tract infection (UTI) detection in the direction of pathogen recognition and anti-microbial susceptibility is under investigation. Detecting end-stage heart failure patients, apt to adverse outcomes during the early phase of left ventricular assisted device implantation, is vital. A hafnium oxide (HfO_2)-based biosensor has been utilized for early stage diagnosis of human interleukin (IL)-10 (Lee *et al.*, 2012). Besides, HfO_2 biosensor has been functionalized for antibody deposition with recognition of a human antigen by electrochemical impedance spectroscopy. Apart from these, heart failure is one of the biggest dilemma that humanity is facing today. There are different approaches for diagnosis of cardiovascular diseases such as immunoaffinity column assay, fluorometric, and enzyme-linked immunosor-bent assay (Ooi *et al.*, 2006; Caruso *et al.*, 2010; Caruso *et al.*, 2012; Watson *et al.*, 2011; Maurer *et al.*, 2010). However, these are arduous, necessitate qualified personnel and are time consuming. Biosensors based on electrical measurements use biochemical molecular identification for desired selectivity with a particular biomarker of interest. Other uses in this area include: quantitative assessment of cardiac markers in undiluted serum, immunosensor array for clinical immunophenotyping of acute leukemias, microfluidic impedance testing for controlling endothelin-induced cardiac hypertrophy, effect of oxazaborolidines on immobilized fructosyltransferase in dental diseases; histone deacylase (HDAC) inhibitor assay from resonance energy transfer, biochip for a rapid and precise diagnosis of multiple cancer markers as well as neurochemical recognition by diamond microneedle electrodes (Mehrotra, 2016).

On the other hand, fluorescent biosensors as imaging agents can be utilized in cancer and drug discovery. They have allowed insights into the role and control of enzymes at

cellular level. This type of biosensors are small scaffolds onto which one or several fluorescent probes are mounted through a receptor. The receptor diagnoses a certain analyte or target, thereby transducing a fluorescent signal which can be identified and measured (Wang *et al.*, 2009; Morris, 2010). They can also explore ions, metabolites and protein biomarkers with great sensitivity and are able to report the presence, activity or status of the target (serum, cell extracts) in the complex solution. According to these specifications, they are used in inquiring gene expression, protein localization, and conformation in fields, such as signal transduction, transcription, cell cycle and apoptosis. Furthermore, indication of arthritis, inflammatory diseases, cardiovascular and neurodegenerative diseases, viral infection, cancer and metastasis can be done using these biosensors.

2.4.4 Military Purposes

In addition to above mentioned applications, biosensors can be also utilized in military purposes at times of biological attacks. The main motivation of such biosensors is to sensitively and selectively detect organisms posing threat in real time called biowarfare agents (BWAs) namely, bacteria (vegetative and spores), toxins and viruses. Many efforts have been made to use such a bio-sensing device using molecular techniques, which are capable of identify the chemical markers of BWAs. Seeing that nucleic acid-based sensing systems give gene-based specificity, they are more sensitive than antibody-based detection methods, without amplification steps to achieve detection sensitivity. The human papilloma virus HPV (double stranded DNA virus) has been classified into two types: HPV 16 and 18; and refers to invasive cervical cancer. HPVs can be quickly diagnosed using a leaky surface acoustic wave peptide nucleic acid biosensor with double two-port resonators, where this probe directly identifies the HPV genomic DNA without polymerase chain reaction amplification, and can also bind to the target DNA sequences with high efficiency and accuracy (Mehrotra, 2016).

2.4.5 Metabolic Approaches

Environmental concerns and shortage of sustainability of petroleum-derived products have steadily increased the development of microbial cell factories for the preparation of chemicals. Researchers find metabolic engineering as a powerful technology for a sustainable bioeconomy (Woolston and Edgar, 2013). They also predicted that a considerable fraction of fuels, chemicals and pharmaceuticals will be synthesized from renewable feedstocks by exploiting microorganisms rather than based on petroleum refining or extraction from plants. The high capacity for a variety of generation also necessitates efficient screening approaches to choose the individuals carrying the desired phenotype. The former approaches were spectroscopy-based enzymatic assay analytics, although had restricted throughput. To evade this hindrance, genetically encoded biosensors that make possible the *in vivo* monitoring of cellular metabolism were developed which presented potential for high-throughput screening using fluorescence-activated cell sorting (FACS) and selection using cell survival.

Förster resonance energy transfer (FRET) sensors includes a pair of donor and acceptor fluorophores, and a ligand-binding peptide sandwiched between the two. As it was bound by a ligand of interest, the peptide underwent a conformational alteration, thereby a FRET change (Peroza *et al.*, 2015; Mohsin and Ahmad, 2014). Although they showed high orthogonality, temporal resolution, and ease of construction, FRET sensors are only capable of report the abundance of the target metabolites and are incapable of exert downstream regulation to the signal (Bermejo *et al.*, 2011).

Moreover, transcription factors (TFs) are natural sensory proteins developed to regulate gene expression in reaction to alterations in environment for high throughput

screening (Zhang *et al.*, 2015). It is accomplished by hacking into host transcription system and employing a synthetic condition specific promoter to drive the expression of a reporter gene. These exhibit poor orthogonality and background noise (Becker *et al.*, 2015; Lefrançois *et al.*, 2009). Another category of biosensors involves riboswitches; the regulatory scope of an mRNA that can selectively bind to a ligand and thus alters its own structure, accordingly regulating transcription of its encoded protein. As compared to TFs, they are faster as the RNA has already been transcribed. Besides, ribosomes do not count on protein–protein or protein–metabolite interactions and so they have been widely engineered in bacterial systems in the recent decades (Berens and Suess, 2015; Groher and Suess, 2014).

2.4.6 Plant Biology

Recent developments in the fields of DNA sequencing and molecular imaging, have led to tremendous breakthroughs in plant science. Traditional approaches of mass spectroscopy for gauging insights into cellular and subcellular localization, and detection of ion and metabolite levels had extraordinary accuracy but lacked the important information regarding location and dynamics of enzyme substrates, receptors and transporters. This information can be effortlessly successfully tapped by means of biosensors. To evaluate a dynamic process under physiological circumstances, must require device tactics to envisage the actual process, for example, the exchange of one metabolite into another or the triggering of signaling events. This apparition can be made by sensors which can respond to dynamic changes (Groher and Suess, 2014; Orij *et al.*, 2012; Jones et al., 2013; Mehrotra, 2016).

Advances of nanomaterials in biosensors open up new opportunities for building up a new generation of biosensor technologies. Therefore, it seems that future research in this field is focused on investigating the interaction mechanism between nanomaterials and

biomolecules on the surface of nanostructured systems and using novel features to manufacture a new generation of biosensors.

2.5 Surface Architecture (Materials and Modifications)

Generally, the surface of electronic biosensors require to be conductive and dependent on the diagnosis approach. Numerous biosensors with some notable exceptions utilize labelling to measure the binding process, e.g., the binding of an additional antibody with a fluorescent label in the case of enzyme-linked immunosorbent assay (ELISA). In the case of electrochemical biosensors, the label is commonly an enzyme which catalyzes specified reactions in cases where the bound molecule in itself does not drastically change the charge transfer process across the electrode interface. Lastly, the electrons produced through the detection event or commonly the enzymatic label reaction with a substrate must be diagnosed as well. It should be noted that mediators can be utilized to transfer the electrons between the reaction site and the surface if the reaction occurs away from the interface of electrode (Grieshaber *et al.*, 2008).

Currently, a broad range of different materials is employed for the preparation of surfaces for biosensing approaches where they require to meet special necessities such as transparency for optical devices and electrical conductivity for electrochemical approaches. Due to the promising features, especially their optical properties, glass and other oxides are the most commonly used surfaces (Wang *et al.*, 2005). Glassy carbon, gold, microporous gold, graphite and indium tin oxide (ITO) are also widely used (Tilke *et al.*, 2003; Khanal *et al.*, 2007; Elfstrom *et al.*, 2007). In addition, conducting polymers, such as polyaniline, polypyrrole and polystyrene are another group of materials that can be utilized for the fabrication of electrochemical biosensors. The polymers are normally adsorbed to gold surfaces, which results in surfaces with good constancy, superb redox recyclability and easy handling (Wang *et al.*, 2005; Chaubey and Malhotra, 2002; Foley

et al., 1999). Besides, gold and other metallic surfaces are coated with self-assembled monolayers (SAMs) of sulfides (thiols) and disulfides. In electrochemical approaches, it is necessary that the SAM allows electron or analyte diffusion (Landauer, 1989). On the other hand, carbon nanotube (CNT)-modified electrodes have benefits of high surface area, good chemical stability, mechanical strength, as well as outstanding electrical conductivity. They are particularly noteworthy as the enzymes can be entrapped in the inner cavity (Agarwal and Sen, 2006; Das and Green, 2003).

In a more distinctive approach, glassy carbon electrodes (GCEs) were tailored with gold nanocrystals followed by gold nanoparticles bounding via cysteamine, which ultimately causes high effectiveness of enzyme immobilization (Mena *et al.*, 2005). Additionally semiconductors, for example ZnO can be employed for the fabrication of nanorods, which commonly functionalizes with e.g. biotin (Yi *et al.*, 2005).

2.6 Biosensors for the Diagnosis of Hydrogen Peroxide

As described above, biosensor is a term utilized for numerous devices either employed to monitor living systems or incorporating biotic elements. Hereon, the main applications in the history of biosensors development are reviewed specifically for the detection of hydrogen peroxide (H_2O_2). The important areas of H_2O_2 application are industrial (pharmaceutical, food, clinical) and environmental analysis. Its application as an antibacterial agent added to milk, and the environmental requirement to prevent halogenated substances for disinfection aims, makes H_2O_2 an important substance in the food and beverage industry. This has raised widespread demands for setting protocols for H_2O_2 diagnosis contingent upon its application. Besides, it is one of the most important substrates of enzyme-catalyzed oxidation reactions. In addition to enzymatic reactions, hydrogen peroxide is by itself an important analyte. H_2O_2 plays a key role in natural oxidation processes as it is found in air, solids and water. In the case of photosystem II

(PS-II), H_2O_2 is an electron donor. This process is through the two-electron oxygen reduction to H_2O_2 by a variety of synthetic quinones that can react directly to the reducing part of photosystem II. For higher plants, this require treatment of the thylakoids in the chloroplast cell to attain H_2O_2 production and detection (Giannoudi *et al.*, 2006).

2.6.1 Hydrogen Peroxide as a Substrate & Analyte

H_2O_2 is one of the most important products/substrate of enzyme catalyzed oxidation reactions. The most common enzymes used in biosensors are oxidases, which catalyze the model oxidation reactions (Tang *et al.*, 2003):

$$Substrate\ S + O_2 \xrightarrow{Oxidase} Product\ P + H_2O_2 \tag{2.1}$$

The operation of enzyme is to selectively oxidize analyte via the reduction of O_2 to H_2O_2 (Vreeke *et al.*, 1992). Oxygen is the natural oxidizing electron acceptor that and is utilized to restore the enzyme throughout the reaction. From the diversity of enzymatic reactions that generate H_2O_2, the most important reaction is the oxidation of glucose catalyzed by glucose oxidase (GO_x) according to the Eq. (2.2).

$$\mathrm{Glucose + H_2O + O_2 \longrightarrow Gluconic\ Acid + H_2O_2} \tag{2.2}$$

This process is utilized broadly in the fabrication of glucose biosensors and assays. The production of H_2O_2 is identified electrochemically and is then related to the glucose concentration. Besides, H_2O_2 is by itself an important analyte. Under different circumstances, very low concentrations of H_2O_2 can be measured. In addition, H_2O_2 can be determined at a single cell level during oxidative stress in food specimens and it is utilized as a substrate in many immunoassays (Zhang and Wong, 1999; Price *et al.*, 1998; Lin *et al.*, 1998; Jianzhong *et al.*, 1994).

2.6.2 Electrochemical Diagnosis of Hydrogen Peroxide

Nanoelectroanalytical chemistry is a growing multidisciplinary field, which combines the unique properties of nanomaterials, e.g., optical, magnetic, electronic, mechanical and catalytic properties, with the electrochemical characterizations, e.g. low cost, rapid detection and high sensitivity, for the production of numerous application devices, such as fuel cells, supercapacitors, catalyst and sensor devices (Guo *et al.*, 2010). Among these applications, electrochemical biosensors have received remarkable attention because of several advantages like simplicity, low cost, high selectivity and sensitivity. On the other hand, H_2O_2 as a strong oxidizing agent and essential intermediate (Lane and Burgess, 2003), is effortlessly miscible with water and extensively utilized in light industry, electronic technology, medical hygiene, biomedical science and pharmaceutical engineering (Tian *et al.*, 2014). Therefore, the rapid, reliable and accurate determination of H_2O_2 is of highly importance in the fields of bioanalysis, food security and environmental protection (Liu *et al.*, 2014). Consequently, various types of H_2O_2 detection and measurement methods have been developed, such as fluorometry (Bortolozzi *et al.*, 2014), cell imaging (Chung *et al.*, 2011), spectrophotometry (Zaribafan *et al.*, 2014), and electrochemical analysis (Kong *et al.*, 2015). Among these methods, the electrochemical recognition technology is considered as the most promising approach due to its outstanding advantages including convenient operation, rapid response and high sensitivity (Tran *et al.*, 2016). The enzymatic and non-enzymatic H_2O_2 biosensors are the most frequently used electrochemical detection methods.

2.6.2.1 Enzymatic- Based Electrochemical Biosensors

Until now, extensive studies have been done on the enzymatic-based H_2O_2 biosensor, which possesses the benefits of high efficiency and good selectivity (Bai *et al.*, 2016). Horseradish peroxidase (HRP) and Catalase (CAT) are the two types of enzymes that are generally utilized for H_2O_2 recognition. Nevertheless, the immobilization and

stabilization protocol of the enzyme are complex, and thus it is arduous to attain the direct electron transfer on the bare electrode (Vilian *et al.*, 2014; Liu *et al.*, 2017). After that, the admirable support materials are expanded, which supply better environment for loading the enzyme proficiently and encourage direct electron transfer. Accordingly, polymer, metal nanoparticles and carbon-based nanomaterials have been produced and utilized in fabricating enzymatic-based H_2O_2 biosensors. In this regard, the introduction of nanomaterials can enhance the enzyme loading area, contact with more detectors, and improve the transfer rate of electrons. In fact, the nanomaterials, such as graphene, carbon nanotubes, Au nanoparticles, molybdenum disulfide, polyaniline and their hybrid nanostructures can effectively enhance the biosensor performance (Shu *et al.*, 2017; Hong *et al.*, 2013; Nandini *et al.*, 2014). Various enzymatic-based H_2O_2 biosensors are presented in Table 2.1. These biosensors commonly have superior detection limit (LOD) but low sensitivity and narrow linear range. Besides, the enzymatic-based biosensors suffer from environmental instability, high cost and complex immobilization process due to the intrinsic nature of enzymes.

Table 2.1 Various enzymatic-based H_2O_2 biosensors.

Type of Biosensor	LOD (nm)	Linear Range	Sensitivity	Reference
CAT/PLL/f-MWCNT/GCE*	8	1n-3.6μM	$0.39\mu A \cdot mM^{-1} \cdot cm^{-2}$	Vilian *et al.*, 2014
NF/CAT/MWCNTs-COOH/Cys- AuNPs[2]	0.5	1nM-1μM	-	Hong *et al.*, 2013
CAT/MoS_2-Au	100	0.5μ-0.2mM	$0.18\mu A \cdot mM^{-1} \cdot cm^{-2}$	Shu *et al.*, 2017
PANI/CAT/glutaraldehyde	2.18μM	5μ-0.1mM	-	Akyilmaz *et al.*, 2017
HRP/Graphene	0.026	80n-0.66μM	-	Liu *et al.*, 2017
HRP-Au-CPE	210	0.48-50μM	-	Liu *et al.*, 2002
HRP-Au thin-film gold	16μM	20-500μM	$12\mu A \cdot mM^{-1} \cdot cm^{-2}$	Koposova *et al.*, 2014

*Catalase (CAT), L-Lysine/multiwalled carbon nanotube (PLL/*f*-MWCNT), glassy carbon electrode (GCE), Nafion (NF), functionalized multi-walled carbon nanotubes (MWCNTs-

COOH), L-cysteine (Cys) modified AuNPs (Cys-AuNPs), polyaniline (PANI), horseradish peroxidase (HRP), gold-modified carbon paste electrode (Au-CPE).

2.6.2.2 Non-Enzymatic-Based Electrochemical Biosensors

Though enzyme-based biosensors might obtain higher sensitivity, many drawbacks hinder the universal applications of them. Firstly, the immobilization and stabilization protocol of the enzyme is very complicated. Secondly, the activity of oxidase can be easily affected by the temperature, pH value, humidity, toxic chemicals, and so on, which lead to poor stability and low reproducibility of enzymatic sensors. Thirdly, enzymes are expensive and thus lead to a high cost. Considering these respects, the developing of the non-enzymatic H_2O_2 sensor has become a highly desirable project. On the other hand, non-enzymatic electrochemical sensors are the industry standard for sensing applications because these sensors exhibit quite low detection limits, have enhanced response times, and are of much lower cost compared to the sensors based on other detection mechanisms. Among the non-enzymatic electrochemical detection approaches, two specific methods, named potentiometry and amperometry, have been used quite extensively. In potentiometric sensors, the potential difference between a reference electrode and a working electrode is measured at zero applied currents. The potential of the working electrode changes depending on the analyte concentration. It has been shown that these sensors can measure analyte concentrations of μM or higher. In amperometric sensors, a constant bias potential is applied and the resulting current, which scales linearly with analyte concentration, is measured. Amperometric sensors have been shown to possess almost similar analyte detection limits as their potentiometric counterparts, typically in the μM to M range. Thus, this approach provides an effectual platform for the diagnosis of H_2O_2 (Zhao *et al.*, 2009; Jiaojiao *et al.*, 2015; Xu *et al.*, 2013). The non-enzymatic biosensor is on the basis of the electrocatalytic reduction, wherein the reaction

occurs on the electrode surface. The electrochemical recognition on the electrode's needs requires a relatively high over-potential (Nguyen *et al.*, 2016; Kivrak *et al.*, 2015). Accordingly, some attempts have been made to minimize the over-potentials by employing nanomaterials. It has been found that the nanoelectronic medium can enhance the electron transfer rate and improve the capability of the anti-interference of the biosensor. Among various nanoscale materials, transition metal oxide, for example, MnO_2, CuO and Co_3O_4 have advantages of easy preparation, environmentally friendly and low cost, and also have the high electrocatalytic performance of H_2O_2 (Huang *et al.*, 2014; Wu *et al.*, 2017; Wang *et al.*, 2015). Nevertheless, its consistency and sensitivity are undesirable. In fact, although non-enzymatic biosensors can avoid the inherent shortcomings of enzymatic biosensors, particularly environmental factors such as temperature, oxygen, pH and coexisting chemicals; the kinetics and over potential of the electrochemical reaction are crucial factors that influence the Faradaic current and analytical performance (Wu *et al.*, 2014). Thus, these sensors depend on electrode modification.

So far, several attempts have been focused on electrode modification for the fabrication of new electrocatalytic materials to improve the kinetics of electron transfer. In this regard, noble metal catalysts, such as Au, Ag, Pd, and Pt have received wide recognition in non-enzymatic H_2O_2 biosensors (Wan *et al.*, 2012; Wang *et al.*, 2013; Mattarozzi *et al.*, 2016).

Table 2.2 A range of Ag nanomaterial-based non-enzymatic H_2O_2 biosensors.

Type of Biosensor	LOD(μm)	Linear Range (mM)	Sensitivity	Ref.
AgNPs/MWCNT/GCE*	0.5	0.05-17	1.42 $\mu A \cdot mM^{-1}$	Zhao *et al.*, 2009
AgNPs–rGO-/ITO	5.0	0.1-100	-	Golsheikh *et al.*, 2013
PQ11-AgNPs/GCE	33.9	0.1-180	-	Lu *et al.*, 2011a

AgNPs/F-SiO_2/GO	4	0.10-260	128 $\mu A \cdot mM^{-1}$	Lu *et al.*, 2011b
AgNPs–rGO/GCE	1	0.04-6	128 $nA.\mu M^{-1}$	Guascito *et al.*, 2008
AgNPs–PMPD/GCE	4.7	0.1-30	-	Tian *et al.*, 2011
AgNPs-NFs/GCE	62.0	0.1-80	-	Tian *et al.*, 2010
Ag/FeOOH/GCE	15.1	0.03-11	9.34 $\mu A \cdot mM^{-1} \cdot cm^{-2}$	Zhang and Zheng, 2015
Al/LDH/AgNPs/CPE	6.0	0.01-10	1.863 $\mu A \cdot mM^{-1} \cdot cm^{-2}$	Habibi *et al.*, 2017
AgNPs-P(ABA)-Fe_3O_4/MCPE	1.74	0.005-5.5	-	Chairam *et al.*, 2015
AgNPs/MoS_2/GCE	3.5	0.025-135.2	54.5 $\mu A \cdot mM^{-1} \cdot cm^{-2}$	Zhao *et al.*, 2017

*Ag nanoparticles (AgNPs), multiwall carbon nanotube (MWCNT), glassy carbon electrode (GCE), reduced graphene oxide (rGO), indium tin oxide (ITO), poly [(2-ethyldimethylammonioethyl methacrylate ethyl sulfate)-co-(1-vinylpyrrolidone)] (PQ11), polyvinyl alcohol (PVA), AgNP-decorated nanofibers (AgNPs-NFs), layered double hydroxide (LDH), poly(o-aminobenzoic acid) (P(ABA)), magnetic carbon paste electrode (MCPE).

Among them, the Ag nanostructures have high activity towards H_2O_2 reduction, due to its good stability, distinctive electronic and catalytic features. Nevertheless, Ag nanostructures exhibit a high tendency to agglomerate due to the strong van der Waals force between nanoparticles, which degrades the performance of the system. To overcome this issue, a variety of support nanomaterials such as graphene (Liu *et al.*, 2011), amorphous carbon (Tang *et al.*, 2016), carbon nanodots (Jiang *et al.*, 2014), and poly microparticles (Tian *et al.*, 2011) are utilized for immobilizing Ag nanomaterials, which are verified to be a successful approach for enhancing the sensing performance of the as-manufactured biosensors. A range of Ag nanomaterial based non-enzymatic H_2O_2 biosensors are summarized in Table 2.2. It has been reported that these biosensors have outstanding sensing features for the diagnosis of H_2O_2 due to the excellent electrocatalytic of Ag and synergistic effect between the nanomaterials.

Table 2.3 A summary of the Pt based non-enzymatic H_2O_2 biosensors.

Type of Biosensor	LOD (µm)	Linear Range (mM)	Sensitivity ($\mu A \cdot mM^{-1}$)	Ref.
Pt-Carbon nanofiber/GCE *	1.7	0.005-100	-	Yang *et al.*, 2015
Pt-Polyaniline/MSF	0.24	0.001-2	50	Ding and Su, 2015
Pt-Polypyrrole/GCE	1.2	1-8	80.4	Bian *et al.*, 2010
Pt-Poly melamin/GCE	0.65	0.005-1.65	-	He *et al.*, 2014
Pt-PVA-CNT/GCE	0.7	0.002-3.8	122.63	Fang *et al.*, 2012
Pt/Au	60	0.1-0.9	22.18	Wan *et al.*, 2012
Pt/NG/ITO	0.34	0.001-1	61.23	Tajabadi *et al.*, 2016

*Glassy carbon electrode (GCE), mesoporous silica film (MSF), polyvinyl alcohol (PVA), carbon nanotube (CNT), indium tin oxide (ITO).

On the other hand, Pt shows high catalytic activity for many reactions and has found application in a variety of fields, for example, catalytic hydrogenation, oxygen reduction and fuel-cell catalysis (Kulp *et al.*, 2013). However, Pt is expensive and rare, and new approaches are required to minimize the amount of Pt needed for different technological applications. Accordingly, the support materials on which the Pt catalysts are attached, have also received much attention for the reason that they play an important role in intensification of the performance of analytical method. The support materials of the catalysts are impacted by many factors, for instance, the surface roughness and morphology, hydrophobicity and biocompatibility. In fact, an ideal catalyst support material as the sensing inter-face should exhibit a strong affinity in the direction of the catalyst particles for their immobilization, high electrical conductivity and good chemical stability. Besides, the support materials should be non-toxic and have a high surface area and long-period stability (Vinayan *et al.*, 2012). Therefore, materials such as redox proteins (Liu *et al.*, 2004), conductive polymers (Mahmoudian *et al.*, 2014) and carbon

(Lawal, 2015), have been utilized as support materials for non-enzymatic biosensors. A summary of the Pt based non-enzymatic H_2O_2 biosensors is presented in Table 2.3.

CHAPTER 3: MATERIALS AND EXPERIMENTAL PROCEDURE

This chapter presents a detailed description of the preparation methods of AgNDs/NG-modified ITO electrode (Ag/NG) and PtNFs/NG-modified ITO electrode using electrophoretic and electrochemical deposition as well as its characterization in order to improve the sensitivity of non-enzymatic H_2O_2 biosensors. Figure 3.1 displays the flowchart of the experimental procedures.

3.1 Chemicals

All chemicals, e.g. monosodium phosphate (NaH_2PO_4), disodium phosphate (Na_2HPO_4), hydrogen peroxide (H_2O_2 30 wt%), silver nitrate ($AgNO_3$), magnesium nitrate ($Mg(NO_3)_2$), hydrazine (N_2H_4), ethanol (C_2H_5OH), urea (CH_4N_2O), sulfuric acid (H_2SO_4, 98%), phosphoric acid (H_3PO_4, 98%), potassium permanganate ($KMnO_4$, 99.9%), hydrochloric acid (HCl, 37%), and chloroplatinic acid solution (H_2PtCl_6) were purchased from Sigma Aldrich and were of analytical grade and utilized without purification. In all experiments, double distilled water (resistance = 18.3 MΩ) was used. Phosphate buffered saline (PBS) solution was prepared by mixing stock solutions of NaH_2PO_4 and Na_2HPO_4. Each experimental detection of H_2O_2 was carried out using a freshly prepared solution. It should be noted that all experiments were conducted at ambient temperature.

3.2 Preparation of Graphene and NG

In the case of Ag/NG, NG was prepared using a simple method that employed GO as a starting material. Hereon, the Hummers approach was employed to synthesize GO (Sookhakian *et al.*, 2014a). The exfoliation process comprised of sonicating the graphite oxide dispersion (0.2 mg mL^{-1}) in an ultrasonic bath for 30 min to attain a yellow-brown dispersion. The chemical reduction reaction was initiated by adding 0.8 mL hydrazine

into 30 mL GO dispersion. Afterward, the as-prepared product was irradiated under high power mode in a microwave oven for 5 min to obtain a stable black dispersion of NG sheets. The lower density NG suspension was collected from the solution by centrifuging and was dried at 50 ºC. It should be mentioned that graphene was produced using the same procedure but with the absence of the hydrazine solution.

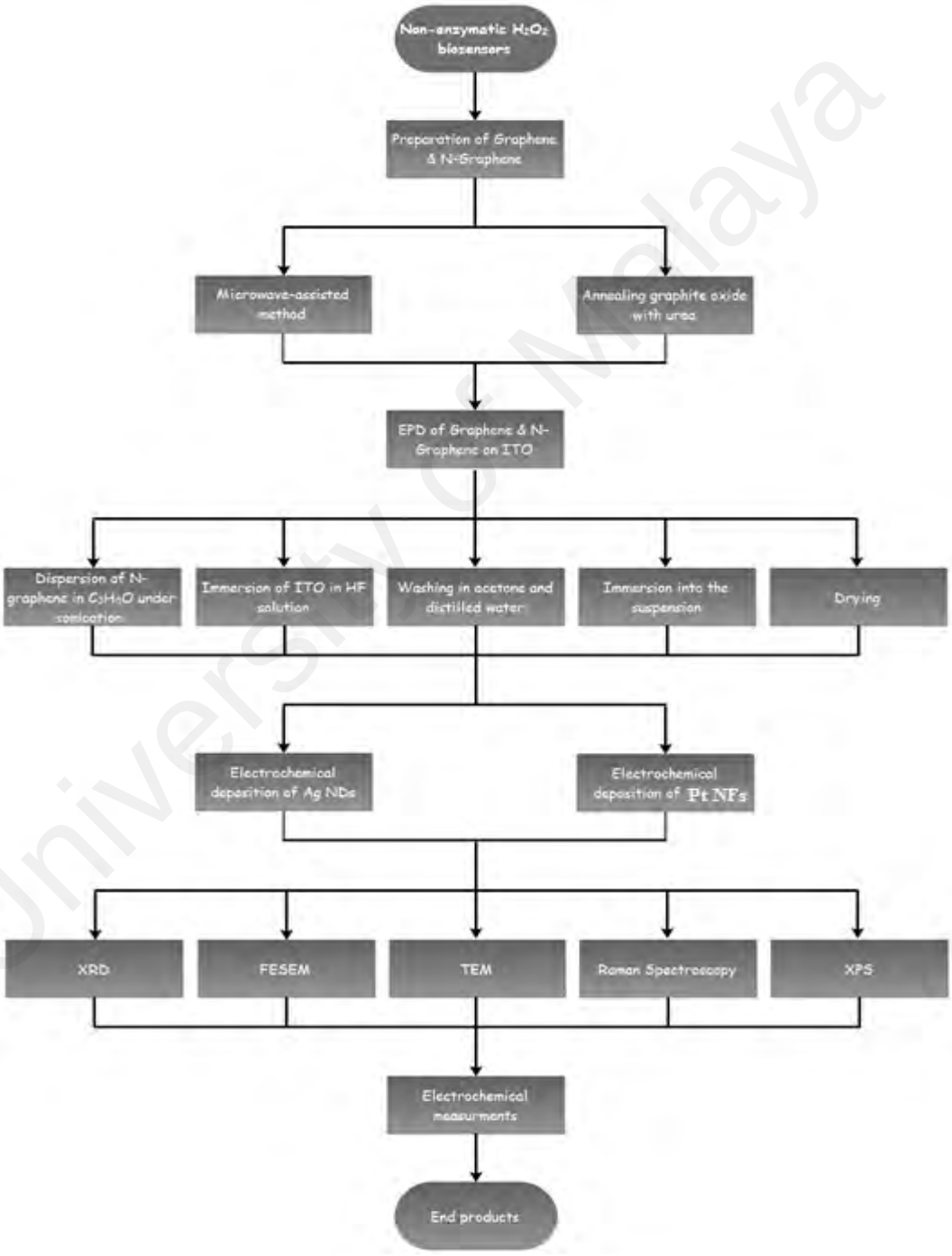

Figure 3.1: Flowchart of the experimental procedures.

In the case of Pt-NG, graphite powder (1–2 μm, Aldrich) was used for the preparation of GO using the modified Hummers method (Azarang *et al.*, 2015). The synthesis of NG is described elsewhere (Teridi *et al.*, 2015). Briefly, 50 ml of a GO dispersion in ethanol (1 mg/mL) was added with 100 mg of urea. The dispersion was heated to 80 °C with stirring until it dried. The powders were then placed in an Al_2O_3 crucible in a tube furnace and flushed with Ar gas to completely remove the oxygen in the medium. After the flow of Ar gas (100 sccm), the temperature was increased to 600 °C at a heating rate of 3 °C min^{-1} for 1 h. After that, the temperature increased to 900 °C at a rate of 5 °C min^{-1} and maintained at this temperature for 4 h. Then the furnace was cooled to room temperature, to collect the as-synthesized NG.

3.3 Electrophoretic deposition of NG-Modified ITO

The experimental set-up for the electrophoretic deposition (EPD) of NG-modified ITO and graphene-modified ITO electrodes is reported elsewhere (Sookhakian *et al.*, 2014a). For AgNDs/NG, two milligrams of the as-synthesized NG was dispersed in 40 mL of isopropyl alcohol under sonication for 5 min to obtain a homogeneous suspension (0.05 mg L^{-1}). The suspension was adjusted to pH 3 with a dilute HCl solution before EPD. In the case of Pt-NG, the suspension contained 40 ml of different concentrations of NG (0.01, 0.05, and 0.1 mg ml^{-1}) in 0.025 M $Mg(NO_3)_2$ in isopropyl alcohol, and was sonicated for 30 min to obtain a homogeneous suspension. In both cases, ITO glass substrates with an area of 10 mm × 20 mm were immersed in a 5% HF solution for a few minutes to remove the native oxide layer, followed by washing in acetone and distilled water before being vertically immersed into the suspension. During the EPD, the DC potential and deposition time were set at 20 V and 5 min, respectively, to form an NG-modified ITO electrode film. The freshly coated film was dried at 50 ºC in an oven to remove the excess solvent from the EPD process.

3.4 Electrochemical Deposition of metals based NG-mofied ITO electrode

3.4.1 Electrochemical Deposition of AgNDs

The electrochemical deposition of AgNDs was executed in a three-electrode electrochemical cell by chronoamperometry at -0.6 V with respect to an Ag/AgCl reference electrode. The NG-modified ITO electrode (with an active area of 1 cm^2) and a platinum foil (with an area of 2 cm^2) were utilized as the working electrode (WE) and the counter electrode (CE), respectively. The solution contained 40 mM $Ag(NH_3)_2OH$, which was prepared by adding ammonia (1 wt%) into a 50 mM $AgNO_3$ solution until the complete dissolution of the precipitates. Distilled water at a volume ratio of 1:12 ($Ag(NH_3)_2OH$: water) was subsequently added for the chronoamperometric deposition of the AgNDs/NG modified ITO electrode for 10 min. The final product (AgNDs/NG) was washed with distilled water and dried at 50 ºC in a conventional oven. The same procedure was used for the electrochemical deposition of AgNDs-graphene modified-ITO electrode (Ag-G).

3.4.2 Electrochemical Deposition of PtNFs

The electrochemical deposition of PtNF was performed by cyclic voltammetry (CV). For the PtNFs deposition in five voltammetric cycles, the fresh NG-modified ITO thin film electrodes with different NG loadings were used as the working electrode. The same reference and counter electrodes were used. The solution contained 20 µl of H_2PtCl_6 in 15 ml of a 0.05 M $Mg(NO_3)_2$ as the supporting electrolyte. The potential scan was from −0.2 to −0.8 V at 10 mV s^{-1}. The as-fabricated Pt-NG with different NG loadings (i.e. 0.01, 0.05, and 0.1 mg ml^{-1}) are referred to as PNG-1, PNG-2, and PNG-3, respectively. The electrochemical deposition of pure PtNF-modified-ITO was performed with the same procedures. Similarly, the electrodes were washed with distilled water and finally dried at 50 ºC in an oven. Figure 3.2 shows the schematic of the overall fabrication of AgNDs/NG and PtNFs/NG biosensors.

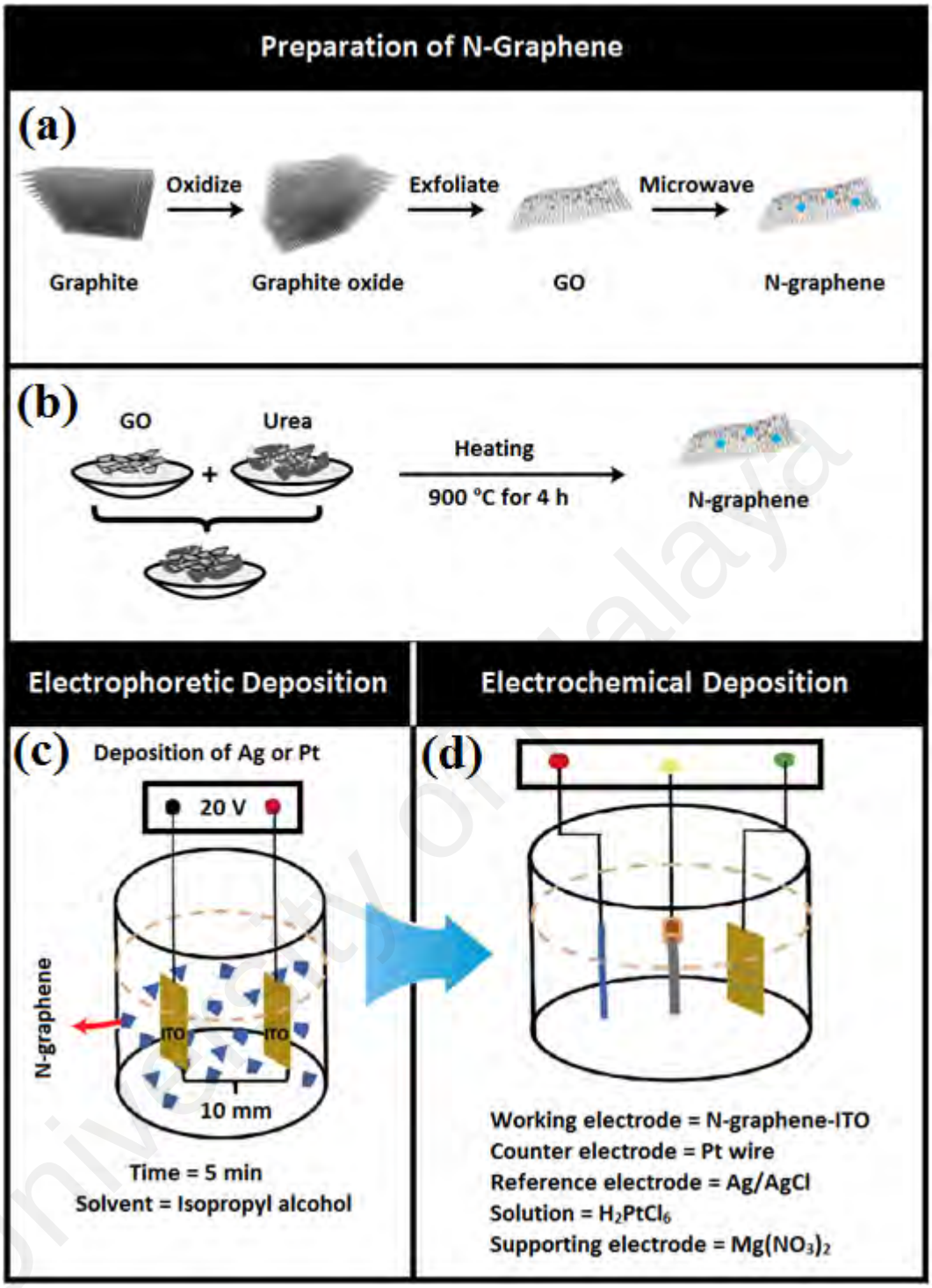

Figure 3.2: Schematic of the overall fabrication of (a) NG with microwave-assisted; (b) NG with annealing; (c) Electrophoretic deposition of NG-modified ITO; (d) Electrochemical deposition of AgNDs and PtNF.

3.5 Characterization Techniques

3.5.1 X-ray Powder Diffraction (XRD)

Prior to the characterization, the electrodes were ultrasonicated in distilled water. A X-ray powder diffractometer (XRD, PANalytical's Empyrean) with a monochromated *CuKa* radiation (λ = 1.54056 Å) over 2 theta range of 10°–80° was utilized to characterize the powders. "*PANalytical X'Pert HighScore*" software was also used to assay the XRD profiles, wherein all the patterns were compared with the standards of Joint Committee on Powder Diffraction and Standards (JCPDS) including card no. 00-004-0802 for Pt and card no. 01-087-0597 for Ag.

3.5.2 Morphological Analysis

A field emission scanning electron microscope (FESEM-Hitachi SU8000) with an acceleration voltage of 2 kV and transmission electron microscope (TEM-FEIG-4020) with an acceleration voltage of 120 kV were utilized to assay the particle size and the morphology of the experimental outputs.

3.5.3 X-ray Photoelectron Spectroscopy (XPS) Analysis

The XPS analysis was executed using an ESCALAB MK II X-ray photoelectron spectrometer with Mg as the excitation source to measure the elemental composition and to corroborate the presence of nitrogen-bonded groups in NG.

3.5.4 Raman Spectroscopy Analysis

A Renishaw Invia Raman Microscope instrument (laser excitation = 514 nm) was used for the Raman spectroscopy analysis. In the present study, Raman spectroscopy was employed to further investigate the structural and electronic properties of the as-synthesized NG.

3.5.5 Electrochemical Experiments

The electrochemical experiments were performed using a potentiostat/galvanostat (Autolab PGSTAT30, Ecochemie Netherlands). The catalytic activity toward H_2O_2 reduction was analyzed by performing cyclic voltammetry at different scan rates to investigate the sensitivity of the AgNDs/NG-modified ITO electrode. The detection of H_2O_2 was also performed using the PtNF/NG -modified ITO electrode to gain insight into the effect of NG loading on the analytical performance of the non-enzymatic sensor electrode. Moreover, the amperometric current-time technique as an effective approach was employed to examine the performance of the fabricated electrochemical sensors. Accordingly, the amperometric response of the modified ITO electrodes in nitrogen saturated 0.1 M PBS solution was assessed with successive additions of H_2O_2. The limit of detection (LOD) of the modified ITO electrodes was determined using the following equation (Mahmoudian *et al.*, 2014):

$$LOD = \frac{3S_B}{b} \tag{3.1}$$

Where b is the slope of the analytical curve and S_B is the standard deviation of the solution.

CHAPTER 4: RESULTS AND DISCUSSION

This chapter provides the results of the experimental studies and related descriptions of the AgNDs/NG-modified ITO electrode and PtNFs/NG-modified ITO electrode.

4.1 Characterization and Electrochemical Behavior of AgNDs/NG

4.1.1 Phase Analysis

Figure 4.1a shows the XRD patterns of GO and NG-modified ITO electrodes after EPD. An intense and sharp diffraction peak for GO appears at 2θ = 9.8º, which is attributed to the (0 0 1) lattice plane, corresponding to an interlayer *d*-spacing of 0.90 nm between the stacked GO nanosheets (Sookhakian *et al.*, 2013). As a comparison, the diffractogram shows the absence of this strong peak and the presence of a (0 0 2) peak at 2θ = 32.62º and 31.58º after the microwave irradiation of GO, corresponding to the *d* spacing of 0.27 and 0.28 nm, for graphene and NG, respectively (Wu *et al.*, 2013; Wang *et al.*, 2012). This suggests that the GO has been reduced to graphene sheets during the microwave-assisted process, with the removal of the functional groups. Moreover, the downshift of the (0 0 2) peak from graphene to NG indicates that the interlayer spacing in NG was enhanced due to the nitrogen doping. The crystal structures of the Ag-G-modified and AgNDs/NG modified ITO electrodes at -0.6 V after 30 min of electrochemical deposition are illustrated in Figure 4.1b. The remaining peaks at 2θ values of 38.115º, 44.229º, 64.443º and 77.397º can be indexed to the (1 1 1), (2 0 0), (2 2 0) and (3 1 1) lattice planes, respectively, of the cubic structure of electrodeposited Ag (JCPDS card no. 01–087–0597), with the lattice constant $a = b = c$ = 4.086 Å. Moreover, the appearance of the high intensity peak of the (1 1 1) plane indicates dendritic growth along the (1 1 1) plane of cubic silver. The ratio of the peak intensity of (1 1 1) / (2 0 0) and (1 1 1) / (2 2 0) of AgNDs/NG are 3.16 and 6.25, respectively, and are higher than

the conventional values *viz.* 2.5 and 4.0. This result is due to the formation of a non-spherical morphology of Ag (Sivasubramanian and Sangaranarayanan, 2013).

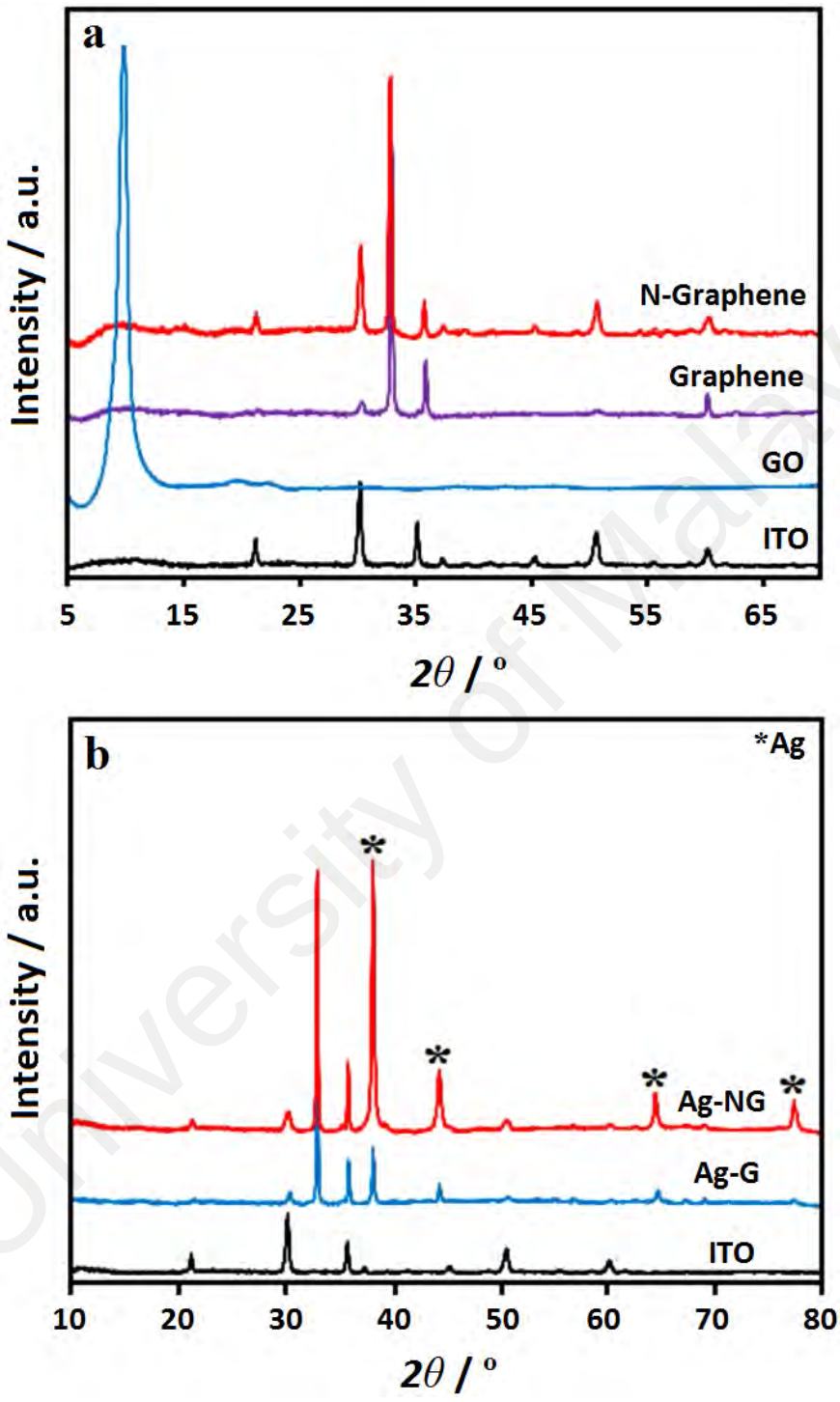

Figure 4.1: (a) XRD patterns of bare ITO electrode, bare GO, and graphene-modified and NG-modified ITO electrodes; (b) XRD patterns of the AgNDs/G-modified and AgNDs/NG modified ITO electrodes.

4.1.2 Morphological Features

Figure 4.2a shows the FESEM image of the NG-modified ITO electrode before the deposition of AgNDs. As shown, the surface of the NG thin film is smooth, while the typical wrinkles and ripple-like features are slightly visible. A representative FESEM image of AgNDs are shown in Figure 4.2b, which demonstrates a well ordered dendritic nanostructure. Figure 4.2c and d presents the FESEM images of the electrochemically deposited AgNDs on the NG-modified-ITO electrode. Figure 4.2c clearly shows that the as-deposited AgNDs are uniformly embedded in the NG surface; however, a number of AgNDs protrude from the edges of the NG sheets. Furthermore, the higher magnification FESEM image in Figure 4.2d clearly reveals the presence of small gaps between the individual AgNDs and NG nanosheets.

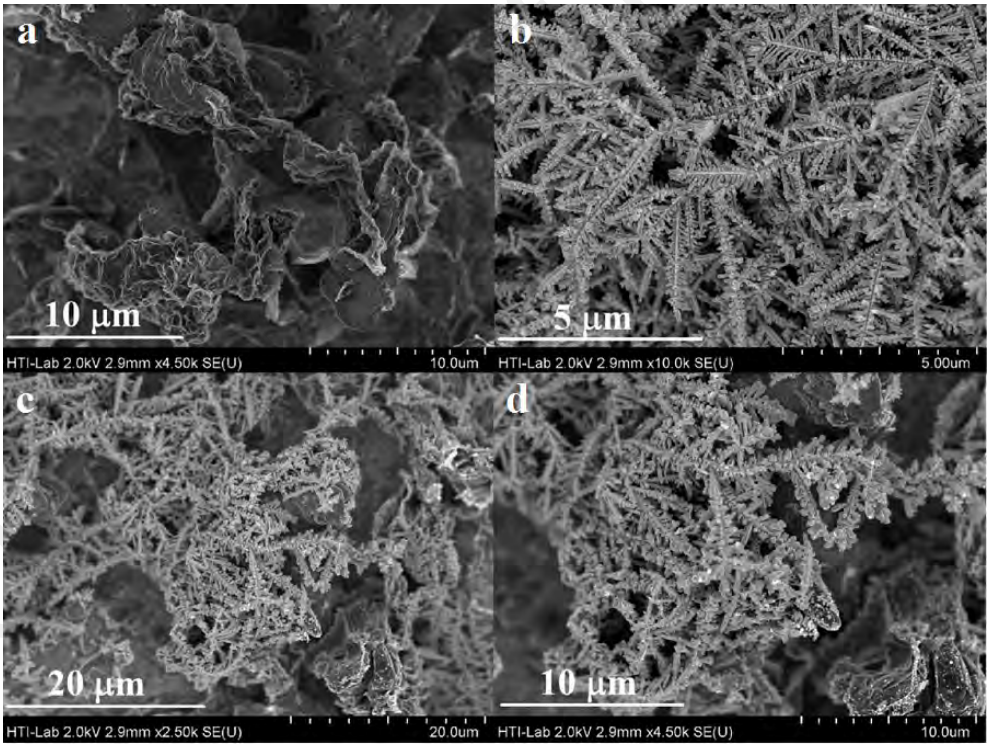

Figure 4.2: (a) FESEM image of NG on an ITO substrate after EPD, (b) FESEM image of AgNDs, (c) low- and (d) high-magnification FESEM images of the AgNDs coated on the NG-modified ITO electrode after electrochemical deposition.

This porous structure could facilitate gas diffusion and ionic transport for enhancing the electrochemical reduction of H_2O_2. Further investigation of the composite

morphology was performed using TEM. Figure 4.3a presents TEM image of the AgNDs/NG composite after its removal from the ITO electrode by ultrasonication. As can be seen, the NG sheets are crumpled due to the local stress induced by the loss of oxygen and the introduction of nitrogen in the NG structure. Moreover, Figure 4.3b clearly shows that the as-fabricated AgNDs/NG composite electrode consists of a large amount of dendritic structures. Furthermore, the Figure 4.3c and d present a representative TEM image of AgNDs.

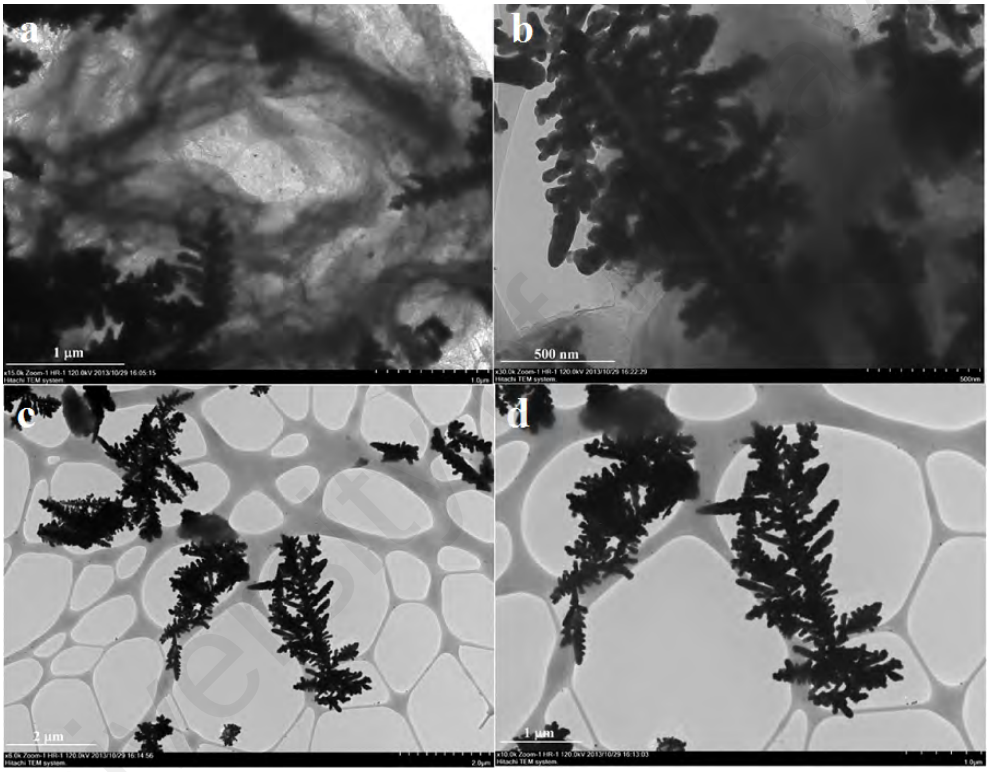

Figure 4.3: (a,b) TEM images of AgNDs deposited on an NG-modified ITO electrode, (c,d) is the TEM image of an individual AgND.

As shown, the individual AgNDs possesses an elegant two-dimensional dendritic structure with long trunks and uniformly arranged parallel branches. The side branches are symmetric and form an angle of approximately 70º. Moreover, the diameters of the trunk and the side branches are approximately 1 µm and 400 nm, respectively.

4.1.3 Structural Analysis by Raman Spectroscopy

As already mentioned, Raman spectroscopy is a powerful technique for examining the structural and electronic features of materials, which is frequently used in chemistry to provide a structural fingerprint to identify molecules. Figure 4.4 shows the Raman spectra of pristine GO Ag-G-modified and AgNDs/NG-modified ITO electrodes, where the *D*, *G* and 2*D* bands are centered at approximately 1359 cm^{-1}, 1587 cm^{-1} and 2681 cm^{-1}, respectively.

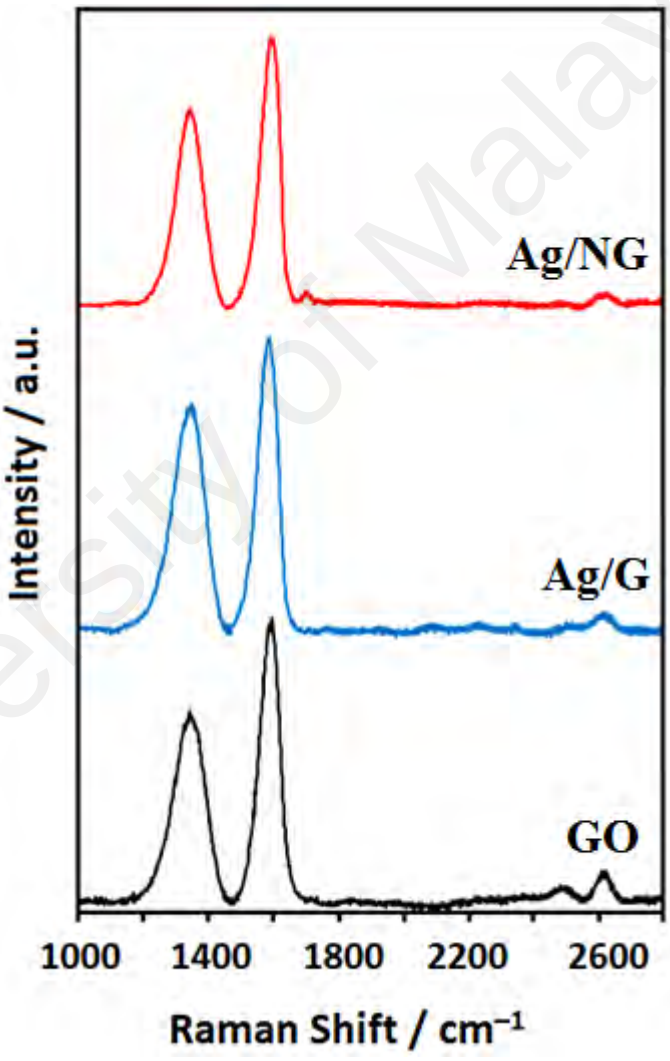

Figure 4.4: The Raman spectra of GO, graphene and NG.

In addition to these three peaks, the AgNDs/NG-modified ITO electrode presents a weak *D′* band located at 1628 cm^{-1} (Zafar *et al.*, 2013). The *G* band arises from the in-plane bond stretching of the C–C sp^2 bond, whereas the *D* and *D′* bands (activated by

inter-valley and intra-valley double-resonant Raman process, respectively) are associated with the various types of defects, such as vacancy-like defects and sp^3 defects, that can be produced by oxidation and hydrogenation, grain boundary edges, domain boundaries and electron doping (Zafar *et al.*, 2013). However the nature of these defects differs although both the *D* and *D′* bands are activated by the defects. Nitrogen doping in the graphene lattice leads to the presence of a *D′* band in the Raman spectrum of AgNDs/NG. The presence of a *D* band in the Raman spectra of both AgNDs/G and AgNDs/NG indicates that the densities of defects in these samples are similar due to the introduction of vacancies during the microwave-assisted process.

In contrast, the intensity of the 2*D* band (activated by a two-phonon double-resonant Raman process) is reciprocal to the electron-hole scattering rate (Ferrari and Basko, 2013). Moreover, the intensity ratios of the *D* to *G* band (I_D/I_G) in GO, Ag-G-modified and AgNDs/NG-modified ITO electrodes are 0.61, 0.74 and 0.79, respectively, indicating an increase in the defect density of graphene and NG after the microwave-assisted reaction and nitrogen doping. However, the intensity of the 2*D* band in pristine GO is higher compared to the Ag-G-modified and AgNDs/NG-modified ITO electrodes. Thus, the intensity ratio of the 2*D* to *G* band (I_{2D}/I_G) decreases from 0.28 for GO to 0.19 and 0.17 for Ag-G and AgNDs/NG, respectively, which further confirms for the increase in the defect density and successful reduction of GO. Note that the intensity of the 2*D* band is reciprocal to the electron-hole scattering rate. Thus, nitrogen doping creates defects in the graphene lattice, which leads to an increase in electron-hole scattering and a decrease in the 2*D* band intensity.

4.1.4 Chemical Composition Analysis by XPS

X-ray photoelectron spectra (XPS) are presented in Figure 4.5 to further investigate the chemical composition and nitrogen content in NG. The wide-scan spectra of GO reveals the presence of carbon and oxygen, and the presence of nitrogen in NG clearly indicates that nitrogen was successfully doped into the graphene lattice during the reduction of GO. The spectrum of GO shows the C 1s peak at 283.2 eV and the O 1s peak at 531.6 eV (Wu *et al.*, 2012). The calculated C:O atomic ratio is approximately 0.69. However, the intensity of the O 1s peak significantly decreased and the C:O atomic ratio reached 3.31 after the microwave-assisted reduction with hydrazine, indicating a successful reduction of GO. Moreover, the N 1s peak at 400 eV is clearly observed in the NG spectrum with a N:C atomic ratio of 0.17. The oxygen functionalities on the surface of GO and NG are identified by deconvoluting the C 1s peak into three different regions. As shown in Figure 4.5b, the high-resolution C 1s spectra of GO can be deconvoluted into two different strong peaks at 284.6 and 286.9 eV, which are assigned to C–C epoxide and C–O hydroxyl groups, respectively (Wu *et al.*, 2012), and the weak peak at 288.8 eV is attributed to the O–C bond of GO (Wu *et al.*, 2012). In addition, the C 1s spectrum of NG exhibits the same oxygen groups as for GO, but with a considerable decrease in the intensity of the oxygenated carbons (C–O and O–C=O) in the higher energy region (286–290 eV) after the microwave-assisted process in the presence of hydrazine, confirming the effective recovery of the p-electron system of graphene, as shown in Figure 4.5c (Wu *et al.*, 2012). Deconvolution of the N 1s peak of NG can provide detailed information on the nitrogen functional groups. As shown in Figure 4.5d, the N 1s peak can be deconvoluted into three different regions at 398.4, 400.2 and 402.6 eV, which are assigned to three different types of N-containing groups: pyridinic N, pyrrolic N and oxidized nitrogen, respectively (Wu *et al.*, 2012). Pyridinic N are the N atoms at the edges of the graphene planes, each of which is bonded to two carbon atoms and donates one p-

electron to the aromatic p-electron system. The pyrrolic N are the N atoms that are bonded to two carbon atoms and contribute two p-electrons to the p-electron system, whereas the pyridinic nitrogen atoms are oxidized, which are bonded to two carbon atoms and one oxygen atom.

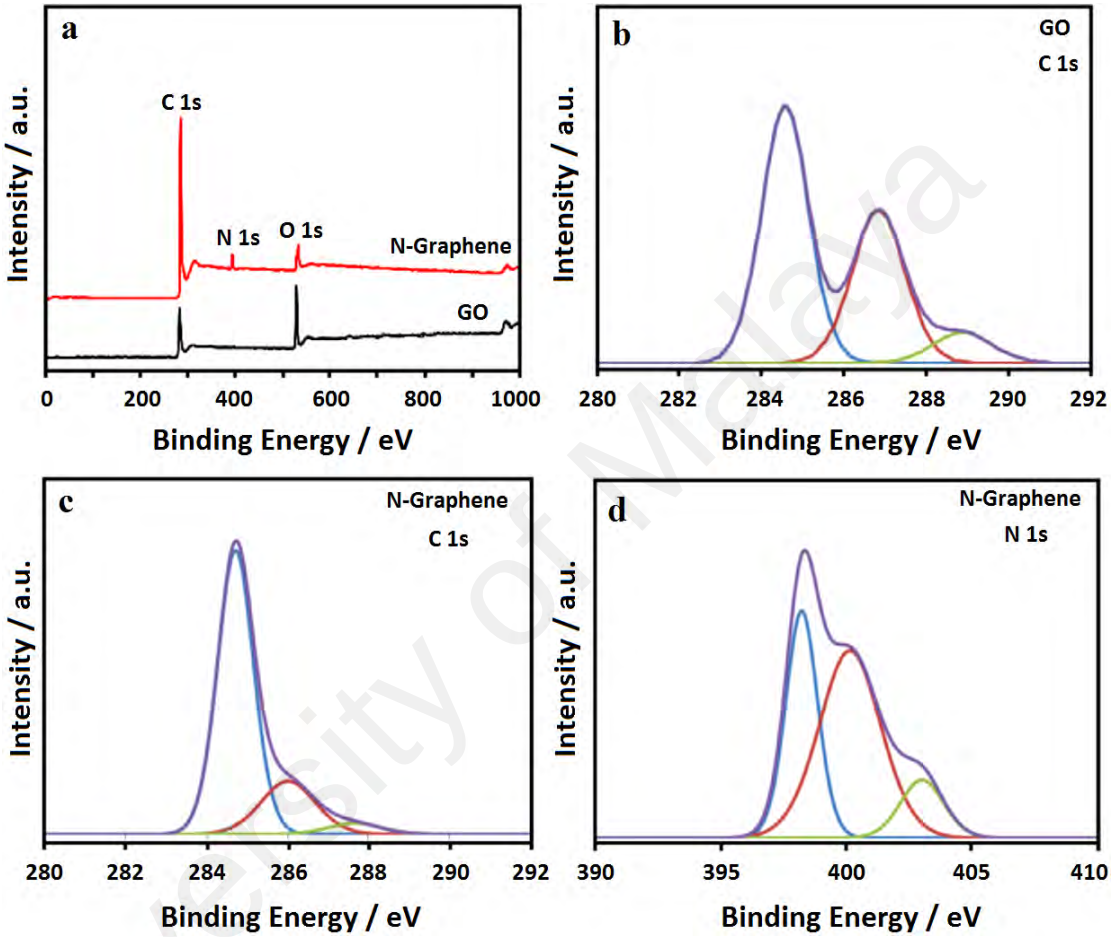

Figure 4.5: (a) XPS spectrum of GO and NG, (b) the high-resolution C 1s spectrum of GO, and the high-resolution (c) C 1s and (d) N 1s spectra of NG.

4.1.5 Nitrogen adsorption-desorption analysis

Nitrogen adsorption-desorption analysis reveals a typical Brunauer–Emmett–Teller specific surface areas (SBET) of 462 m2 g-1 for the AgNDs/NG electrode, with an average pore size of ~32 nm, which is higher compared to the pure NG (316 m2 g-1 and

~25 nm) (Figure 4.6). This could be due to the roughened NG surface with the presence of AgNDs.

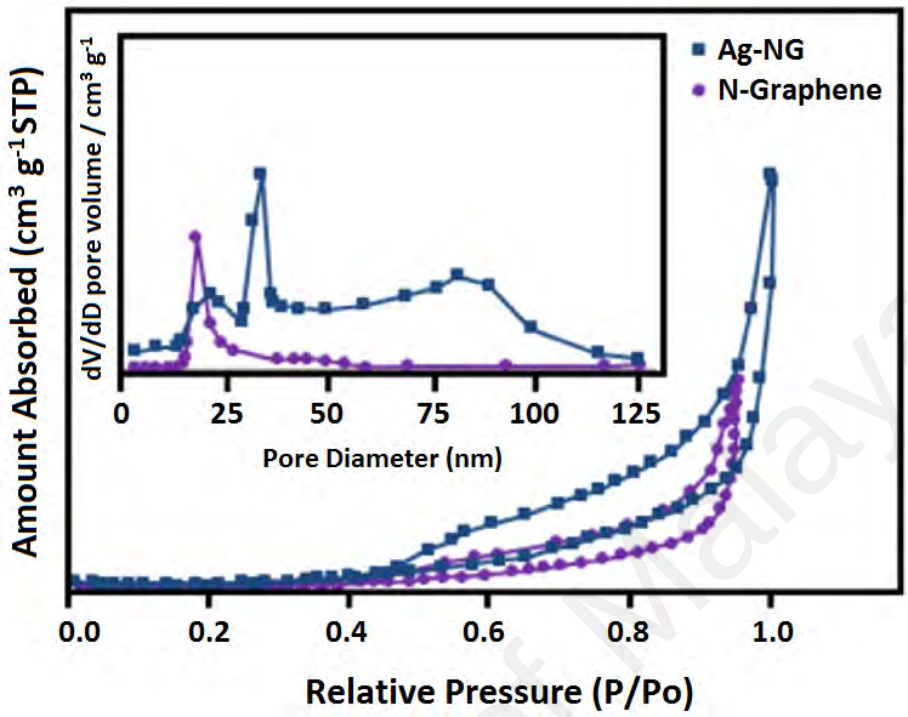

Figure 4.6: Nitrogen adsorption-desorption isotherms of Ag/NG and NG (the inset shows the pore size distribution).

4.1.6 Enhanced Electrocatalytic Activity for H_2O_2 Reduction

The electrochemical detection of H_2O_2 was performed on the AgNDs/NG-modified ITO electrode, and Figure 4.7a presents the cyclic voltammograms (CVs) of bare ITO, graphene-modified ITO, NG-modified ITO, AgNDs-modified ITO and AgNDs/NG-modified ITO in N2-saturated 0.1 M PBS at pH 7.2 in the presence of 1.0 mM H_2O_2. It can be clearly observed that the bare ITO electrode has the weakest response for the detection of H_2O_2. In contrast, the NG-modified ITO electrode exhibits a remarkable catalytic peak current density of approximately 5.6 mA cm-2 at -0.7 V in the presence of H_2O_2, which is considerably higher than the bare ITO, graphene-modified ITO and AgNDs-modified ITO electrodes. However, the AgNDs/NG-modified ITO electrode has

the strongest response among the five electrodes, with the lowest onset reduction potential of -0.40 V and highest current density peak of approximately 7.61 mA cm-2 for H_2O_2 reduction. This result demonstrates that both nitrogen doping in the graphene lattice and the presence of AgNDs can improve the electrocatalytic activity of graphene toward H_2O_2 reduction. Additionally, no obvious reduction current was observed for the AgNDs/NG-modified ITO electrode in the absence of H_2O_2.

The reason for the enhancement of electrochemical detection of H_2O_2 by NG compared to graphene is attributed to the increase in structural defects and oxygen-containing groups, due to the incorporation of nitrogen into the graphene lattice during the microwave-assisted process. As shown in Figures 4.3 and 4.4, the microwave-assisted process creates more structural defects on graphene, which leads to an enhancement in the amount of unsaturated carbon atoms at the graphene edge sites. These unsaturated carbon atoms are very reactive toward oxygen and form oxygen-containing groups when exposed to air during the microwave-assisted process. Therefore, the structural defects and oxygen-containing groups catalyze the reduction of H_2O_2. Furthermore, the background current of NG-modified ITO is higher than the AgNDs-modified ITO electrode which may be attributed to the large surface area of the NG-modified ITO electrode. It should be noted that the reduction peak current of H_2O_2 at the bare ITO, graphene-modified ITO and NG-modified ITO is very low compared to the AgNDs-modified ITO electrode. An obvious reduction peak of H_2O_2 at the AgNDs-modified ITO electrode is observed at -0.35 V, which illustrates the excellent catalytic activity for the reduction of H_2O_2 by the AgNDs. However, the reason for the enhanced reduction of H_2O_2 in AgNDs/NG compared to NG could be due to the increase in the surface area of NG with the presence of AgNDs. According to the BET results in Figure 4.6), the deposition of AgNDs on NG sheets effectively increases the total surface area of NG accompanied by the formation of large numbers of porous channels in the AgNDs/NG

composite. Therefore, O2 gas and OH– anions could be readily transported through these channels while AgNDs facilitates the detection of H_2O_2. Therefore, the AgNDs/NG electrode shows the best performance as a H_2O_2 sensor.

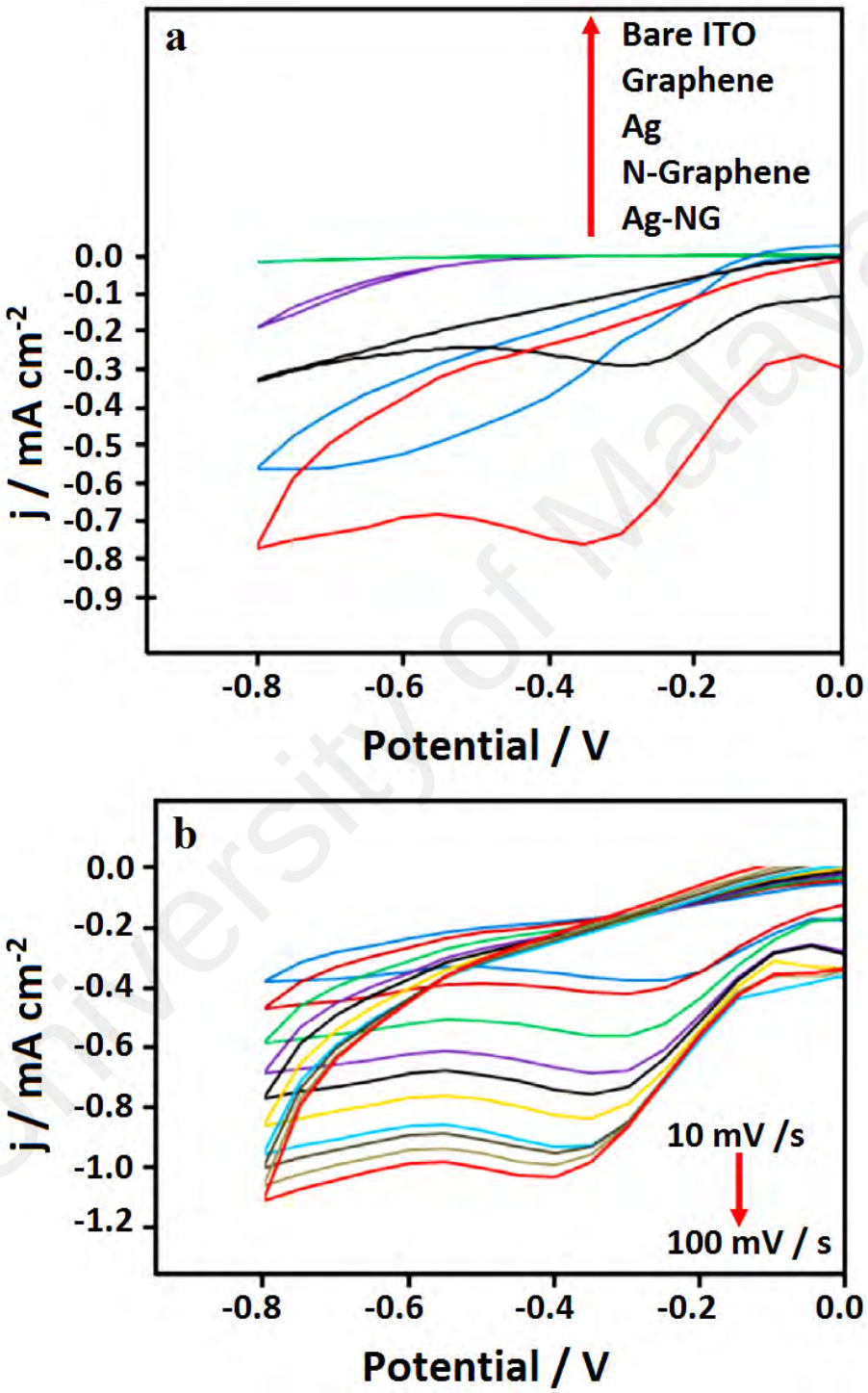

Figure 4.7: (a) CVs of the bare ITO and graphene-modified, NG-modified and AgNDs/NG-modified ITO electrodes; (b) CVs of the AgNDs/NG-modified ITO electrode at different scan rates from 10 mV/s to 100 mV/s in N_2-saturated PBS (0.1 M, pH 7.2) in the presence of 1 mM H_2O_2.

The catalytic activity toward H_2O_2 reduction was examined by performing cyclic voltammetry at different scan rates to investigate the sensitivity of the AgNDs/NG-modified ITO electrode. Figure 4.7b shows the CVs of the AgNDs/NG-modified ITO electrode in a N_2-saturated 0.1 M PBS solution at pH 7.2 with 1 mM H_2O_2 at different scan rates; the peak currents increase linearly as the scan rate increases from 10 to 100 mV s^{-1}. Moreover, the reduction peak is shifted slightly to negative potentials. This could be assigned to changes in the electrocatalytic activity and kinetic effect of AgNDs/NG-modified ITO surface on the reduction of H_2O_2. Therefore, the results illustrate that the electrochemical reduction of H_2O_2 on the AgNDs/NG-modified ITO electrode is a surface-controlled process (Ghadim *et al.*, 2013).

Figure 4.8 presents the amperometric responses of the AgNDs/NG-modified ITO electrode in a N_2-saturated 0.1 M PBS solution at pH 7.2 with successive additions of H_2O_2 at an applied potential of -0.40 V vs. Ag/AgCl. Well-defined steady-state current responses at the AgNDs/NG-modified ITO surface are obtained after each addition of H_2O_2, and the maximum current responses are recorded within 2 s, demonstrating the rapid current response of the electrochemical sensor. The inset of Figure 4.8 shows the calibration curve of the current and H_2O_2 concentration. The AgNDs/NG-modified ITO electrode displays a linear increase as the concentration increases from 100 μM to 80 mM, with a correlation coefficient of 0.9989 and detection limit of 0.26 μM. The linear regression equation can be expressed as I (μA) = 88.47 (μAmM^{-1} cm^{-2}) + 5.348. Moreover, the amperometric response to 1 mM H_2O_2 in PBS (0.1 M, pH 7.2) was obtained over a continuous 45 min period. The response of the AgNDs/NG-modified ITO electrode remained stable throughout the entire experiment, with only 4.3%, 8.6% and 11.2% decreases in current at 10, 30 and 48 min, respectively. The reproducibility of the modified electrode was evaluated by measuring the current response to H_2O_2 under the same conditions. The relative standard deviation (RSD) of the current response to 1 mM

H_2O_2 was 4.1% for 6 successive determinations. All of these measurements indicate that the Ag- NG-modified ITO electrode exhibits good stability and reproducibility for the electrocatalytic reduction of H_2O_2 and that the electrochemical performance of this sensor is comparable with sensors based on other materials, as shown in Table 2.2. It is worth mentioning that the most important achievement of this work is the use of ITO as a cheap substrate compared to the GCE and a facile electrophoretic deposition method for the fabrication of the sensor electrodes. Indeed, electrophoretic deposition can be a substitute for other methods for the preparation of the sensor substrate from carbon materials, conductive polymer and other organic materials, in the fabrication of sensor electrodes based on conductive polymer-metal composite or other organic-metal composite electrodes.

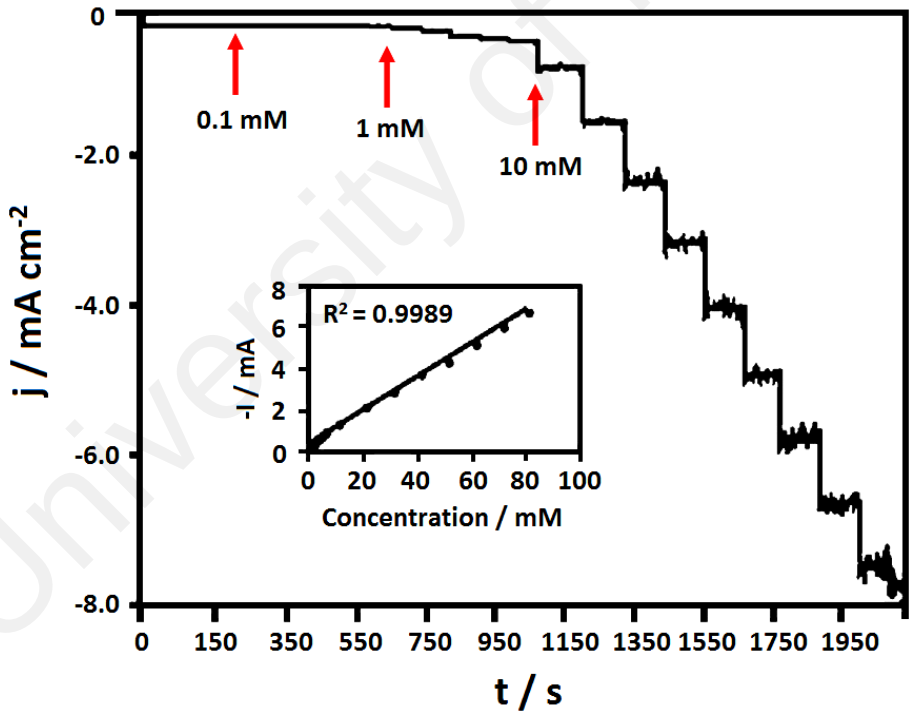

Figure 4.8: Typical amperometric curve of the AgNDs/NG-modified ITO electrode at an applied potential of -0.40 V vs. Ag/AgCl in N_2 saturated PBS (0.1 M, pH 7.2). Inset: calibration curve.

4.2 Characterization and Electrochemical Behavior of Pt-NG

Figure 4.9 shows the effect of NG loading on the color of the electrodes. As can be seen, the thin film electrodes are grayish in color as the NG loading increased due to the increasing thickness of the NG film.

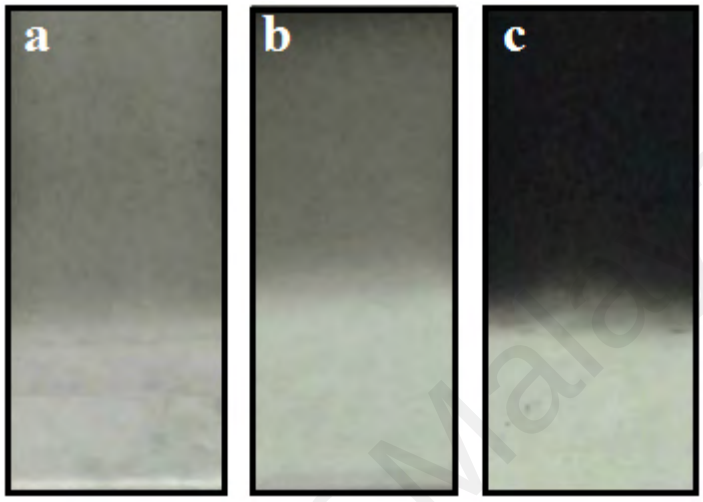

Figure 4.9: The effect of NG loading on the color of the electrodes.

The first cycle in the cyclic voltammograms (CVs) of the electrodeposited PtNF on the surface of NG-modified ITO with 0.05 mg ml^{-1} NG loading is shown in Figure 4.10. Two reduction peaks and one oxidation peak are observed in the negative scan, which indicates the successful reduction of the PtNF. It has been reported that the electrochemical deposition of Pt from the H_2PtCl_6 electrolyte involves a-three step mechanism (Lu and Zangari, 2005):

$$PtCl_6^{2-} + 2e^- \rightarrow PtCl_4^{2-} + 2Cl^- \quad (4.1)$$

$$PtCl_4^{2-} + 2e^- \rightarrow Pt + 4Cl^- \quad (4.2)$$

and/or

$$PtCl_6^{2-} + 4e^- \rightarrow Pt + 6Cl^- \quad (4.3)$$

The peak at −0.38 V might be due to the reduction of Pt (IV) to Pt (II) (Eq. (4.1)) or Pt (IV) to Pt (0) (Eq. (4.3)). The small wave which begins at approximately −0.65 V, could be due to the electro-chemical reduction of Pt (II) to Pt (0) (Eq. (4.2)). However, the anodic peak on the reverse scan is most likely due to desorption and electro-oxidation of the strongly adsorbed hydrogen atoms.

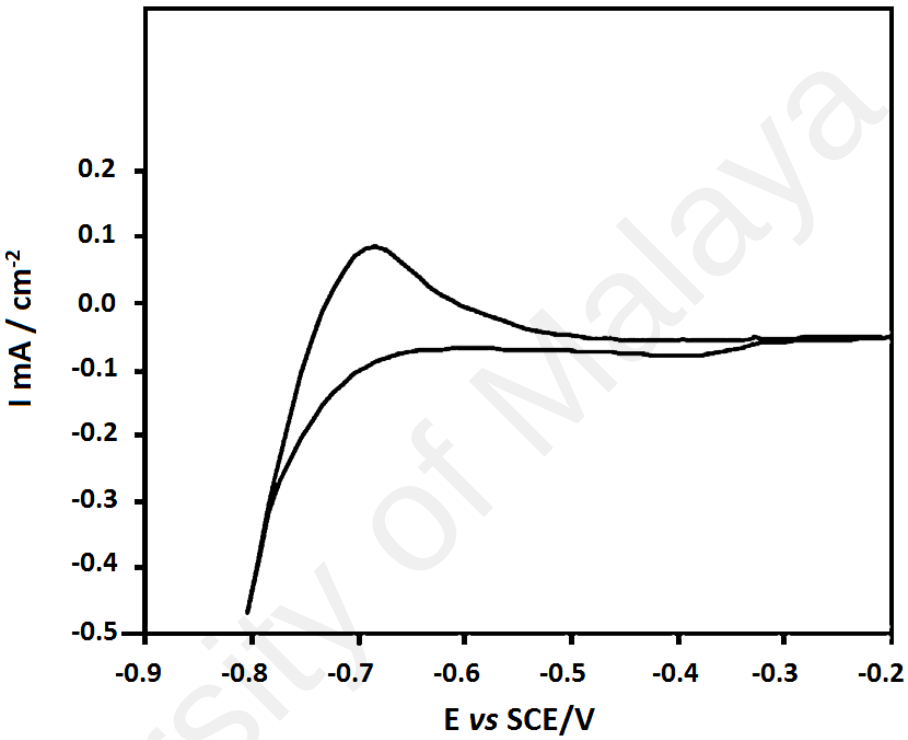

Figure 4.10: CV of the as-electrodeposited PtNF/NG (0.05 mg ml^{-1})-modified ITO electrode. The solution contained 20 µl of H_2PtCl_6 in 15 ml of a 0.05 M $Mg(NO_3)_2$ as the supporting electrolyte. The potential scan was from −0.2 to −0.8 V at 10 mV s^{-1}.

4.2.1 Phase Analysis

Figure 4.11a shows the XRD profiles of graphite, GO and NG. The XRD for GO shows a sharp diffraction peak at $2\theta = 10.6°$, is due to the (0 0 1) lattice plane, with a *d*-spacing of 0.83 nm. This *d*-spacing is much wider than the narrow peak at 26.8° (graphite), with an interlayer spacing of 0.33 nm. This result suggests that the raw graphite was exfoliated into GO sheets, from the presence of the oxygen, carboxyl and other functional groups

(Sookhakian *et al.*, 2015). For comparison, after the annealing of GO with urea at 900 °C in Ar for 4 h, the diffractogram shows the absence of this strong peak, along with the presence of a broad (0 0 2) diffraction peak centered at 2θ of 24.86°, which corresponds to an interlayer spacing of 0.35 nm. This result indicates the formation of graphene, from the removal of the oxygen functional groups during the annealing process (Serov *et al.*, 2015).

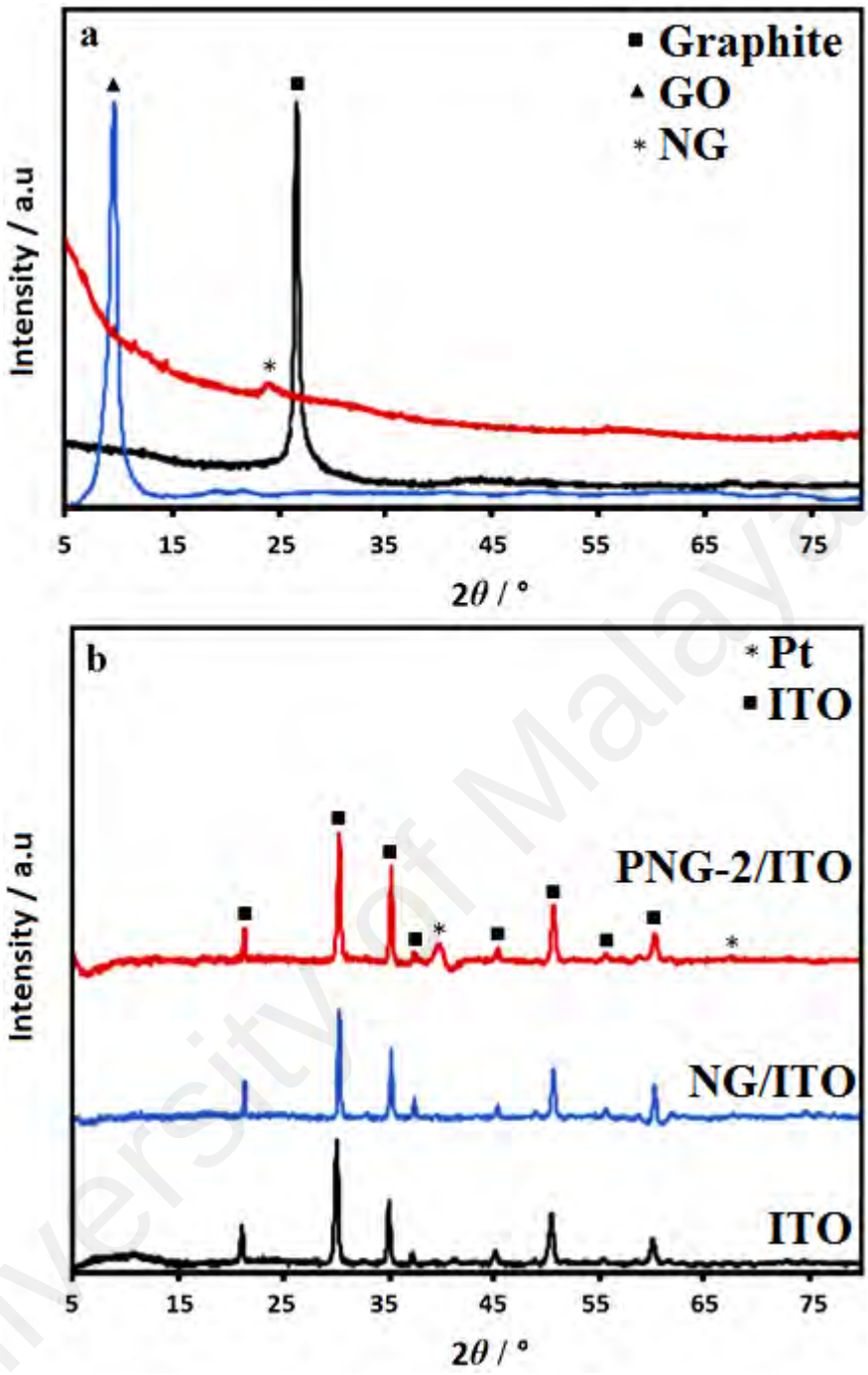

Figure 4.11: XRD profiles of (a) graphite, GO and NG, as well as (b) bare ITO, NG-ITO and PNG-2 electrodes.

The crystalline structure of the PtNF-modified ITO electrode and PNG-2 are shown in Figure 4.11b. The NG-modified ITO electrode exhibits XRD patterns that are similar with the blank ITO electrode, which is due to the small amount of NG. Compared to the NG-modified ITO, the spectra of the PNG-2-modified ITO electrode (after electrodeposition of PtNF in 5 cycles) contain diffraction peaks at 2 theta values of 39.765° and 67.456°,

which is indexed to the (1 1 1) and (2 2 0) lattice planes, respectively, of cubic platinum (JCPDS card no. 00-004-0802) with the following lattice constants: $a = b = c = 3.923$ Å.

4.2.2 Morphological Features

FESEM analysis was performed to study the morphology of the PtNF/NG hybrid as shown in Figure 4.12.

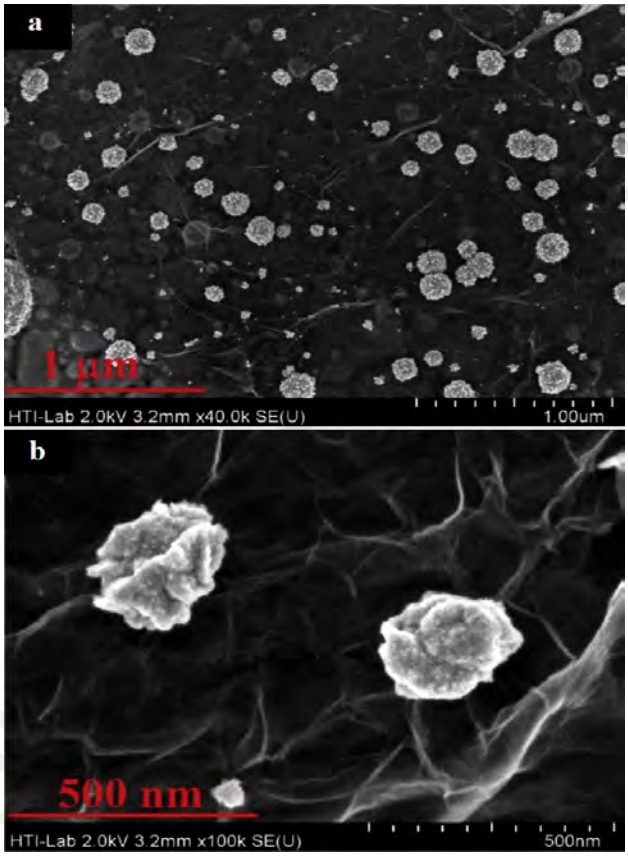

Figure 4.12: (a) Low and (b) high magnification FESEM images of PNG-2-modified ITO electrodes.

The low magnification FESEM image of the as-electrodeposited PtNF on the surface of the NG-modified ITO (Figure 4.12a) shows the presence of Pt nanoflower (NF) structures. In addition, the PtNF was uniform and densely distributed on the surface of the electrophoretically deposited NG-modified ITO electrode. A careful and closer view in Figure 4.12b also reveals that the individual PtNFs are quasi-spherical with sizes in the range of 250–300 nm.

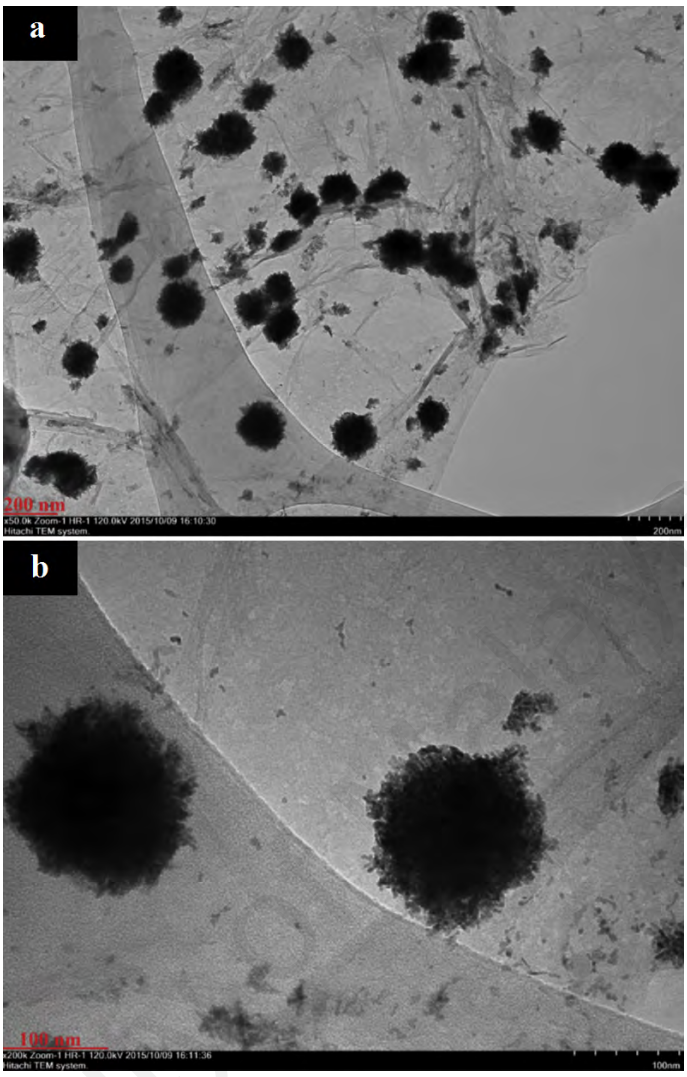

Figure 4.13: (a) Low and (b) high magnification TEM images of PNG-2.

A more detailed investigation of the morphology of the NG and PtNFs was performed using the TEM technique. The TEM image reveals that the Pt nanoflowers are highly decorated on the surface of NG. In addition, the NG exhibits a crumpled sheet-like layer morphology with several micrometers in diameter (Figure 4.13a). The crumpling effect may be due to the defective structures formed during the exfoliation or the doping of nitrogen atoms. The high magnification TEM image of the PtNF (Figure 4.13b) shows that each PtNF consists of randomly shaped nanofibers that point radially outward, and the nanofibers are assembled from tens to hundreds of self-assembled particles growing in all directions.

4.2.3 Structural Analysis by Raman Spectroscopy

Raman spectroscopy was also utilized to further investigate the structural and electronic properties of the as-synthesized NG. Figure 4.14 compares the Raman spectra of pristine GO and NG after the annealing with urea at 900 °C. The Raman spectra of GO contain three peaks located at 1359, 1588 and 2688 cm^{-1}, corresponding to the *D*, *G* and 2*D* bands, respectively. The *G* band is the result of the in-plane bond stretch of the C–C sp^2 bond, and the *D* band is attributed to the different types of defects, such as the vacancy-like and sp^3 defects. These defects are the product of hydrogenation, oxidation, electron doping, domain boundaries and grain boundary edges (Tajabadi *et al.*, 2015). In addition to these three peaks, NG exhibits an extra weak *D′* band located at 1710 cm^{-1} (Zafar *et al.*, 2013). However, the major difference between NG and GO is the degree of disorder, which can be observed from the intensity ratio of the *D* and *G* bands (I_D/I_G). The intensity ratio (I_D/I_G) of GO and NG are 0.66 and 1.28, respectively. The increase of the (I_D/I_G) ratio implies that the annealing process created a large amount of sp^2 bonds and structural defects in the NG lattice. The intensity of the 2*D* band which is attributed to a two-phonon double-resonant process, is reciprocal to the rate of the electron-hole scattering process (Tajabadi *et al.*, 2015). Therefore, the increased intensity of the 2*D* peak at 2703 cm^{-1} is attributed to the increase in the NG layers compared to what is observed in GO, after annealing with urea (Sookhakian *et al.*, 2015).

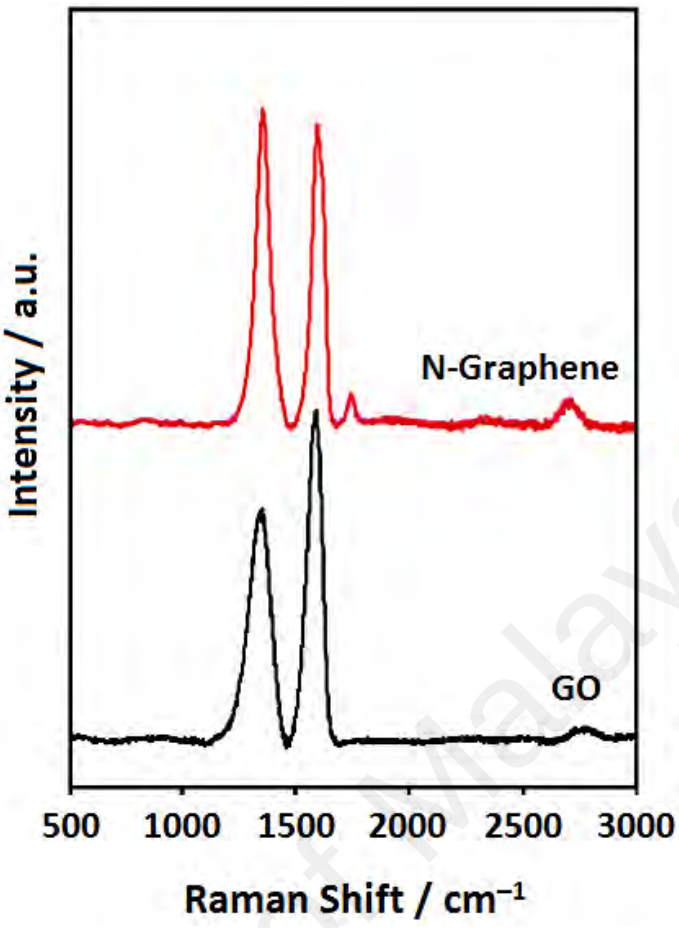

Figure 4.14: Raman spectra of GO and NG.

4.2.4 Chemical Composition Analysis by XPS

Figure 4.15 shows the XPS of GO and the nitrogen-bonded groups in NG. The wide-scan XPS spectrum of GO shows the presence of oxygen and carbon. The wide-scan XPS spectrum of NG shows the presence of nitrogen doping in graphene during the annealing of GO with urea (Figure 4.15a). The GO spectrum shows a C 1s peak at 283.2 eV and O 1s peak at 531.6 eV (Tajabadi *et al.*, 2015). The C:O atomic ratio is 0.69 but the O 1s peak intensity decreases significantly. The C:O atomic ratio of 2.36 indicates the successful reduction of GO, after annealing with urea. Moreover, the NG spectrum shows the N 1s peak at 398.6 eV with a N:C atomic ratio of 0.56 (Figure 4.15a).

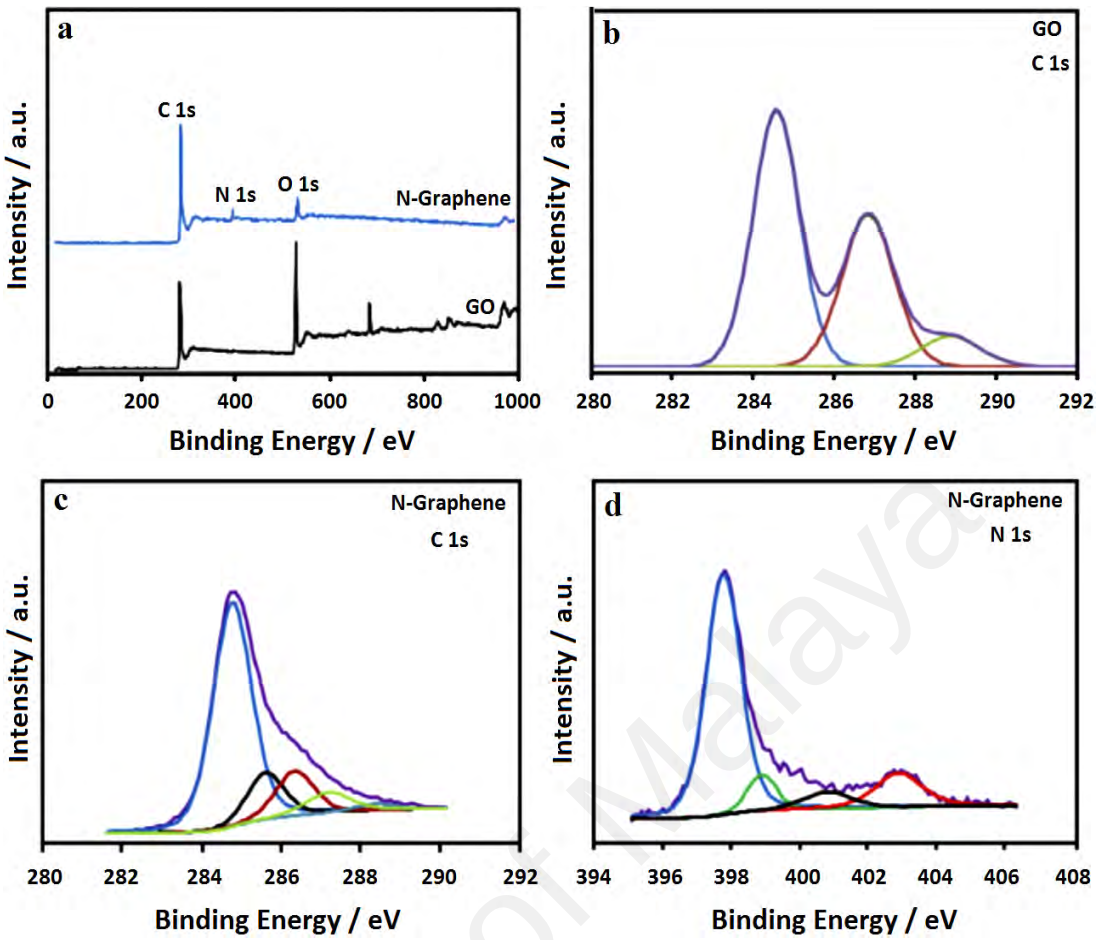

Figure 4.15: (a) Wide scan XPS spectra of GO and NG. The high-resolution XPS spectra of (b) C 1s of GO (c) C 1s of NG, and (d) N 1s of NG.

The oxygen functional groups of GO and NG were identified by the deconvolution of the C 1s peak. The high-resolution C 1s spectrum of GO in Figure 4.15b was deconvoluted into two peaks at 286.9 and 284.6 eV, attributed to the C–O hydroxyl and C–C epoxide groups, respectively. The smaller peak at 288.8 eV was attributed to the O–C=O of GO (Tajabadi *et al.*, 2015). The C 1s spectrum of NG and GO have the same type of oxygen atoms but the NG spectrum shows a decrease in the C–O and O–C=O intensities after annealing with urea. This result confirms the recovery of the π-electron network of graphene after the annealing process, as shown in Figure 4.15c (Tajabadi *et al.*, 2015). Moreover, the C–N groups at 285.7 eV suggest that the nitrogen atoms were incorporated into the graphene nanosheets during the annealing process with urea. A detailed information about the nitrogen functional groups can be provided by the

deconvolution of the N 1s peak in the NG XPS spectrum. As shown in Figure 4.15d, the N 1s peak was deconvoluted into four different regions at 397.9, 399.8, 400.8 and 402.9 eV, which are attributed to the four different types of N-containing groups (i.e., pyridinic N–C, pyrrolic N–C, quaternary N–C and oxidized-N of pyridine, respectively) (Jin *et al.*, 2013). In the pyridinic N–C structure, the N atoms are situated at the edge of the graphene plane, each N atom donates one π-electron to the graphene π-electron system and is bonded to two C atoms. While in the pyrrolic N–C, each N atom contributes two π-electrons to the graphene π-electron network and is bonded to two C atoms. The nitrogen atoms in the quaternary-N–C structures are bonded to three carbon atoms. In addition, the oxidized nitrogens are mostly the nitrogen atoms in the pyridine group, are bonded to one oxygen atom and two carbon atoms.

4.2.5 Enhanced Electrocatalytic Activity for H_2O_2 Reduction

The detection of H_2O_2 was performed using the PtNF/NG-modified ITO electrode to gain insight into the effect of NG loading on the analytical performance of the non-enzymatic sensor electrode. The cyclic voltammograms (CVs) of ITO, pure PtNF-modified ITO, PNG-*x* (*x* = 1, 2, and 3)-modified ITO electrode in nitrogen saturated 0.1 M PBS at pH 7.2 in the presence of 0.1 mM H_2O_2 at 50 mV s^{-1} are shown in Figure 4.16a. In this figure, the ITO electrode shows the weakest response toward H_2O_2 detection (inset of Figure. 16a). The pure PtNF-modified ITO shows a high peak current density of −0.47 mA cm^{-2} at −0.25 V in the presence of H_2O_2, much higher than the ITO electrode.

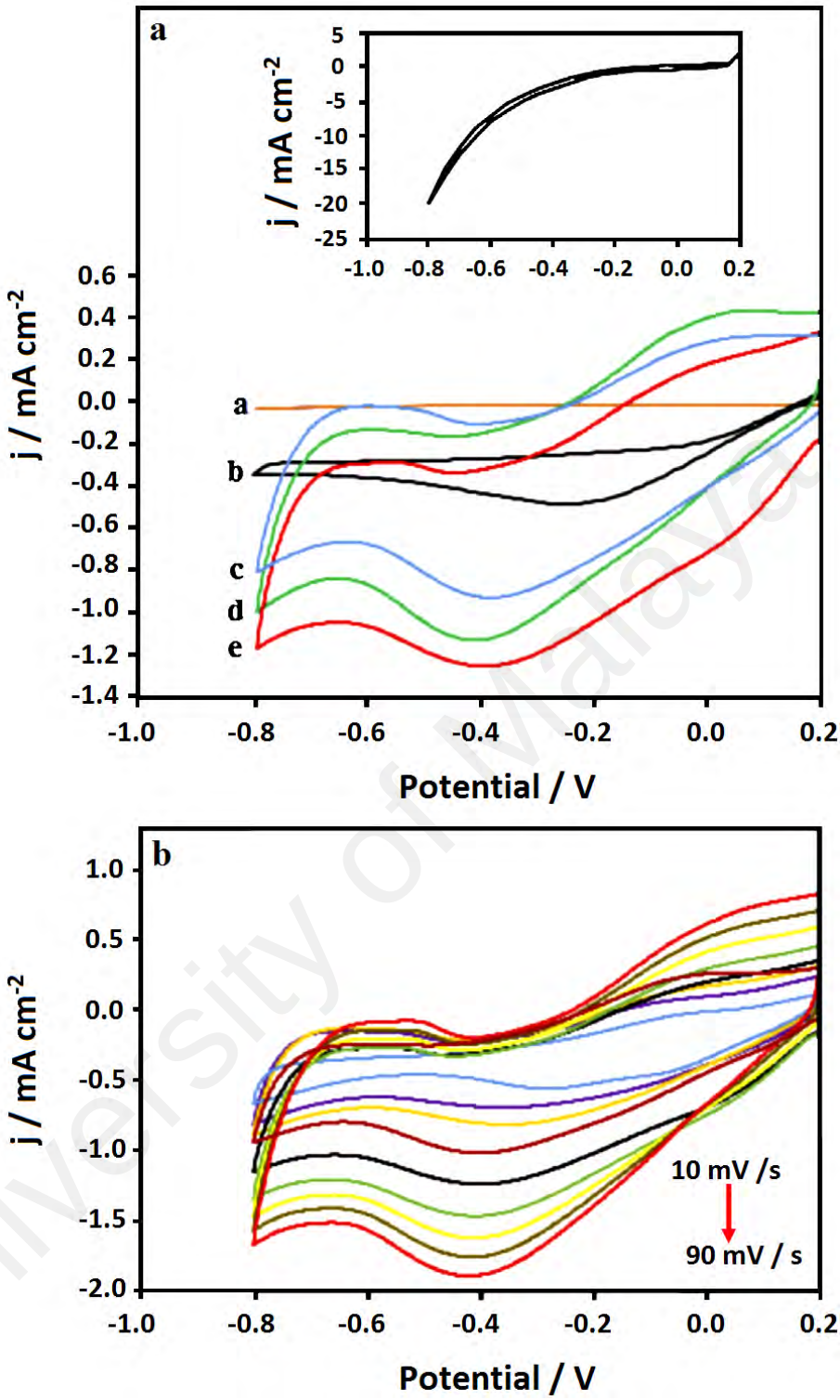

Figure 4.16: (a) CVs of ITO a, PtNF-modified ITO b, and PNG-1 c, PNG-2 d, and PNG-3 e, enlarge inset is CVs of ITO. (b) CVs of PNG-2-modified ITO at various scan rates from 10 mV/s to 100 mV/s in nitrogen saturated PBS (0.1 M, pH 7.2) with 0.1 mM H_2O_2.

The presence of NG leads to a remarkable enhancement in the current density response of the pure PtNF from −0.47 mA cm^{-2} to −1.12 mA cm^{-2} for PNG-1. With an increase in the NG loading up to 0.05 mg ml^{-1}, the current density increases from −1.12

mA cm^{-2} to −1.24 mA cm^{-2} for both PNG-1 and PNG-2. However, a further increase of the NG concentration to 0.1 mg ml^{-1} led to a decrease in the current density from −1.24 mA cm^{-2} to −0.92 mA cm^{-2}. The PNG-2 (PtNF/NG, 0.05 mg ml^{-1}) gave the strongest response at −0.40 V with the highest peak current density (2.5-fold higher than the pure PtNF electrode) for the H_2O_2 reduction. This result demonstrates that the presence of NG enhances the electrocatalytic activity of pure PtNFs toward H_2O_2 reduction.

The catalytic activity for H_2O_2 reduction was examined by cyclic voltammetry of the PNG-2-modified ITO at various scan rates. Figure 4.16b shows the CVs of the PNG-2-modified ITO in nitrogen saturated 0.1 M PBS solution at pH 7.2 with 0.1 mM H_2O_2 at various scan rates. The peak currents rise linearly with the scan rate from 10 to 90 mV s^{-1}. The reduction peak is slightly shifted towards negative region, which may be due to the changes in the activity of the PNG-2-modified ITO during the H_2O_2 reduction. These results indicate that the reduction of H_2O_2 is a surface-controlled process (Tajabadi *et al.*, 2015).

Figure 4.17 shows the effect of the potential on the current density of the PNG-2-modified ITO in nitrogen saturated 0.1 M PBS solution at pH 7.2 in 0.1 mM H_2O_2, between −0.2 to −0.6 V. The plot of current density *vs.* potential indicates that the current density gradually increases with the potential from −0.2 to −0.4 V. However, a further increase in the potential led to a significant decrease in the current density. The best working potential is selected from the least negative potential, which exhibits a high selectivity and high analyte-dependent current. Therefore, a potential of −0.40 V was identified as the best working potential for the reduction of H_2O_2.

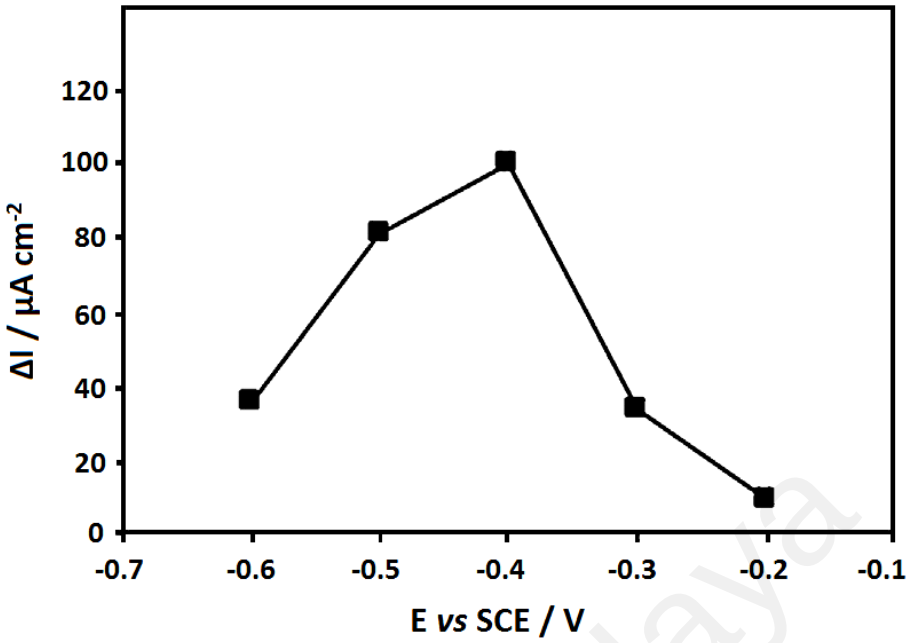

Figure 4.17: The current density *vs.* potential of the PNG-2-modified ITO electrode in 0.1 mM H_2O_2 in 0.1 M PBS at pH 7.2.

The amperometric current-time technique is an effective approach to examine the performance of the fabricated electrochemical sensor. Therefore, the amperometric response of the PNG-2-modified ITO electrode in nitrogen saturated 0.1 M PBS solution with successive additions of H_2O_2 at −0.40 V *vs* Ag/AgCl are shown in Figure 4.18. The current responses of the PNG-2 hybrid are rapid and steady (achieving the steady state current within 5 s) and reproducible when H_2O_2 was added to the PBS solution. The corresponding current-concentration and calibration curve was performed three times, and the standard deviations were calculated (the inset of Figure 4.18). The current response of the as-fabricated PNG-2 electrode is linear when the H_2O_2 concentration increases from 1 μM to 1 mM. The linear regression equation is written as I (mA) = 61.23 ($\mu AmM^{-1}cm^{-2}$) +2.193 with a correlation coefficient of 0.9991. Hereon, the LOD of the PNG-2-modified ITO electrode was calculated using the Eq. (3.1) (Mahmoudian *et al.*, 2014).

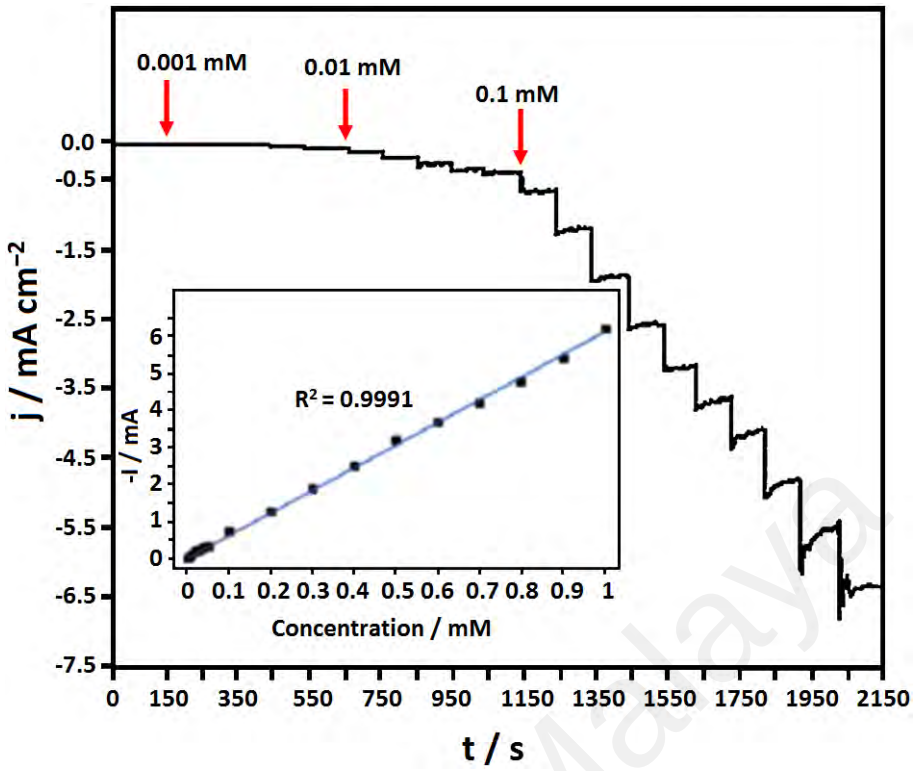

Figure 4.18: Typical amperometric response of the PNG-2-modified ITO electrode at −0.40 V *vs* Ag/AgCl in nitrogen saturated PBS (0.1 M, pH 7.2). Inset: calibration plot.

The estimated LOD is 0.34 µM. Moreover, the amperometric response to 0.1 mM H_2O_2 in PBS (0.1 M, pH 7.2) was obtained over a 48 min time period. The PNG-2-modified ITO electrode remained stable throughout the experiment with only 5.1%, 9.8% and 12.4% decrease in the current at 10, 30 and 48 min, respectively. The reproducibility of the modified electrode was evaluated by measuring the current response to H_2O_2 under the same conditions. The relative standard deviation (RSD) of the current response to 0.1 mM H_2O_2 was 5.1% for 6 successive determinations. Therefore, the PNG-2-modified ITO electrode exhibits good stability and reproducibility for the electrocatalytic reduction of H_2O_2, and the electrochemical performance of this sensor is comparable to the sensors based on other materials, as shown in Table 2.3.

Based on the CV curves and amperometric responses, NG has an important role in the catalytic enhancement of the PtNF-modified ITO electrode. Therefore, electrochemical impedance spectroscopy (EIS) technique was performed with a 5 mV AC

signal with a frequency range of $0.1-10^5$ Hz to evaluate the charge transfer kinetics and ion diffusion process of the sensor electrodes. Figure 4.19 shows the Nyquist plots of the pure PtNF-modified ITO and PNG-*x* (*x* = 1, 2, 3)-modified ITO electrodes in 0.1 M KCl solution containing1 mM $Fe(CN)_6^{3-/4-}$ (1:1). The Nyquist plots of the electrodes exhibit a high-frequency response due to the presence of the charge-transfer resistance (R_{ct}), which is related to the catalytic activity of the reduction of $Fe(CN)_6^{3-}$ to $Fe(CN)_6^{4-}$ across the electrode-electrolyte interface. In addition, the low-frequency response is due to the Warburg diffusion process. The Warburg impedance is attributed to the diffusion controlled process across the deposited layer (Mahmoudian *et al.*, 2014). As shown in Figure 4.19, compared with the pure PtNF-modified ITO electrode, the presence of NG led to a significant decrease in the diameter of the semicircle at higher frequency, which confirms that the conductivity of the electrode is increased due to the presence of NG in the hybrid electrodes. The increased conductivity apparently enhances the catalytic ability of the sensor electrode for faster electron transfer process across the interface, resulting in an improved catalytic performance of the sensor electrodes. However, the diameter of the semicircle is increased when the NG loading is increased beyond the optimum value (0.05 mg ml^{-1}), which indicates a decrease in the catalytic activity of the PNG-3-modified ITO electrode. This phenomenon can be assigned to the decreased in conductivity of the PNG-3 hybrid electrode compared to the PNG-2hybrid electrode due to the excessive NG content, leading to larger agglomeration during the electrophoretic deposition, which substantially decreases the surface area (Sookhakian *et al.*, 2014a) and led to a significant decrease in the analytical performance of the sensor electrode.

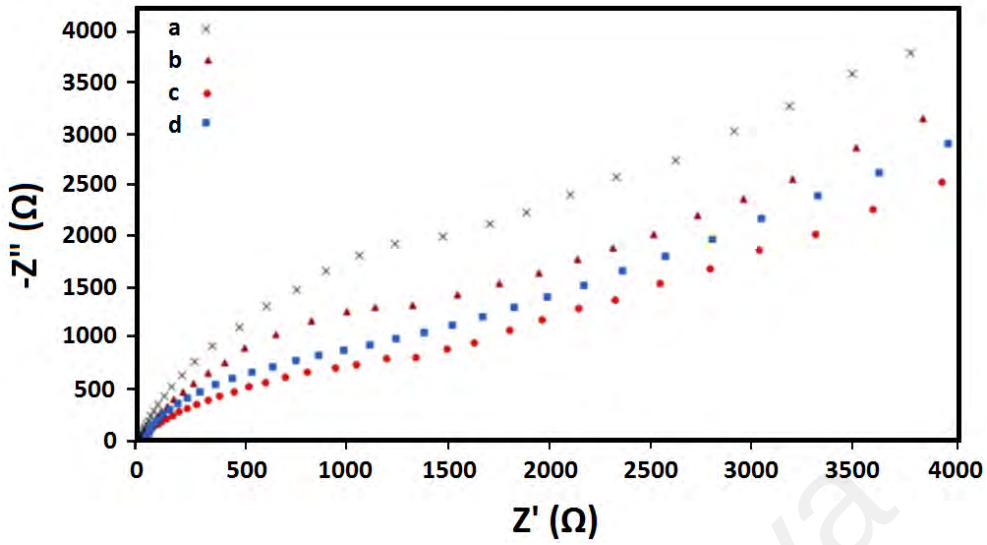

Figure 4.19: Nyquist plots of (a) PtNF, (b) PNG-1, (c) PNG-2, and (d) PNG-3 in 0.1 M KCl solution containing 1 mM $Fe(CN)_6^{3-/4-}$ (1:1).

CHAPTER 5: CONCLUSIONS AND SUGGESTIONS FOR FUTURE WORKS

5.1 Conclusion

In the present work, a hybrid approach was employed for the development of novel nanostructures for the non-enzymatic detection of H_2O_2. To investigate the phase structure/composition and morphological features of the products XRD, FESEM and TEM techniques were utilized. Besides, Raman spectroscopy and XPS were also employed to examine the structural properties and recognize the nitrogen-bonded groups in the as-prepared NG, respectively. The specific conclusions on performance of these products are listed as follows:

5.1.1 Fabrication and Characterization of AgNDs/NG and PtNF/NG

1. NG nanosheets with N:C atomic ratios of up to 0.17 were successfully synthesized at low temperature using a simple microwave-assisted process and were grown on ITO using EPD. In the second step, AgNDs were deposited on the NG-modified ITO electrode via electrochemical deposition for the fabrication of a H_2O_2 sensor.

2. From the XRD profiles, the manifestation of the high intensity peak of the (1 1 1) plane exhibited dendritic growth along the (1 1 1) plane of cubic silver. In addition, the ratios of the peak intensities of (1 1 1) / (2 0 0) and (1 1 1) / (2 2 0) of AgNDs/NG were higher than the conventional values, showing the formation of a non-spherical morphology of Ag.

3. From the FESEM images of the electrochemically deposited AgNDs on the NG-modified-ITO electrode, the as-deposited AgNDs were uniformly embedded in the NG surface. Moreover, according to TEM images, the individual AgNDs had an elegant two-dimensional dendritic structure with long trunks and uniformly arranged parallel branches, where the diameters of the trunk and the side branches were approximately 1 μm and 400 nm, respectively.

4. In Raman spectra of pristine GO, AgNDs/G-modified and AgNDs/NG-modified ITO electrodes, the *D*, *G* and 2*D* bands were centered at approximately 1359 cm^{-1}, 1587 cm^{-1} and 2681 cm^{-1}, respectively. In these cases, the occurrence of the *D* band shows that the defect density in the specimens were similar due to the introduction of vacancies during the microwave-assisted process.

5. The wide-scan XPS spectra of GO confirmed the presence of C and O. Besides, the presence of N in NG clearly confirmed that nitrogen was successfully doped into the graphene lattice during the reduction of GO.

6. In the case of PtNF/NG, NG nanosheets were successfully grown with different degrees of loading on ITO substrate using EPD, where the results confirmed the reduction and nitrogen doping of GO to NG during annealing with urea at 900 °C. After that, the PtNFs were electrodeposited on NG-modified ITO electrode. The PtNF/NG-modified ITO electrodes with different NG loadings were utilized as an advanced biosensor electrode for H_2O_2 detection.

7. The XRD profile of GO exhibited a sharp diffraction peak at $2\theta = 10.6°$ with a *d*-spacing of 0.83 nm, which was much wider than the narrow peak at 26.8° (graphite), with an interlayer spacing of 0.33 nm. This showed that the raw graphite was exfoliated into GO sheets, from the presence of the oxygen, carboxyl and other functional groups. After annealing of GO with urea at 900 °C in Ar for 4 h, the diffractogram showed the absence of this peak, along with the presence of a broad (0 0 2) diffraction peak corresponding to an interlayer spacing of 0.35 nm. This confirmed the formation of graphene, from the removal of the oxygen functional groups during the annealing process.

8. From the FESEM/TEM observations, Pt showed a nanoflower structure, where PtNF was uniform and densely distributed on the surface of the

electrophoretically deposited NG-modified ITO electrode. The individual PtNFs were quasi-spherical in appearance with sizes in the range of 250–300 nm.

9. The Raman spectra of GO showed three peaks at 1359, 1588 and 2688 cm^{-1} that pertained to the *D*, *G* and 2*D* bands, respectively. In addition to these three peaks, NG exhibited an extra weak *D′* band at 1710 cm^{-1}. The intensity ratio (I_D/I_G) of GO and NG were 0.66 and 1.28, respectively. This confirmed that the annealing process created a large amount of sp^2 bonds and structural defects in the NG lattice.

10. The wide-scan XPS spectrum of GO showed the presence of O and C. The wide-scan XPS spectrum of NG also confirmed the doping of N in graphene during the annealing of GO with urea

5.1.2 Electrocatalytic Activity of AgNDs/NG and PtNF/NG for H_2O_2

1. As an advanced sensor electrode, the AgNDs/NG-modified ITO electrode exhibited improved electrochemical performance compared to pure NG-modified and graphene-modified ITO electrodes. The improved electrochemical response was attributed to the enhanced surface area due to the layered structure of NG and the roughened surface from the presence of AgNDs on NG. The response of the as-fabricated electrochemical sensor was rapid, stable and reliable with a detection limit of 0.26 μM in the range from 100 μM to 80 mM.

2. The presence of NG in the PtNF/NG hybrid led to a considerable improvement in the catalytic performance of the pure PtNFs. Thus, the PNG-2-modified ITO electrode with a 0.05 mg ml^{-1} NG loading exhibited the best catalytic performance with a detection limit of 0.34 μM between 1 μM and 1 mM. The EIS measurement confirmed that a further increase in the NG loading up to 0.1 mg ml^{-1} caused an increase in the electrolyte-electrode interfacial resistance of the hybrid electrode, which led to a reduction in the

electrocatalytic performance of the biosensor electrode because of an increase in agglomeration of NG during the EPD.

3. It is worth mentioning that the most important achievement of this work is the use of ITO as a cheap substrate compared to the GCE and a facile electrophoretic deposition method for the fabrication of the sensor electrodes. Indeed, electrophoretic deposition can be a substitute for other methods for the preparation of the sensor substrate from carbon materials, conductive polymer and other organic materials, in the fabrication of sensor electrodes based on conductive polymer-metal composite or other organic-metal composite electrodes.

5.2 Suggestions for Future Work

In a nutshell, with the growth of nanoscience and nanotechnology, numerous types of nanomaterials have been utilized to fabricate electrochemical H_2O_2 biosensors. Accordingly, the performance of the biosensors has been significantly improved during the past decade. The enzymatic biosensors show very low detection limit, which can be considered for biomedical approaches. In contrast, the non-enzymatic H_2O_2 biosensors generally have a larger linear range and better sensitivity, and consequently they are more applicable to industrial and environmental monitoring. Furthermore, the Ag and Pt nanomaterial based non-enzymatic biosensors are highly regarded due to their outstanding features and wide application prospects. It should be noted that although several studies have reported progress in electrochemical H_2O_2 biosensors, some limitations still persist, for instance the preparation method, reliability and reproducibility, which require further investigation before to these biosensors can be employed for routine diagnosis. Some of the valuable titles that can be considered in future research are:

- Preparation of nanocomposites of NG decorated with bimetallic alloy for use as a biosensor for H_2O_2 detection. The influence of alloy loading on the structural and morphological features as well as electrocatalytic activity of the product can be explored.
- In addition to nitrogen, chemical doping of graphene with other foreign atoms, such as boron, fluorine, chlorine, phosphorus, and sulfur, manipulates the surface chemistry and creates a lot of defects into the graphene lattice which ultimately affects the electrocatalytic activity of the experimental outputs.

REFERENCES

Abbasi, N., Shahbazi, P., & Kiani, A. (2013). Electrocatalytic oxidation of ethanol at Pd/Ag nanodendrites prepared via low support electrodeposition and galvanic replacement. *Journal of Materials Chemistry*, *1*, 9966–9972.

Agarwal, A., & Sen, D. (2006). Conductance of quantum wires: A numerical study of effects of an impurity and interactions. *Physical Review B*, *73*, Article#045332.

Arora, P., Sindhu, A., Dilbaghi, N., & Chaudhury, A. (2011). Biosensors as innovative tools for the detection of food borne pathogens. *Biosensors and Bioelectronics*, *28*, 1–12.

Akyilmaz, E., Oyman, G., Cınar, E., & Odabas, G. (2017). A new polyaniline-catalase-glutaraldehyde-modified biosensor for hydrogen peroxide detection. *Preparative Biochemistry and Biotechnology*, *47*(1), 86–93.

Azarang, M., Shuhaimi, A., Yousefi, R., & Sookhakian, M. (2014). Effects of graphene oxide concentration on optical properties of ZnO/RGO nanocomposites and their application to photocurrent generation. *Journal of Applied Physics*, *116*, Article#84307.

Azarang, M., Shuhaimi, A., & Sookhakian, M. (2015). Crystalline quality assessment, photocurrent response and optical properties of reduced graphene oxide uniformly decorated zinc oxide nanoparticles based on the graphene oxide concentration. *RSC Advances*, *5*, 53117–53128.

Bai, J., Sun, C., & Jiang, X. (2016). Carbon dots-decorated multiwalled carbon nanotubes nanocomposites as a high-performance electrochemical sensor for detection of H_2O_2 in living cells. *Analytical and Bioanalytical Chemistry*, *408*(17), 4705–4714.

Ballerstadt, R., & Schultz, J.S. (2000). A fluorescence affinity hollow fiber sensor for continuous transdermal glucose monitoring. *Analytical Chemistry*, *72*, 4185–4192.

Bănică, F.G. (2012). Chemical Sensors and Biosensors: Fundamentals and Applications. Chichester, UK: John Wiley & Sons. p. 576.

Becker, K., Beer, C., Freitag, M., & Kuck, U. (2015). Genome-wide identification of target genes of a mating-type a-domain transcription factor reveals functions beyond sexual development. *Molecular Microbiology*, *96*(5), 1002–1022.

Berens, C., Suess, B. (2015). Riboswitch engineering – making the all-important second and third steps. *Current Opinion in Biotechnology*, *31*, 10–15.

Bermejo, C., Haerizadeh, F., Takanaga, H., Chermak, D., & Frommer, W.B. (2011). Optical sensors for measuring dynamic changes of cytosolic metabolite levels in yeast. *Nature Protocols*, *6*, 1806–1817.

Bian, X., Lu, X., Jin, E., Kong, L., Zhang, W., & Wang, C. (2010). Fabrication of Pt/polypyrrolehybrid hollow microspheres and their application in electrochemical biosensing towards hydrogen peroxide. *Talanta*, *81*, 813–818.

Bonačić-Koutecký, V., Kulesza, A., Gell, L., Mitric, R., Antoine, R., Bertorelle, F., Hamouda, R., Rayane, D., Broyer, M., & Tabarin, T. (2012). Silver cluster–biomolecule hybrids: from basics towards sensors. *Physical Chemistry Chemical Physics*, *14*, 9282–9290.

Bortolozzi, R., von Gradowski, S., Ihmels, H., Schäfer, K., & Viola, G. (2014). Selective ratiometric detection of H_2O_2 in water and in living cells with boronobenzo (b) quinolizinium derivatives. *Chemical Communications*, *50*(60), 8242–8245.

Bragadin, M., Manente, S., Piazza, R., Scutari, G. (2001). The mitochondria as biosensors for the monitoring of detergent compounds in solution. *Analytical Biochemistry*, *292*(2), 305–307.

Brient-Litzler, E., Plückthun, A., & Bedouelle, H. (2010). Knowledge-based design of reagentless fluorescent biosensors from a designed ankyrin repeat protein. *Protein Engineering, Design and Selection*, *23*(4), 229–241.

Cammann, K. (1977). Biosensors based on ion-selective electrodes. *Fresenius' Zeitschrift für Analytische Chemie*, *287*, 1–9.

Campàs, M., Carpentier, R., & Rouillon, R. (2008). Plant tissue-and photosynthesis-based biosensors. *Biotechnology Advances*, *26*(4), 370–378.

Cardini, G., & Muniz-Miranda, M. (2002). Density functional study on the adsorption of pyrazole onto silver colloidal particles. *The Journal of Physical Chemistry B*, *106*, 6875–6880.

Caruso, R., Trunfio, S., Milazzo, F., Campolo, J., De Maria, R., Colombo, T., Parolini, M., Cannata, A., Russo, C., Paino, R., Frigerio, M., Martinelli, L., & Parodi, O. (2010). Early expression of pro-and anti-inflammatory cytokines in left ventricular assist device recipients with multiple organ failure syndrome. *ASAIO Journal*, *56*, 313–318.

Caruso, R., Verde, A., Cabiati, M., Milazzo, F., Boroni, C., Del Ry, S., Parolini, M., Vittori, C., Paino, R., Martinelli, L., Giannessi, D., Frigerio, M., & Parodi, O. (2012). Association of pre-operative interleukin-6 levels with interagency registry for mechanically assisted circulatory support profiles and intensive care unit stay in left ventricular assist device patients. *The Journal of Heart and Lung Transplantation*, *31*(6), 625–633.

Chaubey, A., & Malhotra, B.D. (2002). Mediated biosensors. *Biosensors & Bioelectronics*, *17*(6-7), 441–456.

Chairam, S., Sroysee, W., Boonchit, C., Kaewprom, C., Wangnoi, T.G.N., Amatatongchai, M., Jarujamrus, P., Tamaung, S., & Somsook, E. (2013). Nonenzymatic sensor for hydrogen peroxide using a carbon paste electrode modified with a composite consisting of silver nanoparticles, poly(o-

aminobenzoic acid) and magnetite. *International Journal of Electrochemical Science*, *10*, 4611–4625.

Chung, C., Srikun, D., Lim, C.S., Chang, C.J., & Cho, B.R. (2011). A two-photon fluorescent probe for ratiometric imaging of hydrogen peroxide in live tissue. *Chemical Communications*, *47*(34), 9618–9620.

Cornell, B.A., Braach-Maksvytis, V.L.B., King, L.G., Osman, P.D.J., Raguse, B., Wieczorek, L., & Pace, R.J. (1997). A biosensor that uses ion-channel switches. *Nature*, *387*(6633), 580–583.

Crivianu-Gaita, V., & Thompson, M. (2016). Aptamers, antibody scFv, and antibody Fab' fragments: An overview and comparison of three of the most versatile biosensor biorecognition elements. *Biosensors and Bioelectronics*, *85*, 32–45.

Das, M.P., & Green, F. (2003). Landauer formula without landauer's assumptions. *Journal of Physics-Condensed Matter*, *15*(45), L687–L693.

de Picciotto, S., Dickson, P.M., Traxlmayr, M.W., Marques, B.S., Socher, E., Zhao, S., Cheung, S., Kiefer, J.D., Wand, A.J., Griffith, L.G., Imperiali, B., & Wittrup, K.D. (2016). Design principles for SuCESsFul biosensors: specific fluorophore/analyte binding and minimization of fluorophore/scaffold interactions. *Journal of Molecular Biology*, *428*, 4228–4241.

Ding, L., & Su, B. (2015). A non-enzymatic hydrogen peroxide sensor based on platinum nanoparticle–polyaniline nanocomposites hosted in mesoporous silica film. *Journal of Electroanalytical Chemistry*, *736*, 83–87.

Donzella, V., & Crea, F. (2011). Optical biosensors to analyze novel biomarkers in oncology. *Journal of Biophotonics*, *4*(6), 442–52.

Dubey, R.S., & Upadhyay, S.N. (2001). Microbial corrosion monitoring by an amperometric microbial biosensor developed using whole cell of Pseudomonas sp. *Biosensors and Bioelectronics*, *16*(9–12), 995–1000.

Elfstrom, N., Juhasz, R., Sychugov, I., Engfeldt, T., Karlstrom, A.E., & Linnros, J. (2007). Surface charge sensitivity of silicon nanowires: Size dependence. *Nano Letters*, *7*(9), 2608–2612.

Ercole, C., Del Gallo, M., Mosiello, L., Baccella, S., & Lepidi, A. (2003). Escherichia coli detection in vegetable food by a potentiometric biosensor. *Sensors and Actuators B: Chemical*, *91*, 163–168.

Fang, Y., Zhang, D., Qin, X., Miao, Z., Takahashi, S., Anzai, J.I., & Chen, Q. (2012). Anon-enzymatic hydrogen peroxide sensor based on poly (vinylalcohol)—multiwalled carbon nanotubes—platinum nanoparticles hybrids modified glassy carbon electrode. *Electrochimica Acta*, *70*, 266–271.

Ferrari, A.C., & Basko, D.M. (2013). Raman spectroscopy as a versatile tool for studying the properties of graphene. *Nature Nanotechnology*, *8*, 235–246.

Foley, E.L., Candela, D., Martini, K.M., & Tuominen, M.T. (1999). An undergraduate laboratory experiment on quantized conductance in nanocontacts. *American Journal of Physics*, *67*(5), 389–393.

Gong, Q., Yang, H., Dong, Y., & Zhang, W. (2015). A sensitive impedimetric DNA biosensor for the determination of the HIV gene based on electrochemically reduced graphene oxide. *Analytical Methods*, *7*, 2554–2562.

Hierlemann, A., Brand, O., Hagleitner, C., & Baltes, H. (2003). Microfabrication techniques for chemical/biosensors. *Proceedings of the IEEE*, *91*, 839–863.

Hierlemann, A., & Baltes, H. (2003). CMOS-based chemical microsensors. *The Analyst*, *128* (1), 15–28.

Hong, J., Yang, W.Y., Zhao, Y.X., Xiao, B.L., Gao, Y.F., Yang, T., Ghourchian, H., Moosavi-Movahedi Z., Sheibani, N., Li, J.G., & Moosavi-Movahedi, A.A. (2013). Catalase immobilized on a functionalized multi-walled carbon nanotubes-gold nanocomposite as a highly sensitive bio-sensing system for detection of hydrogen peroxide. *Electrochimica Acta*, *89*, 317–325.

Huang, J., Wang, D., Hou, H., & You, T. (2008). Electrospun palladium nanoparticle-loaded carbon nanofibers and their electrocatalytic activities towards hydrogen peroxide and NADH. *Advanced Functional Materials*, *18*, 441–448.

Ghasemi-Varnamkhasti, M., Rodriguez-Mendez, M.L., Mohtasebi, S.S., Apetrei, C., Lozano, J., Ahmadi, H., Razavi, S.H., & de Saja, J.A. (2012). Monitoring the aging of beers using a bioelectronic tongue. *Food Control*, *25*, 216–224.

Golsheikh, A.M., Huang, N.M., Lim, H.N., Zakaria, R., & Yin, C.Y. (2013). One-step electrodeposition synthesis of silver-nanoparticle-decorated graphene on indium-tin-oxide for enzymeless hydrogen peroxide detection. *Carbon*, *62*, 405–412.

Gough, D.A., Kumosa, L.S., Routh, T.L., Lin, J.T., & Lucisano, J.Y. (2010). Function of an implanted tissue glucose sensor for more than 1 year in animals. *Science Translational Medicine*, *2*(42), 42-53.

Giannoudi, L., Piletska, E.V., Piletsky, S.A. (2006). Development of biosensors for the detection of hydrogen peroxide. in: biotechnological applications of photosynthetic proteins: biochips, biosensors and biodevices. Biotechnology Intelligence Unit. Springer, Boston, MA.

Grieshaber, D., MacKenzie, R., Voros, J., & Reimhult, E. (2008). Electrochemical biosensors - sensor principles and architectures. *Sensors*, *8*, 1400–1458.

Groher, F., Suess, B. (2014). Synthetic riboswitches – a tool comes of age. *Biochimica et Biophysica Acta*, *1839*(10), 964–973.

Guascito, M.R., Filippo, E., Malitesta, C., Manno, D., Serra, A., & Turco, A. (2008). A new amperometric nanostructured sensor for the analytical determination of hydrogen peroxide. *Biosensors and Bioelectronics*, *24*(4), 1057–1063.

Guo, S., Wen, D., Zhai, Y., Dong, S., & Wang, E. (2010). Platinum nanoparticleensemble-on- graphene hybrid nanosheet: one-pot, rapid synthesis, and usedas new electrode material for electrochemical sensing. *ACS Nano*, *4*, 3959–3968.

Habibi, B., Azhar, F.F., Fakkar, J., & Rezvani, Z. (2017). Ni–Al/layered double hydroxide/Ag nanoparticle composite modified carbon-paste electrode as a renewable electrode and novel electrochemical sensor for hydrogen peroxide. *Analytical Methods*, *9*, 1956–1964.

He, S., Chen, Z., Yu, Y., & Shi, L. (2014). A novel non-enzymatic hydrogen peroxide sensor based on poly-melamine film modified with platinum nanoparticles. *RSC Advances*, *4*, 45185–45190.

Ivanov, S., Tsakova, V., & Bund, A. (2013). Formation and electroanalytical performance of polyaniline–palladium nanocomposites obtained via layer-by-layer adsorption and electroless metal deposition. *Electrochimica Acta*, *90*, 157– 165.

Jiang, D., Zhang, Y., Huang, M., Liu, J., Wan, J., Chu, H., Chen, M. (2014). Carbon nanodots as reductant and stabilizer for one-pot sonochemical synthesis of amorphous carbon-supported silver nanoparticles for electrochemical nonenzymatic H_2O_2 sensing. *Journal of Electroanalytical Chemistry*, *728*, 26–33.

Jiaojiao, J., Yangyang, G., Gangying, Z., Yanping, C., Wei, L., & Guohua, H. (2015). D-Glucose, D-Galactose, and D-Lactose non-enzyme quantitative and qualitative analysis method based on Cu foam electrode. *Food Chemistry*, *175*, 485–493.

Jianzhong, L., Zhang, Z., & Ling, L. (1994). A simplified enzyme-based fiber optic sensor for hydrogen peroxide and oxidase substrates. *Talanta 41*, 1999–2002.

Jin, J., Fu, X., Liu, Q., Liu, Y., Wei, Z., Niu, K., & Zhang, J. (2013). Identifying the active site in nitrogen-doped graphene for the VO^{2+}/VO_2^+ redox reaction. *ACS Nano*, *7*, 4764–4773.

Jones, A.M., Grossmann, G., Danielson, J.A.H., Sosso, D., Chen, L.Q., Ho, C.H., & Frommer, W.B. (2013). In vivo biochemistry: applications for small molecule biosensors in plant biology. *Current Opinion in Plant Biology*, *16*, 389–395.

Jost, C., & Plückthun, A. (2014). Engineered proteins with desired specificity: DARPins, other alternative scaffolds and bispecific IgGs. *Current Opinion in Structural Biology*, *27*, 102–112.

Kling, J. (2006). Moving diagnostics from the bench to the bedside. *Nature Biotechnology*, *24*(8), 891–893.

Kong, L., Ren, Z., Zheng, N., Du, S., Wu, J., Tang, J., & Fu, H. (2015). Interconnected 1D CO_3O_4 nanowires on reduced graphene oxide for enzymeless H_2O_2 detection. *Nano Research*, *8*(2), 469–480.

Koposova, E., Liu, X., Kisner, A., Ermolenko, Y., Shumilova, G., Offenhäusser, A., & Mourzina, Y. (2014). Bioelectrochemical systems with oleylamine-stabilized

gold nanostructures and horseradish peroxidase for hydrogen peroxide sensor. *Biosensors and Bioelectronics*, *57*, 54–58.

Kueng, A., Kranz, C., & Mizaikoff, B. (2004). Amperometric atp biosensor based on polymer entrapped enzymes. *Biosensors and Bioelectronics*, *19*(10), 1301–1307.

Kulp, C., Gillmeister, K., Widdra, W., & Bron, M. (2013). Synthesis of CuCorePt Shell nanoparticles as model structures for core–shell electrocatalysts by direct platinum electrodeposition on copper. *Chemical Physics Chemistry*, *14*, 1205–1210.

Kumar, V.S., Nagaraja, B.M., Shashikala, V., Padmasri, A.H., Madhavendra, S.S., Raju, B.D., & Rao, K.S.R. (2004). Highly efficient Ag/C catalyst prepared by electro-chemical deposition method in controlling microorganisms in water. *Journal of Molecular Catalysis A*, *223*, 313–319.

Krishnamurthy, V., Monfared, S., & Cornell, B. (2010). Ion channel biosensors part I construction operation and clinical studies. *IEEE Transactions on Nanotechnology*, *9*(3), 313–322.

Kotanen, C.N., Gabriel Moussy, F., Carrara, S., & Guiseppi-Elie, A. (2012). Implantable enzyme amperometric biosensors. *Biosensors and Bioelectronics*, *35*(1), 14–26.

Khanal, D.R., Yim, J.W.L., Walukiewicz, W., & Wu, J. (2007). Effects of quantum confinement on the doping limit of semiconductor nanowires. *Nano Letters*, *7*(5), 1186–1190.

Kivrak, H., Alal, O., & Atbas, D. (2015). Efficient and rapid microwave-assisted route to synthesize Pt-MnOx hydrogen peroxide sensor. *Electrochimica Acta*, *176*, 497–503.

Kummer, L., Hsu, C.W., Dagliyan, O., MacNevin, C., Kaufholz, M., Zimmermann, B., Dokholyan, N.V., Hahn, K.M., & Plückthun, A. (2013). Knowledge-based design of a biosensor to quantify localized ERK activation in living cells. *Chemistry and Biology*, *20*(6), 847–856.

Lane, B.S., & Burgess, K. (2003). Metal-catalyzed epoxidations of alkenes with hydrogen peroxide. *Chemical Reviews*, *103*(7), 2457–2473.

Landauer, R. (1989). Conductance determined by transmission - probes and quantized constriction resistance. *Journal of Physics-Condensed Matter*, *1*(43), 8099–8110.

Lawal, A.T. (2015). Synthesis and utilisation of graphene for fabrication of electrochemical sensors. *Talanta*, *131*, 424–443.

Lee, M., Zine, N., Baraket, A., Zabala, M., Campabadal, F., Caruso, R., Trivella, M.G., Jaffrezic-Renault, N., & Errachi, A. (2012). A novel biosensor based on hafnium oxide: application for early stage detection of human interleukin-10. *Sensors and Actuators B: Chemical*, *175*, 201–207.

Lefrançois, P., Euskirchen, G.M., Auerbach, R.K., Rozowsky, J., Gibson, T., Yellman, C.M., Gerstein, M., Snyder, M. (2009). Efficient yeast ChIP-Seq using multiplex short-read DNA sequencing. *BMC Genomics*, *10*, 37-42.

Liu, S., Dai, Z., Chen, H., & Ju, H. (2004). Immobilization of hemoglobin on zirconium dioxide nanoparticles for preparation of a novel hydrogen peroxide biosensor. *Biosensors and Bioelectronics*, *19*, 963–969.

Lin, J.M., Arakawa, H., & Yamada, M. (1998). Flow injection chemiluminescent determination of trace amounts of hydrogen peroxide in snow-water using KIO_4-K_2CO_3 system. *Analytica Chimica Acta*, *371*, 171–176.

Liu, Y., Sun, G., Jiang, C., Zheng, X.T., Zheng, L., Zheng, L., & Li, C.M. (2014). Highly sensitive detection of hydrogen peroxide at a carbon nanotube fiber microelectrode coated with palladium nanoparticles. *Microchimica Acta*, *181*(1). 63–70.

Liu, Y., Liu, X., Guo, Z., Hu, Z., Xue, Z., & Lu, X. (2017). Horseradish peroxidase supported on porous graphene as a novel sensing platform for detection of hydrogen peroxide in living cells sensitively. *Biosensors and Bioelectronics*, *87*, 101–107.

Liu, S.Q., & Ju, H.X. (2002). Renewable reagentless hydrogen peroxide sensor based on direct electron transfer of horseradish peroxidase immobilized on colloidal gold-modified electrode. *Analytical Biochemistry*, *307*(1), 110–116.

Liu, S., Tian, J., Wang, L., & Sun, X. (2011). A method for the production of reduced graphene oxide using benzylamine as a reducing and stabilizing agent and its subsequent decoration with Ag nanoparticles for enzymeless hydrogen peroxide detection. *Carbon*, *49*(10), 3158–3164.

Lu, G., & Zangari, G. (2005). Electrodeposition of platinum on highly oriented pyrolyticgraphite. Part I: electrochemical characterization. *The Journal of Physical Chemistry B*, *109*, 7998–8007.

Lu, W., Luo, Y., Chang, G., Sun, X. (2011a). Synthesis of functional SiO_2- coated graphene oxide nanosheets decorated with Ag nanoparticles for H_2O_2 and glucose detection. *Biosensors and Bioelectronics*, *26*(12), 4791–4797.

Lu, W., Liao, F., Luo, Y., Chang, G., Sun, X. (2011b). Hydrothermal synthesis of well-stable silver nanoparticles and their application for enzyme less hydrogen peroxide detection. *Electrochimica Acta*, *56*(5), 2295–2298.

Lud, S.Q., Nikolaides, M.G., Haase, I., Fischer, M., & Bausch, A.R. (2006). Field effect of screened charges: electrical detection of peptides and proteins by a thin film resistor. *Chemical Physics Chemistry*, *7*(2), 379–384.

Mahmoudian, M., Alias, Y., Basirun, W., Meng Woi, P., Baradaran, S., & Sookhakian, M. (2014). Synthesis, characterization, and sensing applications of polypyrrole coated Fe_3O_4 nanostrip bundles. *Ceramics International*, *40*, 9265–9272.

Marazuela, M., & Moreno-Bondi, M. (2002). Fiber-optic biosensors – an overview. *Analytical and Bioanalytical Chemistry*, *372* (5–6), 664–682.

Maurer, M., Burri, S., de Marchi, S., Hullin, R., Martinelli, M., Mohacsi, P., & Hess, O.M. (2010). Plasma homocysteine and cardiovascular risk in heart failure with and without cardiorenal syndrome. *International Journal of Cardiology*, *141*, 32–38.

Mattarozzi, L., Cattarin, S., Comisso, N., Guerriero, P., Musiani, M., & Verlato, E. (2016). Preparation of porous nanostructured Ag electrodes for sensitive electrochemical detection of hydrogen peroxide. *Electrochimica Acta*, *198*, 296–303.

Mayavan, S., Sim, J.B., & Choi, S.M. (2012). Easy synthesis of nitrogen-doped graphene-silver nanoparticle hybrids by thermal treatment of graphite oxide with glycine and silver nitrate. *Carbon*, *50*, 5148–5155.

Mehrotra, P. (2016). Biosensors and their applications – A Review, *Journal of Oral Biology and Craniofacial Research, 6*, 153 –159.

Mena, M.L., Yanez-Sedeno, P., & Pingarron, J.M. (2005). A comparison of different strategies for the construction of amperometric enzyme biosensors using gold nanoparticle-modified electrodes. *Analytical Biochemistry*, *336*(1), 20–27.

Miranda, F.F., Brient-Litzler, E., Zidane, N., Pecorari, F., & Bedouelle, H. (2011). Reagentless fluorescent biosensors from artificial families of antigen binding proteins. *Biosensors and Bioelectronics*, *26* (10), 4184–4190.

Mishra, R., Dominguez, R., Bhand, S., Munoz, R., & Marty, J. (2012). A novel automated flow-based biosensor for the determination of organophosphate pesticides in milk. *Biosensors and Bioelectronics*, *32*, 56–61.

Mohsin, M., & Ahmad, A. (2014). Genetically-encoded nanosensor for quantitative monitoring of methionine in bacterial and yeast cells. *Biosensors and Bioelectronics*, *59*, 358–364.

Mortellaro, M., & DeHennis, A. (2014). Performance characterization of an abiotic and fluorescent-based continuous glucose monitoring system in patients with type 1 diabetes. *Biosensors and Bioelectronics 61*, 227–231.

Morris, M.C. (2010). Fluorescent biosensors of intracellular targets from genetically encoded reporters to modular polypeptide probes. *Cell Biochemistry and Biophysics*, *56*, 19–37.

Nandini, S., Nalini, S., Sanetuntikul, J., Shanmugam, S., Niranjana, P., Melo, J.S., & Suresh, G.S. (2014). Development of a simple bioelectrode for the electrochemical detection of hydrogen peroxide using Pichia pastoris catalase immobilized on gold nanoparticle nanotubes and polythiophene hybrid. *Analyst*, *139*(22), 5800–5812.

Nguyen, T.T., Nguyen, V.H., Deivasigamani, R.K., Kharismadewi, D., Iwai, Y., & Shim, J.J. (2016). Facile synthesis of cobalt oxide/reduced graphene oxide composites

for electrochemical capacitor and sensor applications. *Solid State Sciences*, *53*, 71–77.

Ooi, K.G.J., Galatowicz, G., Towler, H.M.A., Lightman, S.L., & Calder, V.L. (2006). Multiplex cytokine detection versus ELISA for aqueous humor: IL-5, IL-10, and IFN profiles in uveitis. *Investigative Ophthalmology & Visual Science*, *47*, 272–277.

Orij, R., Urbanus, M.L., Vizeacoumar, F.J., Giaever, G., Boone, C., Nislow, C., Brul, S., & Smits, G.J. (2012). Genome-wide analysis of intracellular pH reveals quantitative control of cell division rate by pH(c) in Saccharomyces cerevisiae. *Genome Biology*, *13*, 80-85.

Peroza, E.A., Ewald, J.C., Parakkal, G., Skotheim, J.M., & Zamboni, N. (2015). A genetically encoded Förster resonance energy transfer sensor for monitoring in vivo trehalose-6-phosphate dynamics. *Analytical Biochemistry*, *474*, 1–7.

Price, D., Fauzi, R., & Mantoura, C. (1998). Shipboard determination of hydrogen peroxide in the western Mediterranean Sea using flow injection with chemiluminescence detection. *Analytica Chimica Acta*, *371*, 205–215.

Qiu, J.-D., Peng, H.-Z., Liang, R.-P., Li, J., & Xia, X.-H. (2007). Synthesis, characterization, and immobilization of prussian blue-modified Au nanoparticles: application to electrocatalytic reduction of H_2O_2. *Langmuir, 23*, 2133–2137.

Quesada-González, D., & Merkoçi, A. (2016). Mobile phone-based biosensing: An emerging "diagnostic and communication" technology. *Biosensors and Bioelectronics*, *92*, 549–562.

Rea, G., Polticelli, F., Antonacci, A., Scognamiglio, V., Katiyar, P., Kulkarni, S.A., Johanningmeier, U., & Giardi, M.T. (2009). Structure-based design of novel Chlamydomonas reinhardtii D1-D2 photosynthetic proteins for herbicide monitoring. *Protein Science*, *18*, 2139–2151.

Renard, M., Belkadi, L., Hugo, N., England, P., Altschuh, D., & Bedouelle, H. (2002). Knowledge-based design of reagentless fluorescent biosensors from recombinant antibodies. *Journal of Molecular Biology*, *318*(2), 429–442.

Renard, M., & Bedouelle, H. (2004). Improving the sensitivity and dynamic range of reagentless fluorescent immunosensors by knowledge-based design. *Biochemistry*, *43*(49), 15453–15462.

Renard, M., Belkadi, L., & Bedouelle, H. (2003). Deriving topological constraints from functional data for the design of reagentless fluorescent immunosensors. *Journal of Molecular* Biology, *326*(1), 167–175.

Rizzuto, R., Pinton, P., Brini, M., Chiesa, A., Filippin, L., & Pozzan, T. (1999). Mitochondria as biosensors of calcium microdomains. *Cell Calcium*, *26*(5), 193–199.

Schultz, J.S., & Sims, G. (1979). Affinity sensors for individual metabolites. *Biotechnology and Bioengineering Symposium*, *9*, 65–71.

Schultz, J.S., Mansouri, S., & Goldstein, I.J. (1982). Affinity sensor: a new technique for developing implantable sensors for glucose and other metabolites. *Diabetes Care*, *5*, 245–253.

Scognamiglio, V., Pezzotti, G., Pezzotti, I., Cano, J., Buonasera, K., Giannini, D., & Giardi, M.T. (2010). Biosensors for effective environmental and agrifood protection and commercialization: from research to market. *Microchimica Acta*, *170*, 215–225.

Scognamiglio, V., Arduini, F., Palleschi, G., & Rea, G. (2014). Bio sensing technology for sustainable food safety. *Trends Analytical Chemistry*, *62*, 1–10.

Serov, A., Andersen, N.I., Kabir, S.A., Roy, A., Asset, T., Chatenet, M., Maillard, F., & Atanassov, P. (2015). Palladium supported on 3D graphene as an active catalyst for alcohols electrooxidation. *Journal of the Electrochemical Society*, *162*, F1305–F1309.

Sethi, R.S., & Lowe, C.R. (1990). Electrochemical microbiosensors. In Proceedings of IEE Colloquium on Microsensors, London, UK.

Shishkanova, T.V., Volf, R., Krondak, M., & Kral, V. (2007). Functionalization of pvc membrane with ss oligonucleotides for a potentiometric biosensor. *Biosensors and Bioelectronics*, *22*(11), 2712–2717.

Shu, Y., Chen, J., Xu, Q., Wei, Z., & Liu, F., Lu, R., Xu, S., & Hu, X. (2017). MoS_2 nanosheet-Au nanorod hybrids for highly sensitive amperometric detection of H_2O_2 in living cells. *Journal of Materials Chemistry B*, *5*(7), 1446–1453.

Sivasubramanian, R., & Sangaranarayanan, M. (2013). Electrodeposition of silver nanostructures: from polygons to dendrites, *Crystal Engineering Communication*, *15*, 2052– 2056.

Skrlec, K., Strukelj, B., & Berlec, A. (2015). Non-immunoglobulin scaffolds: a focus on their targets. *Trends in Biotechnology*, *33* (7), 408–418.

Sookhakian, M., Amin, Y., Zakaria, R., Basirun, W., Mahmoudian, M., Nasiri-Tabrizi, B., Baradaran, S., & Azarang, M. (2015). Significantly improved photocurrentresponse of ZnS-reduced graphene oxide composites. *Journal of Alloys Compounds*, *632*, 201–207.

Sookhakian, M., Amin, Y., & Basirun, W. (2013). Hierarchically ordered macro-mesoporous ZnS microsphere with reduced graphene oxide supporter for a highly efficient photo degradation of methylene blue. *Applied Surface Science*, *283*, 668–677.

Sookhakian, M., Amin, Y., Baradaran, S., Tajabadi, M., Golsheikh, A.M., & Basirun, W. (2014a). A layer-by-layer assembled graphene/zinc sulfide/polypyrrole thin-film electrode via electrophoretic deposition for solar cells. *Thin Solid Films*, *552*, 204–211.

Sookhakian, M., Amin, Y.M., Zakaria, R., Baradaran, S., Mahmoudian, M.R., Rezayi, M., Tajabadi, M.T., & Basirun, W.J. (2014b). Enhanced photovoltaic

performance of polymer hybrid nanostructure heterojunction solar cells based on poly (3- hexylthiophene)/ZnS/ZnO/reduced graphene oxide shell–core nanorod arrays. *Industrial & Engineering Chemistry Research*, *53*, 14301–14309.

Sun, Y., & Xia, Y. (2002). Large-scale synthesis of uniform silver nanowires through a soft self-seeding polyol process. *Advanced Materials*, *14*, 833–837.

Sun, Y., Mayers, B., & Xia, Y. (2003). Transformation of silver nanospheres into nanobelts and triangular nanoplates through a thermal process. *Nano Letters*, *3*, 675– 679.

Tajabadi, M., Basirun, W.J., Lorestani, F., Zakaria, R., Baradaran, S., Amin, Y., Mahmoudian, M., Rezayi, M., & Sookhakian, M. (2015). Nitrogen-doped graphene-silver nanodendrites for the non-enzymatic detection of hydrogen peroxide. *Electrochimica Acta*, *151*, 126–133.

Tang, J., Wang, B., Wu, Z., Han, X., Dong, S., & Wang, E. (2003). Lipid membrane immobilized horseradish peroxidase biosensor for amperometric determination of hydrogen peroxide. *Biosensors & Bioelectronics*, *18*, 867–872.

Tang, K., Wu, X., Wang, G., Li, L., Wu, S., Dong, X., Liu, Z., & Zhao, B. (2016). One-step preparation of silver nanoparticle embedded amorphous carbon for nonenzymatic hydrogen peroxide sensing. *Electrochemistry Communications*, *68*, 90–94.

Teridi, M.A.M., Sookhakian, M., Basirun, W.J., Zakaria, R., Schneider, F.K., daSilva, W.J., Kim, J., Lee, S.J., Kim, H.P., & bin Mohd Yusoff, A.R. (2015). Plasmon enhanced organic devices utilizing highly ordered nanoimprinted gold nanodisks and nitrogen doped graphene. *Nanoscale*, *7*, 7091–7100.

Thévenot, D.R., Toth, K., Durst, R.A., & Wilson, G.S. (1999). Electrochemical biosensors: recommended definitions and classification. *Pure and Applied Chemistry*, *71*, 2333–2348.

Thévenot, D.R., Toth, K., Durst, R.A., & Wilson, G.S. (2001a). Electrochemical biosensors: recommended definitions and classification. *Biosensors & Bioelectronics, 16*(1–2), 121–131.

Thévenot, D.R., Toth, K., Durst, R.A., & Wilson, G.S. (2001b). Electrochemical biosensors: recommended definitions and classification, *Biosensors and Bioelectronics*, *16*, 121–131.

Tian, J., Liu, S., & Sun, X. (2010). Supramolecular microfibrils of o-phenylenediamine dimers: oxidation-induced morphology change and the spontaneous formation of Ag nanoparticle decorated nanofibers. *Langmuir*, *26*, 15112–15116.

Tian, J., Li, H., Lu, W., Luo, Y., Wang, L., & Sun, X. (2011). Preparation of Ag nanoparticle-decorated poly (m-phenylenediamine) microparticles and their application for hydrogen peroxide detection. *Analyst*, *136*(9), 1806–1809.

Tian, Y., Wang, F., Liu, Y., Pang, F., & Zhang, X. (2014). Green synthesis of silver nanoparticles on nitrogen-doped graphene for hydrogen peroxide detection. *Electrochimica Acta*, *146*, 646–653.

Tilke, A.T., Simmel, F.C., Lorenz, H., Blick, R.H., & Kotthaus, J.P. (2003). Quantum interference in a one-dimensional silicon nanowire. *Physical Review B*, *68*(7), Article#6.

Tran, H.V., Trinh, A.X., Huynh, C.D., & Le, H.Q. (2016). Facile hydrothermal synthesis of silver/chitosan nanocomposite and application in the electrochemical detection of hydrogen peroxide. *Sensor Letters*, *14*, 32–38.

Turner, A., Wilson, G., & Kaube, I. (1987). Biosensors: Fundamentals and Applications. Oxford, UK: Oxford University Press. p. 770.

US Department of Health and Human Services; Food and Drug Administration; Center for Drug Evaluation and Research; Center for Veterinary Medicine; Office of Regulatory Affairs, eds. (September 2004), Guidance for Industry: PAT — A Framework for Innovative Pharmaceutical Development, Manufacturing, and Quality Assurance

Védrine, C., Leclerc, J.-C., Durrieu, C., & Tran-Minh, C. (2003). Optical whole-cell biosensor using Chlorella vulgaris designed for monitoring herbicides. *Biosensors and Bioelectronics*, *18*(4), 457–63.

Vilian, A.E., Chen, S.M., & Lou, B.S. (2014). A simple strategy for the immobilization of catalase on multi-walled carbon nanotube/ poly (l-lysine) biocomposite for the detection of H_2O_2 and iodate. *Biosensors and Bioelectronics*, *61*, 639–647.

Vinayan, B.P., Nagar, R., Rajalakshmi, N., & Ramaprabhu, S. (2012). Novel Platinum–cobalt alloy nanoparticles dispersed on nitrogen-doped graphene as a cathode electrocatalyst for PEMFC applications. *Advanced Functional Materials*, *22*, 3519–3526.

Vockenroth, I., Atanasova, P., Knoll, W., Jenkins, A., & Köper, I. (2005). Functional tethered bilayer membranes as a biosensor platform. *IEEE Sensors*, 2005 – *the 4th IEEE Conference on Sensors*, *5*, 608–610.

Vo-Dinh, T., & Cullum, B. (2000). Biosensors and biochips: Advances in biological and medical diagnostics. *Fresenius' Journal of Analytical Chemistry*, *366* (6–7), 540–551.

Vollmer, F., & Yang, L. (2012). Label-free detection with high-Q microcavities: a review of biosensing mechanisms for integrated devices. *Nanophotonics*, *1*, 267–291.

Vreeke, M.S., Maidan, R., Heller, A. (1992). Hydrogen peroxide and b-Nicotinamide adenine dinucleotide sensing amperometric electrodes based on electrical connection of horseradish peroxidase redox centers to electrodes through a three-dimensional electron relaying polymer network. *Analytical Chemistry*, *64*, 3084–3090.

Wang, L., Ye, Y., Lu, X., Wu, Y., Sun, L., Tan, H., Xu, F., & Song, Y. (2013). Prussian blue nanocubes on nitrobenzene-functionalized reduced graphene oxide and its application for H_2O_2 biosensing. *Electrochimica Acta*, *114*, 223–232.

Wang, H., Nakata, E., & Hamachi, I. (2009). Recent progress in strategies for the creation of protein-based fluorescent biosensors. *Chemical Biology Chemistry, 10*, 2560–2577.

Wang, D.H., Kou, R., Gil, M.P., Jakobson, H.P., Tang, J., Yu, D.H., & Lu, Y.F. (2005). Templated synthesis, characterization, and sensing application of macroscopic platinum nanowire network electrodes. *Journal of Nanoscience and Nanotechnology*, *5*(11), 1904–1909.

Wang, F., Liu, X., Lu, C.H., & Willner, I. (2013). Cysteine-mediated aggregation of Au nanoparticles: the development of a H_2O_2 sensor and oxidase-based biosensors. *ACS Nano*, *7*(8), 7278–7286.

Wang, H., Maiyalagan, T., & Wang, X. (2012). Review on recent progress in nitrogen-doped graphene: synthesis, characterization, and its potential applications. *ACS Catalysis, 2*, 781–794.

Wan, J., Wang, W., Yin, G., & Ma, X. (2012). Nonenzymatic H_2O_2 sensor based on Pt nanoflower electrode. *Journal of Cluster Science*, *23*, 1061–1068.

Watson CJ, Ledwidge MT, Phelan D, Collier, P., Byrne, J.C., Dunn, M.J., McDonald, K.M., Baugh, J.A. (2011). Proteomic analysis of coronary sinus serum reveals leucine-rich 2-glycoprotein as a novel biomarker of ventricular dysfunction and heart failure. *Circulation: Heart Failure*, *4*, 188–197.

Wiley, B.J., Chen, Y., McLellan, J.M., Xiong, Y., Li, Z.Y., Ginger, D., & Xia, Y. (2007). Synthesis and optical properties of silver nanobars and nanorice. *Nano Letters*, *7*, 1032–1036.

Wiley, B., Sun, Y., Mayers, B., & Xia, Y. (2005). Shape-controlled synthesis of metal nanostructures: the case of silver. *Chemistry*, *11*, 454–463.

Woolston, B.M., Edgar, S., & Stephanopoulos, G. (2013). Metabolic engineering: past and future. *Annual Review of Chemical and Biomolecular Engineering*, *4*, 259–288.

Wu, P., Qian, Y., Du, P., Zhang, H., & Cai, C. (2012). Facile synthesis of nitrogen-doped graphene for measuring the releasing process of hydrogen peroxide from living cells. *Journal of Materials Chemistry*, *22*, 402–6412.

Wu, H., Fan, S., Jin, X., Zhang, H., Chen, H., Dai, Z., & Zou, X. (2014). Construction of a zinc porphyrin–fullerene-derivative based nonenzymatic electrochemical sensor for sensitive sensing of hydrogen peroxide and nitrite. *Analytical Chemistry*, *86*, 6285–6290.

Wu, P., Cai, Z., Gao, Y., Zhang, H., & Cai, C. (2011). Enhancing the electrochemical reduction of hydrogen peroxide based on nitrogen-doped graphene for

measurement of its releasing process from living cells. *Chemical Communications*, *47*, 11327–11329.

Wu, P., Du, P., Zhang, H., & Cai, C. (2013). Microscopic effects of the bonding configuration of nitrogen-doped graphene on its reactivity toward hydrogen peroxide reduction reaction. *Physical Chemistry Chemical Physics*, *15*, 6920–6928.

Xiao, J.P. , Xie, Y., Tang, R., Chen, M., & Tian, X.B. (2001). Novel ultrasonically assisted templated synthesis of palladium and silver dendritic nanostructures. *Advanced Materials*, *13*, 1887–1891.

Xu, Y., Zhang, X., Chen, D., Hou, J., Li, C., & Zhu, X. (2013). A layered nano-structured perovskite-type oxide $LaNiTiO_3$ for nonenzymatic catalytic detection of hydrogen peroxide. *Current Nanoscience*, *9*(6), 737–741.

Yang, G.-H., Zhou, Y.-H., Wu, J.-J., Cao, J.-T., Li, L.-L., Liu, H.-Y., & Zhu, J.-J. (2013). Microwave- assisted synthesis of nitrogen and boron co-doped graphene and its application for enhanced electrochemical detection of hydrogen peroxide. *RSC Advances*, *3*, 22597–22604.

Yang, Y., Fu, R., Yuan, J., Wu, S., Zhang, J., & Wang, H. (2015). Highly sensitive hydrogenperoxide sensor based on a glassy carbon electrode modified with platinum nanoparticles on carbon nanofiber heterostructures. *Microchimica Acta*, *182*, 2241–2249.

Yan, C., Dong, F., Chun-yuan, B., Si-rong, Z., & Jian-guo, S. (2014). Recent progress of commercially available biosensors in china and their applications in fermentation processes. *Journal of Northeast Agricultural University*, *21*, 73–85.

Yi, G.C., Wang, C.R., & Park, W.I. (2005). ZnO nanorods: synthesis, characterization and applications. *Semiconductor Science and Technology*, *20*(4), S22–S34.

You, T., Niwa, O., Tomita, M., & Hirono S. (2003). Characterization of platinum nanoparticle-embedded carbon film electrode and its detection of hydrogen peroxide. *Analytical Chemistry*, *75*, 2080–2085.

Zafar, Z., Ni, Z.H., Wu, X., Shi, Z.X., Nan, H.Y., Bai, J., & Sun, L.T. (2013). Evolution of Raman spectra in nitrogen doped graphene. *Carbon*, *61*, 57–62.

Zaribafan, A., Haghbeen, K., Fazli, M., & Akhondali, A. (2014). Spectrophotometric method for hydrogen peroxide determination through oxidation of organic dyes. *Environmental Studies of Persian Gulf, 1*(2), 93–101.

Zhang, L.S., & Wong G.T.F. (1999). Optimal conditions and sample storage for the determination of H_2O_2 in marine waters by the scopoletin-horseradish peroxidase fluorometric method. *Talanta*, *48*, 1031–1038.

Zhang, J., Jensen, M.K., & Keasling, J.D. (2015). Development of biosensors and their application in metabolic engineering. *Current Opinion in Chemical Biology*, *28*, 1–8.

Zhang, J., & Zheng, J. (2015). An enzyme-free hydrogen peroxide sensor based on Ag/FeOOH nanocomposites. *Analytical Methods*, *7* (2015) 1788–1793.

Zhao, W., Wang, H., Qin, X., Wang, X., Zhao, Z., Miao, Z., Chen, L., Shan, M., Fang, Y., & Chena, Q. (2009). A novel nonenzymatic hydrogen peroxide sensor based on multi-wall carbon nanotube/silver nanoparticle nanohybrids modified gold electrode. *Talanta*, *80*(2), 1029–1033.

Zhao, Z., Liu, J., Wang, W., Zhang, J., Li, G., Liu, J., Lian, K., Hu, J., & Zhuiykov, S. (2017). Ag functionalized molybdenum disulfide hybrid nanostructures for selective and sensitive amperometric hydrogen peroxide detection. *International Journal of Electrochemical Science*, *12*, 8761–8776.

Zhou, Y., Chiu, C.W., & Liang, H. (2012). Interfacial structures and properties of organic materials for biosensors: an overview. *Sensors*, *12*(11), 15036–15062.

Zhu, Y., Zheng, H., Li, Y., Gao, L., Yang, Z., & Qian, Y. (2003). Synthesis of Ag dendritic nanostructures by using anisotropic nickel nanotubes. *Materials Research Bulletin*, *38*, 1829–1834.

LIST OF PUBLICATIONS AND PAPERS PRESENTED

LIST OF PUBLICATIONS

1. **Tajabadi, M.T.,** Basirun, W.J., Lorestani, F., Zakaria, R., Baradaran, S., Amin, Y.M., Mahmoudian, M.R., Rezayi, M., & Sookhakian, M. (2015). Nitrogen-doped graphene-silver nanodendrites for the non-enzymatic detection of hydrogen peroxide. *Electrochimica Acta, 151*, 126–133.

2. **Tajabadi, M.T.,** Sookhakian, M., Zalnezhad, E., Yoon, G.H., Hamouda, A.M.S., Azarang, Majid, Basirun, W.J., & Alias, Y. (2016). Electrodeposition of flower-like platinum on electrophoretically grown nitrogen-doped graphene as a highly sensitive electrochemical non-enzymatic biosensor for hydrogen peroxide detection. *Applied Surface Science, 386*, 418–426.

LIST OF PAPERS PRESENTED

1. Sookhakian, M., Amin, Y.M., Baradaran, S., **Tajabadi, M.T.,** Moradi Golsheikh, A., & Basirun, W.J. (2014). A layer-by-layer assembled graphene/zinc sulfide/polypyrrole thin-film electrode via electrophoretic deposition for solar cells. *Thin Solid Films, 552*, 204–211.
2. Sookhakian, M., Amin, Y.M., Basirun, W.J., **Tajabadi, M.T.,** & Kamarulzaman, N. "Synthesis, structural, and optical properties of type-II ZnO–ZnS core–shell nanostructure. (2014). *Journal of Luminescence*, *145*, 244–252.